Granular segregation dynamics in a rotating drum

by

Zeina Khan

A thesis submitted in conformity with the requirements
for the degree of Doctor of Philosophy
Graduate Department of Physics
University of Toronto

Abstract

Heterogeneous granular mixtures tend to segregate by size when tumbled in a partially filled, horizontal rotating drum. After a few drum rotations the small grains move towards the axis of rotation and form a buried radial core, which, after several hundred drum rotations, splits into axial bands. This process can display complex, oscillatory wave dynamics during the transient before segregation saturates. In this thesis, we report on measurements of the axial transport of grains in the radial core, the dynamics of the axial segregation process, and the oscillatory wave transient. We show experimentally that two fields, the concentration and dynamic angle of repose, whose coupling was theoretically postulated, do not evolve as predicted, which falsifies a recent model. We also report that the axial transport of small grains in the radial core is subdiffusive. This does not depend on grain type or rotation rate. We show that the self-mixing of monodisperse grains is as well a subdiffusive mixing process. Lastly, we find that the growth rate scaling of the axial segregation pattern increases as a function of drum diameter and grain size ratio. None of these findings are accounted for by any theoretical model of this system.

Acknowledgements

I would like to thank my advisor, Stephen W. Morris, for introducing me to the fascinating field of granular materials, and for the freedom he has allowed me in pursuing my own ideas and interests. He was always available to discuss the progress of this research, and his enthusiasm for it was infectious. I deeply appreciate the guidance, support, and inspiration he has given me.

I would also like to thank Professors Rashmi Desai and Jerry X. Mitrovica for their input into this research as committee members. They have helped to focus and refine this work, and have given many helpful comments in the preparation of this thesis.

I am extremely grateful to my dear friend and collaborator, Wayne A. Tokaruk, for his guidance in the technical aspects of research in general, and for never being afraid to ask tough questions. I have enjoyed and benefitted from his passion for physics over the years. I am also grateful to Amy Daradich for being such a good friend and an excellent physicist, for offering her opinion on every talk I have ever practiced, and for helping me to overcome my fears of public presentation.

I would also like to express my gratitude to my fellow group members for their helpful discussions and support. I would especially like to thank Peichun Tsai for her good advice and friendship, and Chris Charles for his contribution to this research as an undergraduate thesis student.

I would like to thank my mother Marta for her appreciation of the human side of physics, and my father Ata, for his generosity, enthusiasm, and computers. My sister Ayla was always full of good practical advice, and I am grateful for it. I would especially like to thank my husband, Frank Van Bussel, for his patience, good humour, willingness to read and re-read everything I have written in the last six years, and for just being himself. He is truly my better half, and I dedicate this work to him.

Contents

List of Tables

List of Figures

Chapter 1

Introduction

Granular media are everywhere. From sand grains, which can be several microns to several hundred microns in size, to lentils and other dried foodstuffs, to boulders in rock slides, to the constituents of the rings of Saturn, they are ubiquitous and easily taken for granted – that is, until you consider the complex behaviour these materials can display. What happens when granular media are in motion has interested and puzzled thinkers, starting with Appolonius of Perga around 200 B.C., including Coulomb and Reynolds in the modern era, to the present day [1]. Moreover, mixing, demixing, and pattern formation of sands, powders, and grains is of immense practical interest; it is estimated that 10 % of the world's energy is used in the processing of grains [1, 2].

The physics of granular materials is complex, and the field is still in an early stage of development. In some ways one can consider granular materials as a new state of matter which is not a traditional solid or fluid; for example, in a narrow pipe a granular material can flow as a liquid, but it can also form an arch and jam the pipe like a solid [1]. Driven granular systems are systems far from equilibrium because they are dissipative due to the frictional interactions between grains, and they have strong spatial and temporal variations in density and local particle velocity [3]; the patterns which emerge in these strongly dissipative systems can be quite striking. An example of this corresponds to

the surface patterns which develop spontaneously when several layers of particles are vertically oscillated, a behaviour similar to Faraday patterns observed in a shaken fluid layer, and convection patterns in fluids [1, 4]. In these experiments the granular material organizes itself into stripes, squares and hexagons for particular values of acceleration [5].

Another interesting phenomenon is often observed when one attempts to mix two different granular materials which have different grain properties such as size, density, or surface roughness. Instead of mixing, the materials tend to segregate partially or completely. The segregation of granular mixtures occurs in a wide variety of circumstances, which have attracted the attention of the physics community in recent years. When grains of different sizes are vibrated vertically, it has been observed that the large grains typically rise to the top of the container. This so-called *Brazil-nut effect*, which gets its name from the way large brazil nuts are inevitably at the top of a can of mixed nuts, has been investigated using many different imaging, data analysis, and simulation techniques [6, 7, 8, 9, 10]. Another example of a spontaneously-forming segregation pattern arises when grains of different sizes are poured in a Hele-Shaw cell, which approximates a two-dimensional geometry; in this case they separate into alternating layers of different components of the mixture [11, 12, 13, 14]. This effect has been proposed as a possible cause of sandstone or river bed stratification [11]. An example of this segregation pattern in a mixture of large salt grains and small sand grains is shown in figure 1.1.

Segregation by size has also been investigated in a two-dimensional rotating drum geometry. Typically in these experiments, small and large grains with mixed initial conditions are placed in the drum, which is then rotated at a slow rate, where the flowing layer forms intermittent avalanches or is smoothly streaming [15, 16]. The smaller grains filter to the axis of rotation of the materials in the drum and form a core, surrounded by the larger grains, as illustrated in figure 1.2; this effect is called *radial segregation*.

When a long cylindrical drum is partially filled with a mixture of grains and rotated

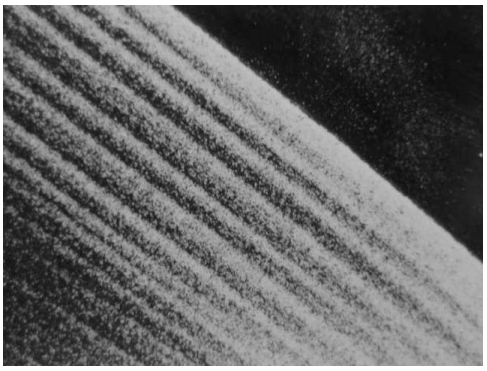

Figure 1.1: An example of the segregation pattern which forms when large white table salt grains and small black hobby sand grains are poured into a Hele-Shaw cell.

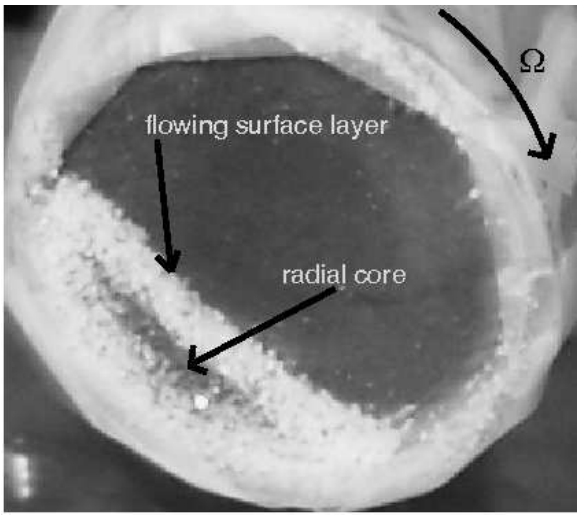

Figure 1.2: An example of a radial segregation pattern which forms when small black 177-212 μm sand grains and large 300-420 μm salt grains are placed in a 2.7 cm diameter rotating drum which is 3 mm long. The drum rotation rate is 0.62 rev/s and the mixture is composed of 1/3 sand grains and 2/3 salt grains.

about its long axis, as shown in figure 1.3, the mixture may separate by size into bands of each of the components of the mixture along the length of the drum. This effect was first observed by Oyama in 1939 [17], and was given the name *axial segregation*. Though it has been more than six decades since the phenomenon was first discovered as

yet very little is known about the mechanism of formation of these axial bands, despite the apparent simplicity of the pattern. This is the most widely studied and modeled segregation experiment [15]. In this thesis we will investigate the dynamics of axial band formation, as well as subsurface phenomena that may give rise to it.

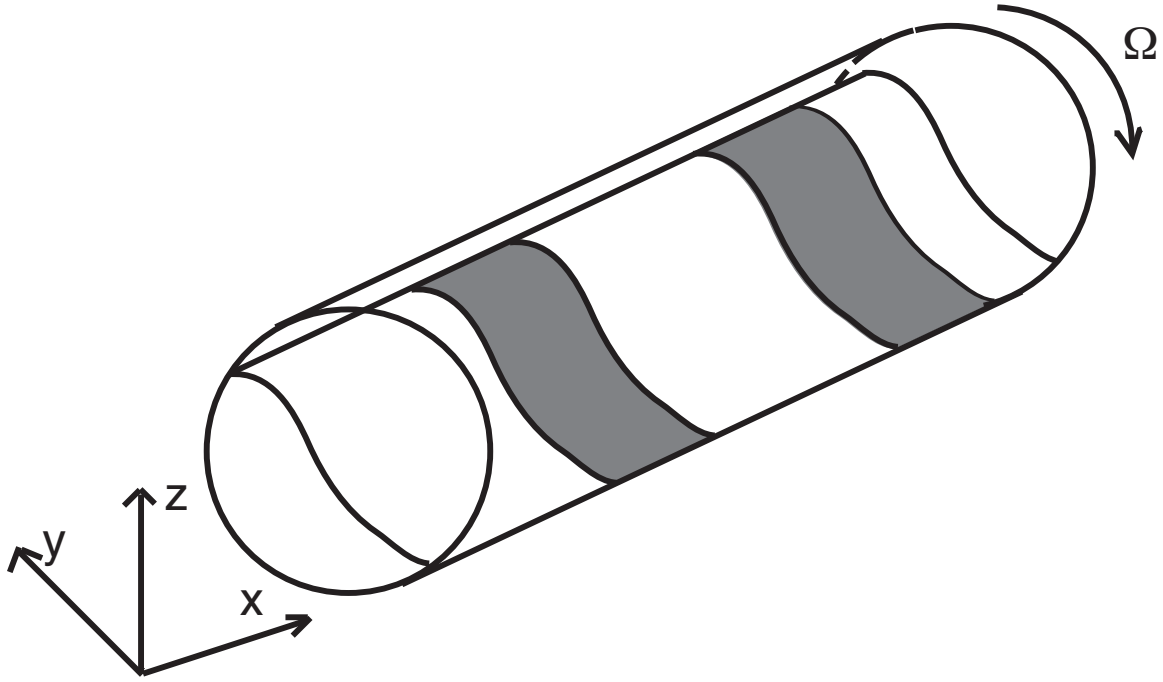

Figure 1.3: A schematic diagram of the rotating drum used in experiments. The mixture of grains typically used in experiments consists of small black hobby sand grains and large white table salt grains. The x axis runs along the axis of the drum, the y axis runs along the cross section of the drum perpendicular to the axis, and the z axis points vertically upwards. Ω refers to the drum rotation rate.

1.1 Phenomenology of the rotating drum system

Figure 1.4 shows a rotating drum filled with a mixture of small salt grains and large black sand grains at different times during the segregation process. As can be seen in figure 1.4a, bands near the end caps appear prior to axial band formation, within a few

drum rotations. Donald and Roseman [18] were the first to report end-band formation in the literature, and attributed the full axial segregation phenomenon to end-wall effects. Later experiments showed that end-bands are an experimental artifact due to the fact the caps sealing the tube were made from a material with different frictional properties than the tube and grains [19].

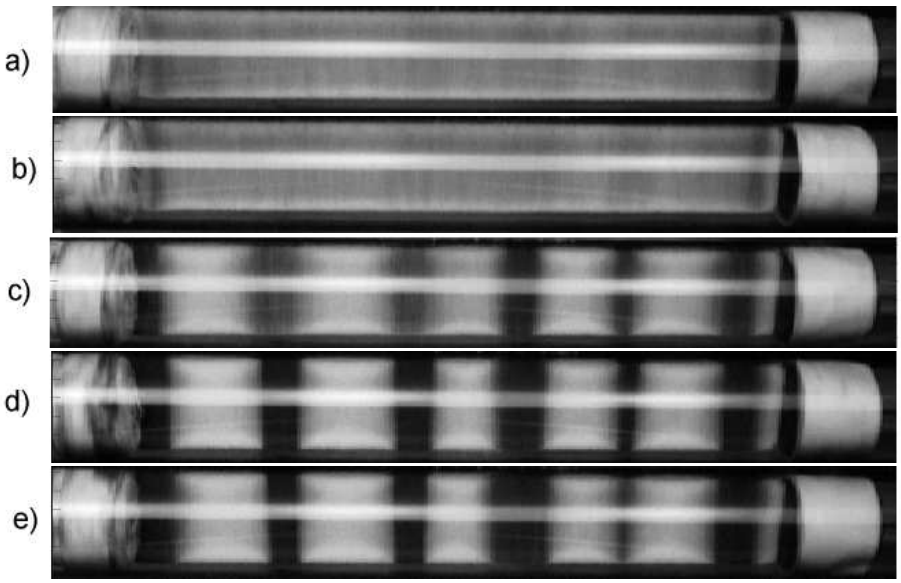

Figure 1.4: a) An image of the rotating drum after 0 s of rotation, b) 50 s, c) 500 s, d) 1500 s and e) 2500 s. The mixture consists of large white table salt grains with sizes in the range of 500-600 μm and small black hobby sand grains with sizes in the range of 177-212 μm. The drum diameter is 2.85 cm, its length is 20 cm and the rotation rate is 0.3 rev/s.

As first reported by Donald and Roseman [18], the segregation of grains in a rotating drum is actually a two-stage process. First the smaller grains filter through the larger ones forming a core at the axis of rotation of the mixture in the drum. This occurs via a "dynamic sieve effect" which takes place quickly, within a few drum rotations, as shown in figure 1.2 [18, 20, 21, 22, 23]. Under the influence of gravity, the small grains filter through voids in between the larger ones when the particles are dilated due to the flow in the drum. This is similar to the mechanism by which small particles penetrate through mesh screens in mechanical size separation [24]. After several hundred to several thousand drum rotations, axial bands form. While it was speculated as early as 1962 that these effects were related [18], only recently has radial core instability has been investigated as the mechanism responsible for axial band formation [20, 21, 22, 23, 25, 28, 29, 30]. In this view, quasi-periodic modulations on the core grow and break through the flowing surface layers of materials in the drum, forming axial bands. In the work presented here, we greatly expand upon this idea.

Most axial segregation studies focus on bidisperse mixtures of grains in a circular rotating drum [17, 20, 25, 26, 27]. In 1962, it was observed that, for mixtures consisting of more than two components, the axial bands order themselves by particle size [31]; this effect has been termed *band-in-band segregation* [29]. It has also been noted that the radial core was comprised of the smallest grain size in the deepest layer, surrounded by rings of increasing grain sizes.

In 1969, a new type of segregation called *floating segregation* was reported by Bridgwater and co-authors [24]; here segregation occurs in the avalanching surface layer of grains in the rotating drum. This was attributed by the authors to percolation effects, since the large grains in the study were two orders of magnitude larger than the small grains.

In 1994, Hill and Kakalios reported on the systematic variation of grain sizes in bidisperse mixtures rotated at different rates. They observed three types of behaviour

depending on the size of the grains involved: axial banding which would occur at high rotation rates and re-mix at lower rotation rates, axial segregation which was not reversible at lower rotation rates, and finally, no segregation [32]. Measurements of the *dynamic angle of repose*, the angle the flowing granular surface forms with the horizontal (shown schematically in figure 1.5), revealed that when there was little difference in dynamic angle of the small and large consitutents the mixture never formed axial bands, but when the difference was large, axial bands formed and were non-reversible. Finally, when the difference of the angles of repose increased with rotation rate, reversible axial segregation occurred. It was also reported that small grains typically have higher angles of repose than large grains.

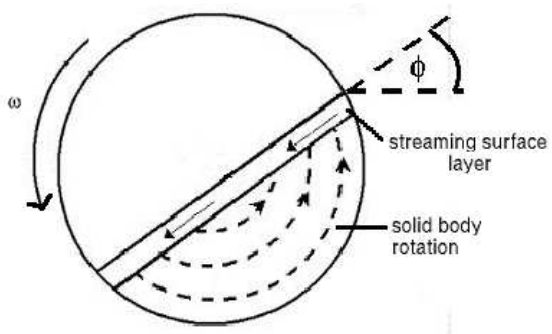

Figure 1.5: A schematic illustration of the dynamic angle of repose, the angle ϕ the flowing granular surface forms with the horizontal cross-section of the drum.

The so-called *reverse diffusion model* was first proposed by Savage [33], and further developed by Zik *et al.* [34]. The "effective" diffusion coefficient is the difference between the diffusion coefficient and a quantity β with the same dimensions whose value is determined by the difference in angles of repose of the mixed and large grain phases. If the difference of the angles of repose of the mixed and large (grain) phases is small, β will have a very small value and and normal positive diffusion will dominate, resulting in a mixed phase as has been observed experimentally [18, 32, 34]. If the difference in dynamic angles is large, the sign of the effective diffusion coefficient becomes negative, and

initial concentration fluctuations grow, leading to the collection of grains in areas of high concentration, which correspond to axial bands. The reverse diffusion model developed is described in more detail in chapter 3.

In 1997, a travelling wave transient occurring prior to axial segregation was first reported by Choo *et al.* [35, 36]. Travelling waves were observed in mixtures consisting of 1/3 sand and 2/3 salt, whose sizes were taken from non-overlapping distributions. Video imaging techniques were adapted to construct space-time diagrams in which the waves are clearly seen passing to the left and right, and through each other. As well, standing wave transients were observed in runs starting from presegregated initial conditions; these decayed until they were absorbed by nearby axial bands. One example of a space-time diagram of these traveling waves is shown in figure 1.6, from reference [35]. In this experiment, a mixture of black sand and white table salt was presegregated into 1 and 2 cm bands respectively. Choo *et al.* performed a detailed study of the wave-speed dependence on presegregated wavelength; they found that the wave speed decreases as a function of wavelength, with a long wavelength cutoff above which the presegregated bands remain in a frozen state [35, 36].

These results demonstrated that the Zik *et al.* theory mentioned above, which describes axial segregation as a reverse diffusion process, is insufficient to explain axial banding since a diffusion equation cannot sustain standing or travelling waves. Recently, this travelling wave transient was found in a bidisperse mixture of glass spheres [37], suggesting that differences in frictional properties of the grains is not a potential driving mechanism of the travelling wave transient [30]. It has also been reported that some mixtures composed of three particle sizes, so-called *ternary* mixtures of glass beads, can display an oscillatory band instability; the widths of small-particle bands oscillate in time while the band widths of the larger particles remain unchanged in time [29].

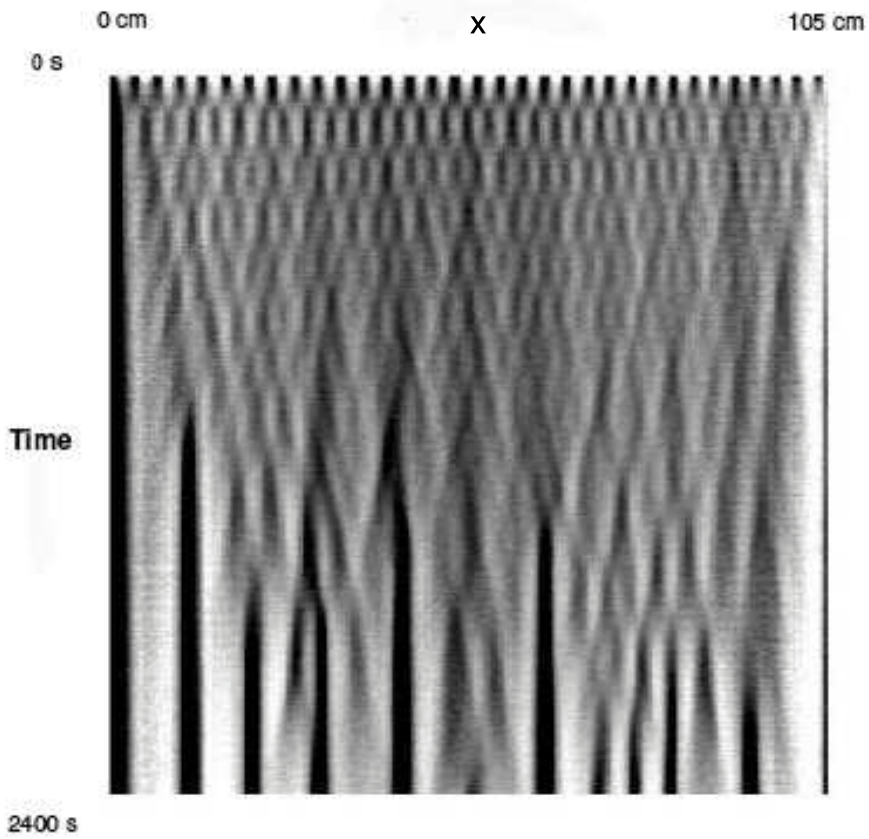

Figure 1.6: A space-time diagram of an oscillatory transient found in a presegregated mixture of large white table salt grains and small black hobby sand grains, with a 3 cm presegregated initial wavelength. From reference [42].

The work of Choo *et al.* was a significant innovation in the study of axial segregation. Prior to the publication of this work, authors in this field presented images of the initial and final states with perhaps a few snapshots at intermediate times [17, 18, 23, 32]. By taking many digital images of the drum in time and vertically averaging over them, and effectively stacking them in time to create a space-time representation of the dynamics, Choo and co-workers were able to determine that interesting phenomena are present that are too slow to be observed by eye. One period of the travelling waves is typically 100 drum revolutions. It is possible that previous studies of axial segregation missed interesting dynamical behavior of grains in the drum because they did not capture a complete picture of the evolving pattern.

In light of Choo *et al.*'s work, a comprehensive new model was proposed by Aranson *et al.* which reproduces axial segregation as well as the oscillatory travelling wave transient which may occur prior to the axially segregated state [38, 39]. The main feature of this model is that two reaction-diffusion fields, the relative concentration of large to small grains and the dynamic angle of repose, are coupled such that they oscillate ninety degrees out of phase during the oscillatory transient. They are in phase for later times, in the axially segregated state. This promising theory, which is described in detail in chapter 3, was able to reproduce the wave speed dependence on initial wavelength as found by Choo *et al.* Testing the predicted phase relationships between the two coupled fields was a goal of this thesis; a new measurement device, the *scanning profilometer*, was developed to simultaneously measure both evolving fields and is described in chapter 2. The experiments described in chapter 3 using the scanning profilometer showed that concentration and dynamic angle do not have the required phase relationship, thereby falsifying this model.

In the last decade, attention has turned to non-invasive magnetic resonance imaging (MRI) techniques to elucidate the dynamics of flow within the bulk of the rotating drum system, using mixtures of MRI and non-MRI active particles [20, 21, 22, 23, 40]. One

study shows that radial segregation evolves to axial segregation [23]. While this was a reasonable assumption made four decades ago, it was not proven definitively until this thesis study, as described in chapters 3 and 4.

Another report shows that the velocity in the flowing layer of grains is not uniform, but varies with depth in a complex manner, depending on grain size and surface roughness [20]. It was determined that the flowing surface layer intrudes upon material deeper within the bulk and that the radial core is not isolated from the flow dynamics, as was previously assumed. This report indicates that there is a complicated relationship between the dynamics of the radial core and axial segregation that are not addressed in theories that only consider surface flows, such as the reverse-diffusion model mentioned above. While use of non-invasive MRI techniques have advantages for studying these complex bulk flows, they have serious limitations as well. MRI techniques are getting faster, but they are still too slow to determine the short-time development of segregation transients. Typically, drums are rotated slowly within the device [23], or the drum is rotated away from the magnet and stopped at discrete intervals, during which very detailed images of the internal structure of the grains in the drum are produced [20, 40]. The choice of grains suitable for MRI studies is restricted as well. At least one of the grains must contain some type of fluid, and the drum must be small enough to fit within the bore of the magnet. As a consequence, the systematic variation of parameters is limited in MRI studies. For this thesis, we developed a new bulk visualization technique which does not suffer from these limitations in order to examine the radial core dynamics; this technique is discussed in chapter 2.

Ristow and Nakagawa have recently investigated the transport properties of different-sized grains in the rotating drum [40]. Starting from a two-band initial condition with a sharp interface between the large and small grains, they rotated the drum and observed the evolution of the radial core from the interface. Stopping the drum at regular intervals, they measured detailed spatial concentration profiles of small to large grains and the

shape of the interfacial front between the radial core and surrounding larger grains using MRI techniques. They showed that the propagating front is described well by a one-dimensional diffusion process, but they find that the agreement with a diffusion process is better when a concentration dependent diffusion coefficient is used. Their concentration profiles are slightly asymmetric since the small grain interface propagating into the larger grains appears more quickly than the larger grains travelling over the surface of the radial core. This model is described in detail in chapter 4. For this thesis, we conducted detailed studies of the axial transport of grains in the radial core and the self-mixing of one grain type and find that these processes are slower than diffusion i.e *subdiffusive*. These experimental results are discussed in chapter 4.

Over the last four decades, only a few attempts have been made to determine the parametric dependencies of axial segregation despite the enormous parameter space to be explored. It was noted in 1962 that when the ratio of the large to small grains exceeds 1.2, axial segregation occurs [31]. The same authors also noted that the number of axial bands increased with increasing surface roughness of grains by examining 30 different binary mixtures of sands, salt and glass beads [18]. Alexander *et al.* [25] report that the occurrence of axial segregation depends on the ratio of the drum diameter to average particle diameter. When this ratio is smaller than a critical value, axial bands do not appear at any drum rotation rate, and when this ratio is large, axial bands occur at all rotation rates within the smoothly streaming regime. In between these extremes lies a regime of "reversible segregation" as reported by Hill and Kakalios [32].

In collaboration with C. R. J. Charles, I examined the dependence of wavelength and growth rate of the axial band pattern on drum diameter [27]. Charles *et al.* determined that the wavelength to diameter ratio approaches a constant for drum diameters larger than 120 times the average grain size. This study also determined that axial segregation did not occur below a critical ratio of drum diameter to grain size. This work was also the first to show that the growth rate of axial bands increases as a function of drum diameter.

The results of these experiments are described in chapter 4. It is also interesting to note that none of the current theoretical descriptions of axial segregation correctly predicts any of the parametric dependencies or scaling regimes described above [32, 33, 34, 38, 39, 41].

1.2 Outline of the thesis

In chapter 2, the scanning profilometer, and bulk and surface visualization techniques are described, as well as data analysis methods. In chapter 3, Choo's discovery of traveling waves is elucidated in detail. We examine the early theoretical model due to Zik *et al.* [34] and offer a detailed description of Aranson *et al.*'s model [38, 39]. The experimental tests of this model are then described, as well as investigations of the oscillatory instability in the radial core.

Chapter 4 describes detailed experimental investigations of the transport of grains within the radially segregated core in the absence of the oscillatory instability, and how the growth rate of undulations on the core forming axial bands is enhanced as the drum diameter and grain size differences are increased. The influences of varying these parameters on the axial transport of grains within the radial core is investigated, as well as the axial self-mixing of the larger grains alone.

Chapter 5 describes promising new areas of theoretical investigation in granular phenomena that could be extended to describe the dynamics observed here. Chapter 6 provides a summary of our results and suggestions for future experiments.

Chapter 2

Experimental Methods and Data Analysis

This chapter describes the experimental methods used to measure both surface and bulk flow properties of grains in the rotating drum. Grain preparation techniques and the setup of well controlled and reproducible initial conditions are discussed in section 2.1, and the apparatus used to rotate the grains is described in section 2.2. The scanning profilometer device, described in section 2.3, was developed to simultaneously measure the relative concentration of large to small grains and their dynamic angle of repose in order to test a continuum model of axial segregation proposed by I. Aranson and L. Tsimring [38, 39]. Surface imaging, described in section 2.4, is a standard tool used to measure time and length scales relevant to axial segregation and granular mixing. Discrete Fourier transforms can then be used on digital images obtained with a CCD camera to provide detailed information about the pattern evolution. A new bulk visualization technique was developed over the course of this study in order to elucidate the role of the radial core in the traveling wave transient [28, 35, 36] and the axial segregation process. This chapter is concluded with a discussion of this technique in section 2.5.

2.1 Grain Preparation Techniques

For a majority of the experiments described in this thesis, the grains used were Sifto brand white table salt and black "Scenic Sand" purchased from Activa Products Inc. [60]. The density of the salt grains used here was measured to be 2.2 ± 0.1 g/mL and the density of the sand grains was 2.0 ± 0.1 g/mL. The volume of the grains was measured using a fluid displacement method, and the mass was measured using a laboratory scale. Glass and bronze beads were also used in some experiments, their densities were measured to be 2.3 ± 0.1 g/mL and 8.6 ± 0.2 g/mL respectively. In order to create grain mixtures with consistent grain sizes, all grains were sieved using U.S. Standard mesh sieves and a mechanical sieve shaker. The mesh sizes used for this work were 75, 106, 149, 177, 212, 250, 300, 420, 500, 600 and 750 micrometers. The sieves were stacked so grains would be obtained between two of the mesh sizes listed above, and the sieves were always stacked in the above order so no grain size range would be larger than 120 micrometers. Grains with a size distribution of 100 micrometers or smaller were considered to be a monodisperse mixture for the purpose of this study. Most of the work described in this thesis consists of studies of bidisperse mixtures in a variety of initial configurations. These mixtures consist of one sieve cut of small grains and one sieve cut of large grains, where the grain types are different. These mixtures are described in context. However the travelling wave study described in chapter 3 requires the use of certain polydisperse mixtures of both sand and salt, the mixture components are shown in histogram form in figure 2.1. This travelling wave mixture is composed of 1/3 of the sand mixture and 2/3 of the salt mixture, and was used because of the need to reproduce the results of Choo *et al.* [35, 36].

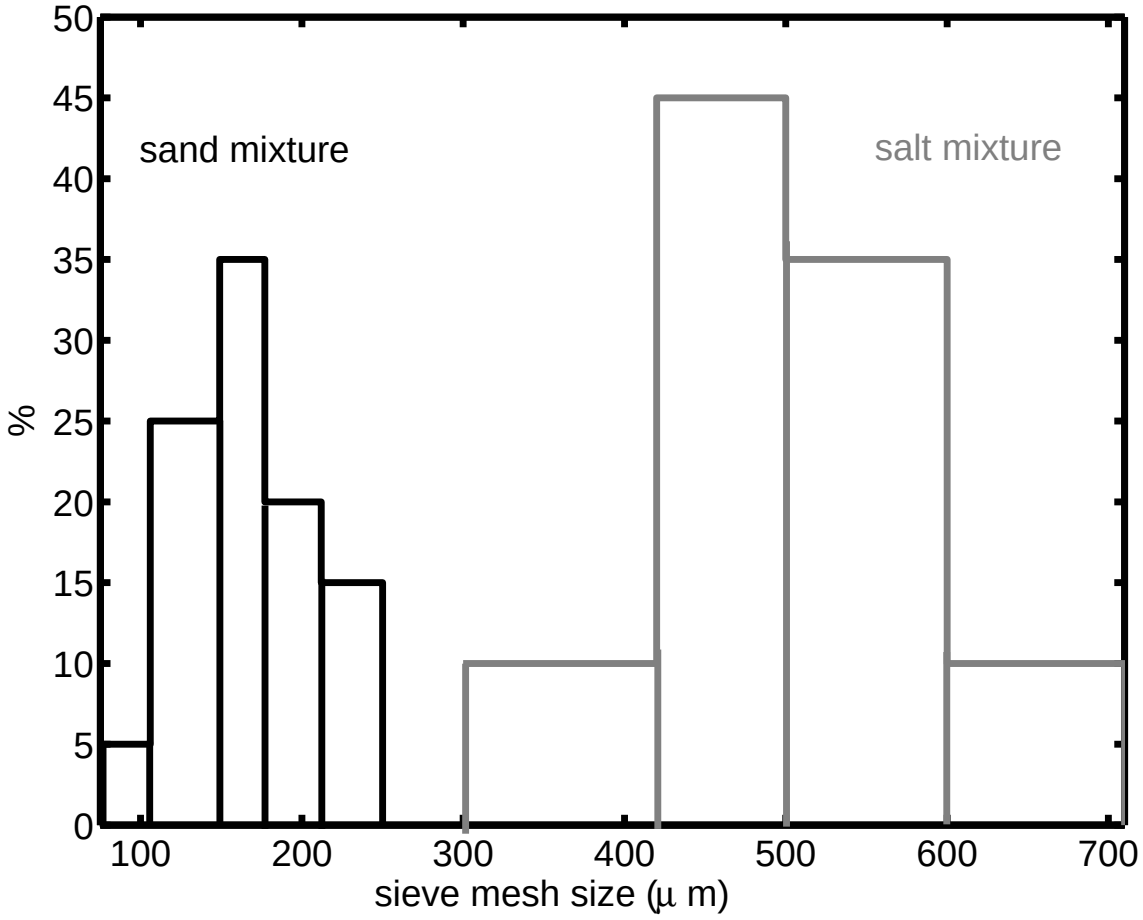

Figure 2.1: Histogram of salt and sand grain sizes in a mixture which exhibits a travelling wave and standing wave instability occurring prior to axial segregation. This was the mixture used by Choo *et al.* in references [35, 36].

It is possible for an accumulation of static charge between the rolling grains and the drum walls to interfere with accumulating experimental data. The grains may collect on drum walls obscuring visualization or may slip in the drum [50]. Humidity control was sufficient to reduce static charge in experiments where table salt was used. For these experiments either humidifiers were used in the winter in an enclosed space to increase the humidity to 40-60 percent, or in the summer a dehumidifier was used to reduce the humidity to the same range. For experiments using glass spheres increasing the ambient humidity had little effect, so small amounts of a powdered antistatic agent was used. We used Larostat FPE-S antistatic powder, which is manufactured by BASF Specialty Products [62]. No information about its composition could be obtained due to the proprietary nature of this product.

2.1.1 Initial Conditions

In order to cite reasonable statistics on the errors of the experiments, it was necessary to start from reproducible initial conditions for most of these experiments since the largest potential source of error is related to lack of reproducibility of initial conditions. The spatial resolution error is on the order of one pixel (typically one-third of a millimeter) and the temporal resolution error is on the order of 10 milliseconds, because we used a real-time operating system, QNX, to perform digital image aquisition with time stamps on each image.

For segregation experiments with randomly mixed initial conditions, the grains were combined by mass in the smallest quantities before being loaded into the drum at the desired filling fraction of 28-30 %. To ensure that the desired proportions did not segregate in the handling of the mixtures, the grains were spooned into a U-shaped channel, and a ruler was run along the top of the channel to remove excess grains and ensure that each and every filling was performed consistently. Then this channel was inserted lengthwise into the drum and rotated to deposit its contents.

Segregation experiments with presegregated initial conditions were performed in a similar manner, but first a threaded rod with thin aluminum spacers aligned according to the presegregated wavelength desired was placed in the channel. The large and small grains were placed between the appropriate spacers with the use of a narrow funnel, and a small flat piece of metal was used to flatten each filled space and remove any excess grains. The rod was carefully removed, and the channel inserted into the drum and rotated to deposit its contents. This method was originally developed by Choo and co-authors [35, 36].

2.2 Experimental Apparatus

The drum used in the majority of experiments described in this thesis was a precision Ace Glass pyrex drum of length 90 cm and inner diameter 2.85 cm [61] with teflon endcaps. It was used to rotate mixtures of white sand and black table salt. The drum was driven at one end by a motor controlled by a Hewlett-Packard function generator which controlled the drum rotation rate, and was supported by a pair of black rubber wheels at the opposite end. The drum and wheels were placed on a leveling table, one end of which could be raised or lowered by turning a screw. The drum was kept horizontally leveled to avoid axial tilt since the wave speed of left and right-going traveling waves are not equal if the drum is tilted. In fact, we were able to use the wave speeds of left and right-going traveling waves to verify that the drum was level. All data were captured using a high-speed black and white CCD camera. The camera was a Dalsa black and white CCD with 512×512 pixel resolution, and a maximum frame rate of 77 Hz. The segregation dynamics were measured using three different visualization techniques, scanning profilometry described in section 2.3, surface video imaging described in section 2.4 and backlit bulk visualization described in section 2.5. An image of the drum, wheels, leveling table, lights and camera are shown in figure 2.2, in addition to the scanning profilometer device.

In some experiments described in chapter 4 drums with inner diameters of 4.4 and 5.6 cm with acrylic endcaps were used to determine the dependence of axial grain transport properties on drum diameter. The apparatus used to rotate these drums was constructed by C. R. J. Charles, and is described in his undergraduate thesis report [63]. The backlit bulk visualization technique was used to capture data from this apparatus, and this technique is described in section 2.5. A software control loop written in the C programming language and implemented on the QNX operating system by Z. S. Khan rotated the drum at the input frequency, and gave commands to the high speed black and white CCD camera to obtain images at predetermined intervals.

2.3 The Scanning Profilometer Visualization Technique

The scanning profilometer was developed to measure the relative concentration of large (white) to small (black) grains, and their dynamic angle of repose. From this data, we obtained space-time diagrams of the dynamics of these two fields, wave speed information, and their phase relationship, as described below.

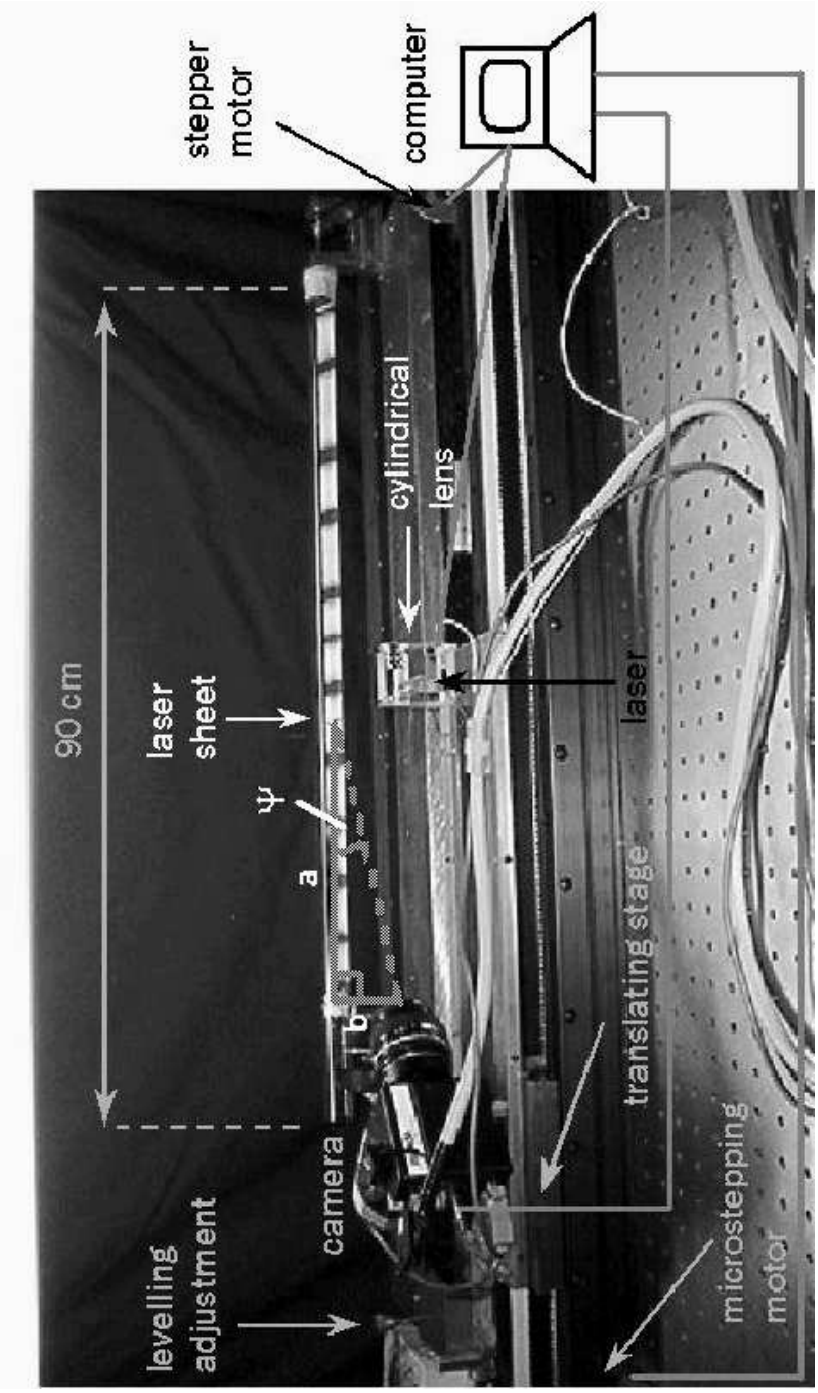

Figure 2.2: Image of the scanning profilometer experimental apparatus. The camera, laser, microstepping motor controlling the translating stage and stepper motor controlling the drum rotation are computer controlled. The angle Ψ was used to correct foreshortening of the images obtained, as described in the text.

An image of the scanning profilometer device is shown in figure 2.2. The streaming surface layer of grains was illuminated by a diode laser obtained from a laser pointer. The beam was spread into a thin vertical sheet using a horizontally mounted cylindrical lens with a 2.1 mm diameter. The laser sheet was visualized using a CCD video camera which views the light sheet with a 50 mm focal length lens at an angle of $\Psi = 41.2 \pm 0.2^o$. This angle was determined by measuring the distance of the center point of the lens to the drum perpendicular to the drum, and by measuring the distance of that point to the position on the drum where the light sheet struck the drum. The camera, laser and lens were mounted on a translation stage which slides parallel to the drum, so the surface could be observed at multiple locations along the drums axis. The translation stage was driven by a Compumotor microstepping motor whose rotation rate was controlled by a computer interface card.

To track the position of the camera, the Compumotor was given a command to rotate 206600 microsteps. The resulting displacement of the translation stage was measured to be 909.6 mm, which results in a conversion factor of 227.1 microsteps per mm. This conversion factor was then used to translate the scanning distance to Compumotor microsteps, and the position of the camera could then be determined. The timing of the measurements was done using the QNX real-time operating system. The entire setup was enclosed in a black canvas tent to eliminate all outside light. The video signal was captured by a frame-grabber card and stored as 8-bit TIFF images on the computer.

The software control was developed in collaboration with W. A. Tokaruk, and implemented in the C programming language. The software moved the translating stage to the input locations given as a length along the axis of the drum with stops every given distance, typically 20 cm and 2 mm, respectively. At each stop, the camera took ten images with the laser sheet on, and the laser was turned off and an image was taken with no laser sheet present, a background image. The images were labeled by software to record the time, axial position and whether the image taken is a background image. The

images with a laser sheet present were averaged to correct for uneven lighting conditions and the average time of the ten images were recorded on the resulting image. Each scan took approximately 7.5 seconds or 6 drum revolutions.

2.3.1 Analysis of Scanning Profilometer Data

Data from the camera were stored in 8 bit format as black and white tiff files, one file for each image captured. Two types of image were collected, some with the laser sheet striking the granular surface and some without the laser sheet present.

To isolate the laser image from background data and noise, the background was subtracted from the laser image. The remaining signal is composed of all the pixels in the laser image where the sheet is present. The laser images and background images were taken 0.2 seconds apart to ensure that the background lighting did not change significantly within the black canvas enclosure. Then a circle was cropped around the image of the laser sheet, and the pixel grey-scale values outside of that circle were set to 0 (black), this eliminated unwanted signals such as the laser sheet reflecting off the back of the rotating drum. Finally the images were read into Matlab as unsigned 8-bit matrices and converted to double precision. This allowed mathematical operations to be performed on the images.

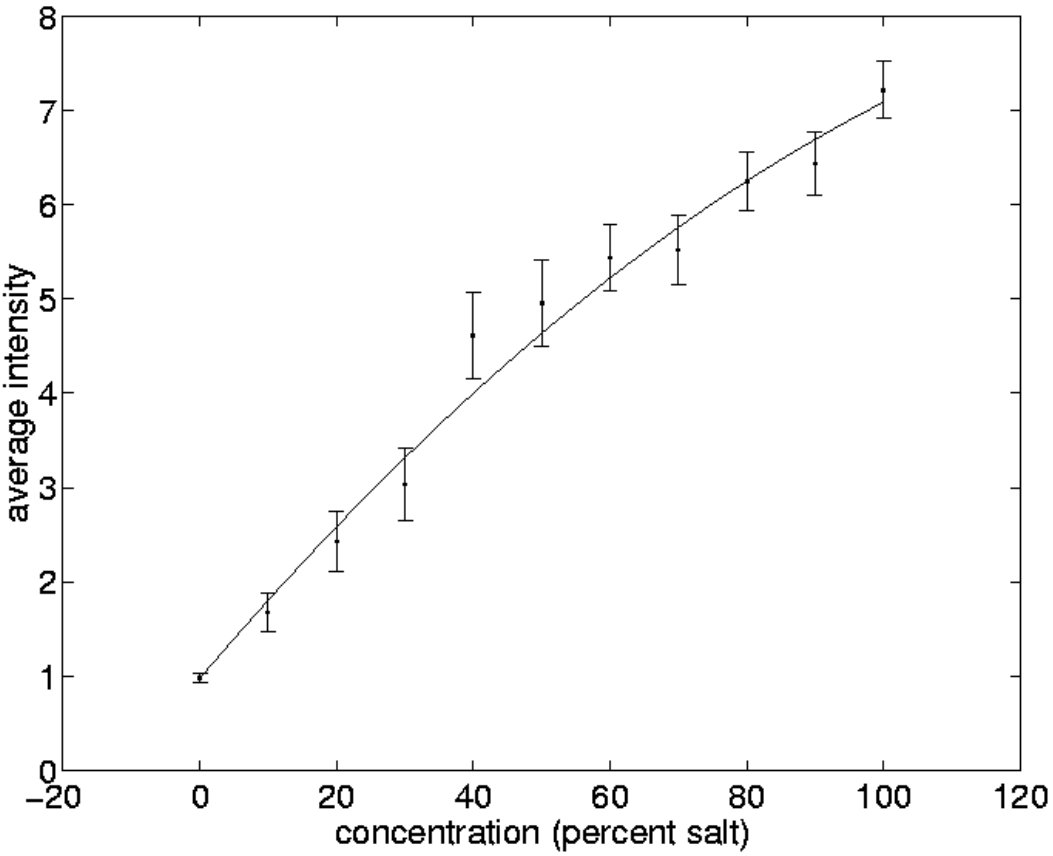

Figure 2.3: Calibration curve relating average image intensity to the relative concentration of grains.

To calibrate intensity levels of a laser sheet image to a concentration or ratio of large white to small black grains, samples with concentrations ranging from 0 percent salt to 100 percent salt in increments of 10 percent were imaged as described above. For each mixture 200 frames were analyzed. The integrated intensity was calculated for each image by adding the pixel greyscale values ranging from 0 to 255 and dividing by the number of pixels in the image. This was done for each of the 200 frames corresponding to a particular mixture concentration, and the average value of these was taken to represent the intensity corresponding to that particular concentration value. The standard deviation was used as the uncertainty in the measurement. These data are shown in figure 2.3. A weighted quadratic least-squares fit to the data yields, where I is the image intensity and C is the concentration of large to small grains,

$$I = \left(-2.00 \times 10^{-5}\right) C^2 + \left(8.52 \times 10^{-2}\right) C + \left(9.75 \times 10^{-1}\right) \tag{2.1}$$

This curve is also shown in figure 2.3. From this calibration curve, intensity measurements of the laser image constitute measurements of the concentration at a given axial position.

After calibration, extracting data from the double-precision image matrices was completed in four steps: determining the concentration, applying a foreshortening correction, thresholding the image to eliminate noise, and fitting the resulting data to a fifth-order polynomial to determine the surface profile and dynamic angle of repose. Each of these steps are described in detail below.

The quadratic polynomial calibration curve given above has two roots for the concentration C, both real valued in the range of I that is measured. One is always between 0 and 100 and the other is greater than 100. We discarded the latter as unphysical and used the former to calculate the concentration of large to small grains from the average laser intensity of the image we measured.

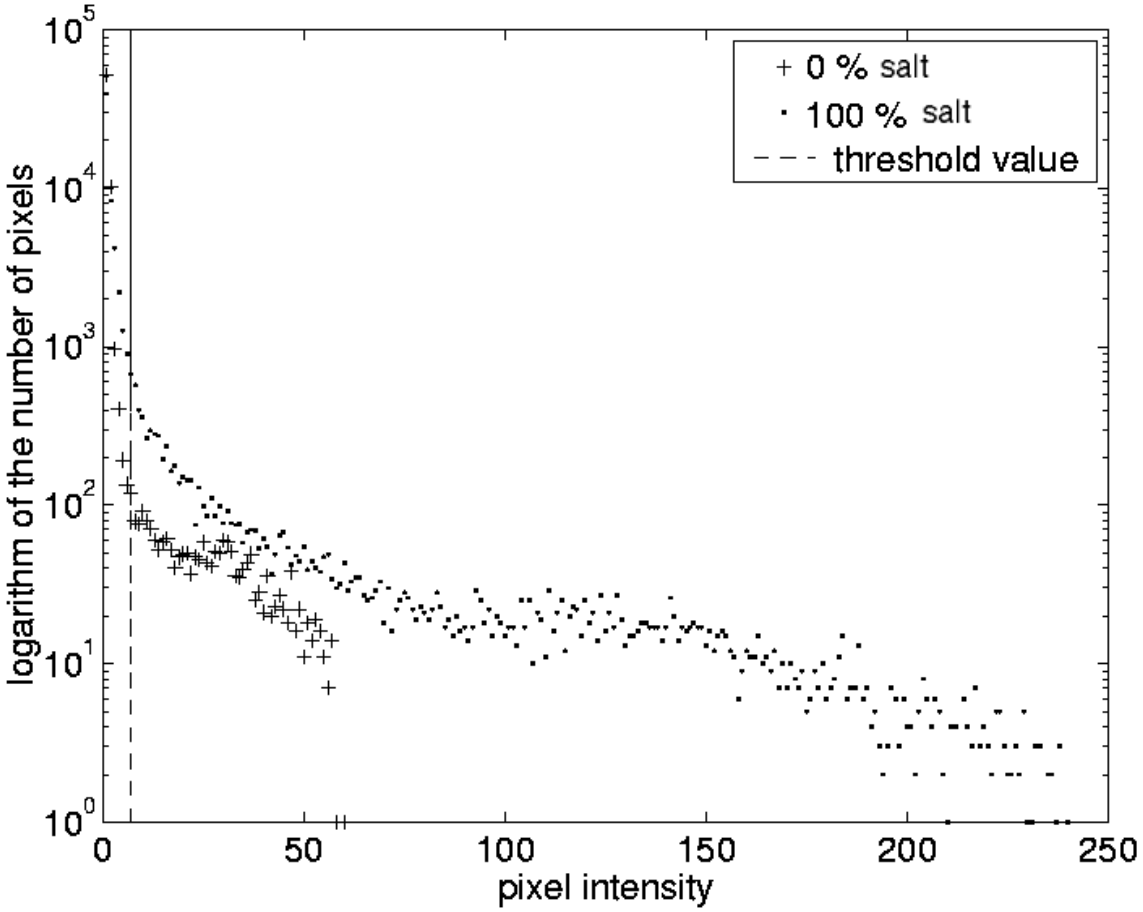

Figure 2.4: Histogram of image intensity, and the threshold value used to eliminate noise pixels.

To eliminate noise pixels from the images, a reasonable threshold value was determined by examining histograms of pixel intensities, such as in figure 2.4. This figure shows the pixel intensity values on the horizontal axis and the logarithm of the number of pixels having the corresponding intensity on the vertical axis. The data was taken from two calibration images, one with a relative concentration value of 100 percent, the other 0 percent. From the histograms it can be seen that a threshold value of 7 (also shown in figure 2.4) adequately reduces the noise from the large number of pixels with low intensity while retaining information from the black sand mixtures. All pixels whose intensity was larger than the threshold value were output to data sets as (x, y, I) points, where the x and y values correspond to the position of a pixel in a Cartesian coordinate system. From images of the laser sheet viewed at an angle Ψ such as that from figure 2.2, we determined the surface profile as though it were taken from the end of the drum. To do this we needed to effectively elongate the image along the horizontal x-direction while the keeping the vertical length unaffected. By applying the foreshortening correction

$$x' = x/\cos\Psi \tag{2.2}$$

$$y' = y \tag{2.3}$$

we obtained this end view, where x' and y' are the corrected pixel positions. As mentioned earlier for the experiments cited here, $\Psi = 41.2 \pm 0.2^o$.

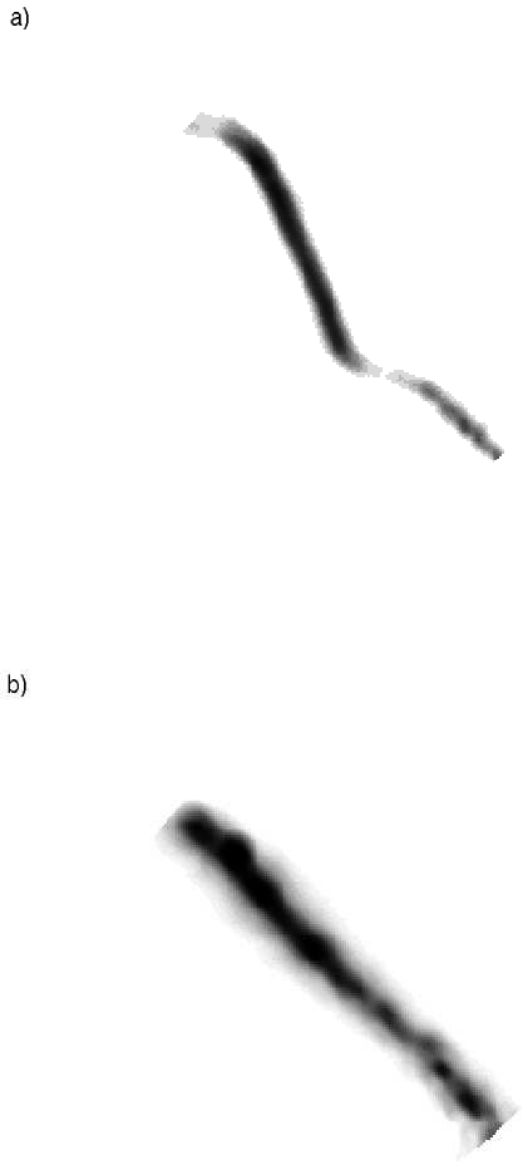

Figure 2.5: a) Image of the laser sheet for a pure sand mixture, b) image of the laser sheet for a pure salt mixture. These images have been inverted to aid in the visualization of the laser sheet. Note the kink in the sand image.

Once the foreshortening correction was applied to an image of the laser sheet, the resulting data were fit to a fifth-order polynomial. This high order was chosen as mixtures with a high sand concentration generally have a kink in their surface profile, as can be seen in figure 2.5a, where the relative concentration is 0 percent salt. Figure 2.5b shows that the profile of a 100 percent salt mixture is much closer to a straight line. A weighted least-squares scheme was used for the fit, as the coefficients of higher-order terms vanish if they are not necessary to describe the data. Figure 2.5b shows that the beam spreads when it strikes the grains. To compensate for this effect each pixel was assigned a weight of $(1/I)$ in the fitting scheme. Recall that for a general least-squares fitting scheme, the χ^2 merit function is defined as

$$\chi^2 = \sum_{i=1}^{N} \left[\frac{y_i - \sum_{k=1}^{M} a_k X_k(x_i)}{\sigma_i} \right]^2$$

where the X_k are basis functions, y_i are the data points and the a_k are the linear coefficients to be determined [58]. If the error σ_i is set as $(1/I)$ then brighter pixels carry more weight in the fitting scheme. Since brighter pixels carried more weight the polynomial was fit to the center of the width of the laser sheet. The surface slope below the kink was rather insensitive to the concentration. We therefore calculated the dynamic angle of repose from the average arctangent of the slope of the polynomial profile above the kink. Further details about this measurement technique, such as the reconstruction of surface profiles of flowing grains in the drum can be found in Z. S. Khan's M. Sc. report [64].

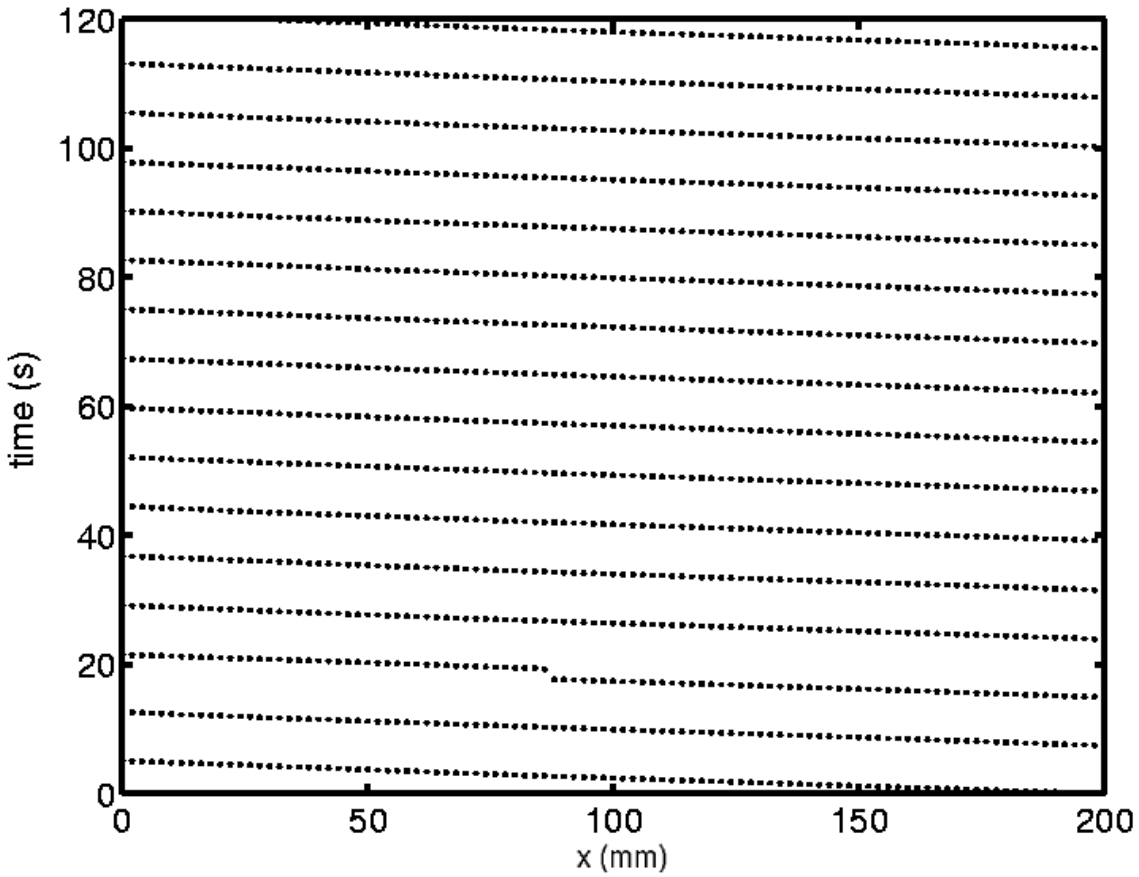

Figure 2.6: Graph of the time and position of each scanning profilometer measurement for a section of the data run. The mixture being imaged is a standing wave mixture with a presegregated wavlength of 33 mm and with a drum rotation rate of 0.77 rev/s.

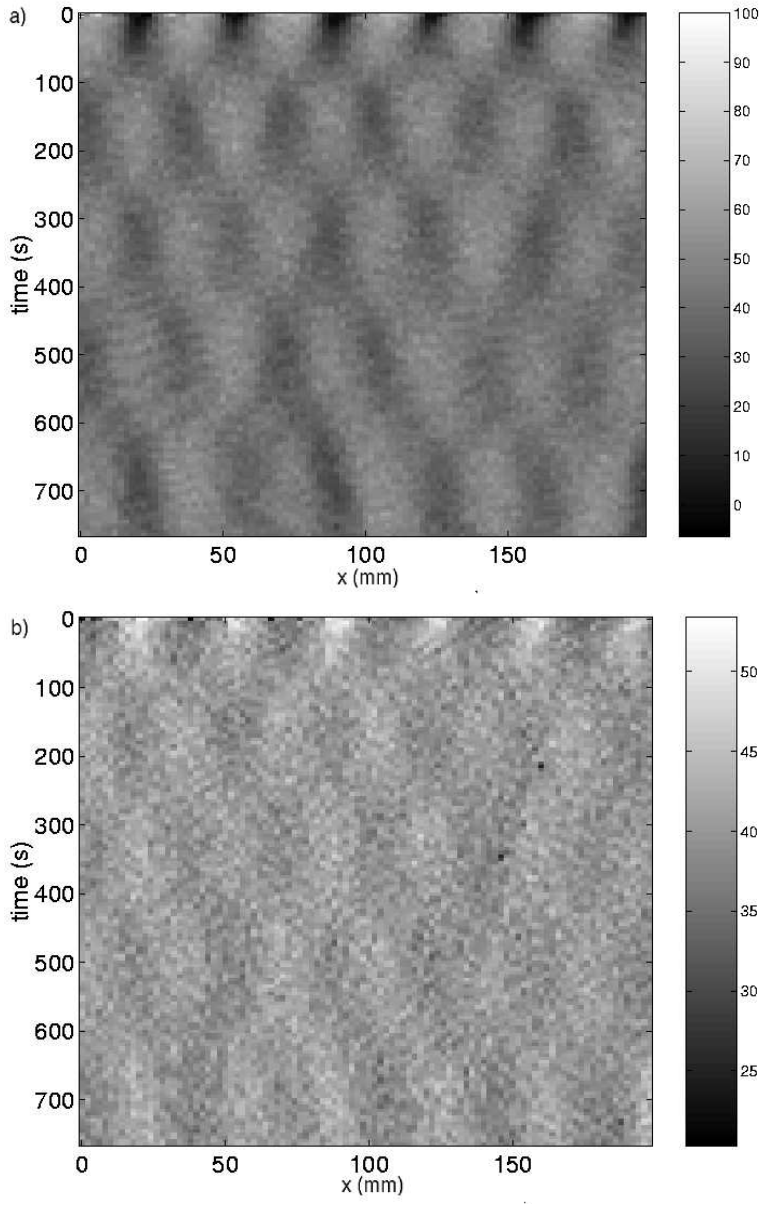

Figure 2.7: a) a space-time diagram of the concentration field corresponding to the graph in figure 2.6. The concentration values of each pixel in the image are shown in the colourbar to the right, b) the space time diagram of the dynamic angle of repose field corresponding to figure 2.6 and (a).

Space-time diagrams of the relative concentration of grains and dynamic angle of repose are necessary to analyze the evolution of the travelling wave transient and axial segregation. These diagrams were constructed as follows: A portion of the scanning profilometers' space-time trajectory is shown in figure 2.6. The translating stage begins at the far right, at a position labeled 200 mm and travels to the left by 2 mm steps, to a position labeled as the axis origin, 0 mm. At each step a measurement is taken. When it reaches the origin it returns quickly to the starting position and repeats the measurement. Each scan takes approximately 7.5 seconds to complete, or 6 drum revolutions

To reconstruct the space-time evolution from this data set, we interpolated to obtain values of concentration and dynamic angle at regular time intervals. Linear interpolation at constant positions was performed for 5 second intervals. Then a space-time diagram was constructed from the measured positions at the interpolated time values. Figure 2.7a is an example of a space time diagram of relative concentration values of a standing wave transient which occurs in a presegregated mixture of sand and salt whose presegregated wavelength is 3.3 cm. Its composition and the setup of the initial condition are described in section 2.1. Figure 2.7b shows the corresponding space-time diagram of the dynamic angle of repose.

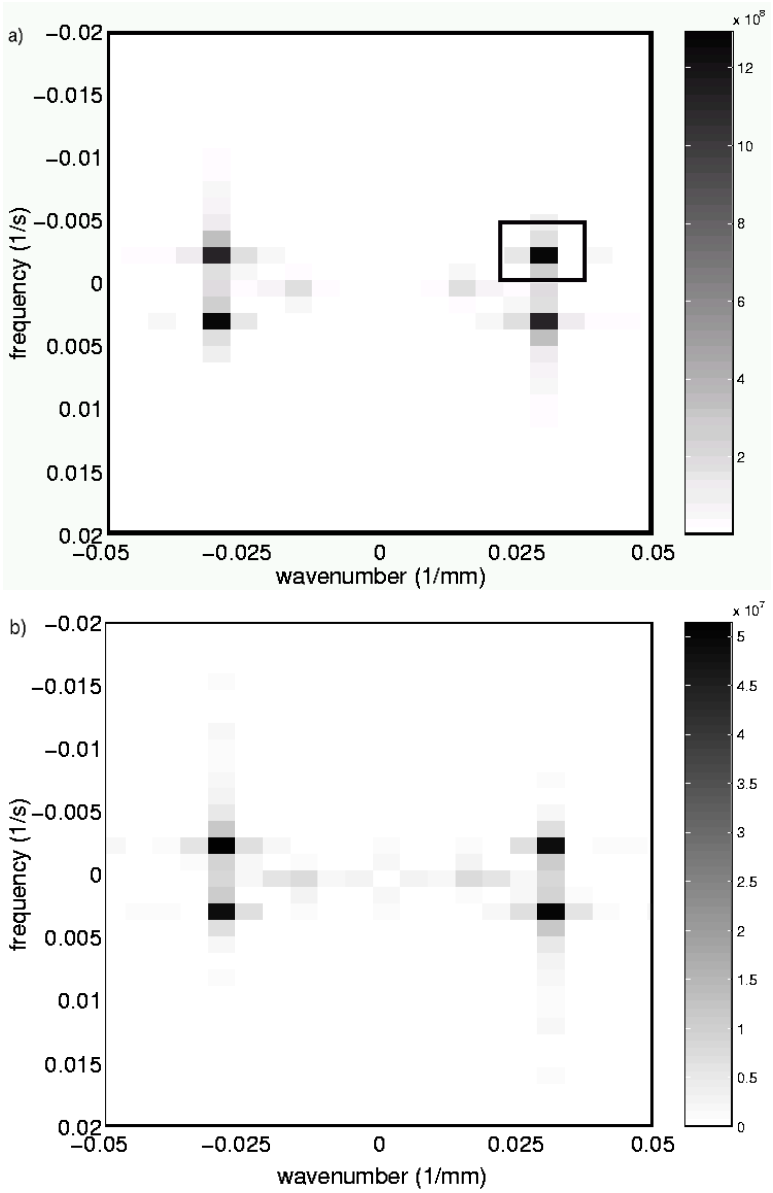

Figure 2.8: a) The power spectrum of the discrete two-dimensional fast-Fourier transform (fft) of the concentration field shown in figure 2.7a). b) The power spectrum of the discrete two-dimensional fft of the dynamic angle of repose field shown in figure 2.7b).

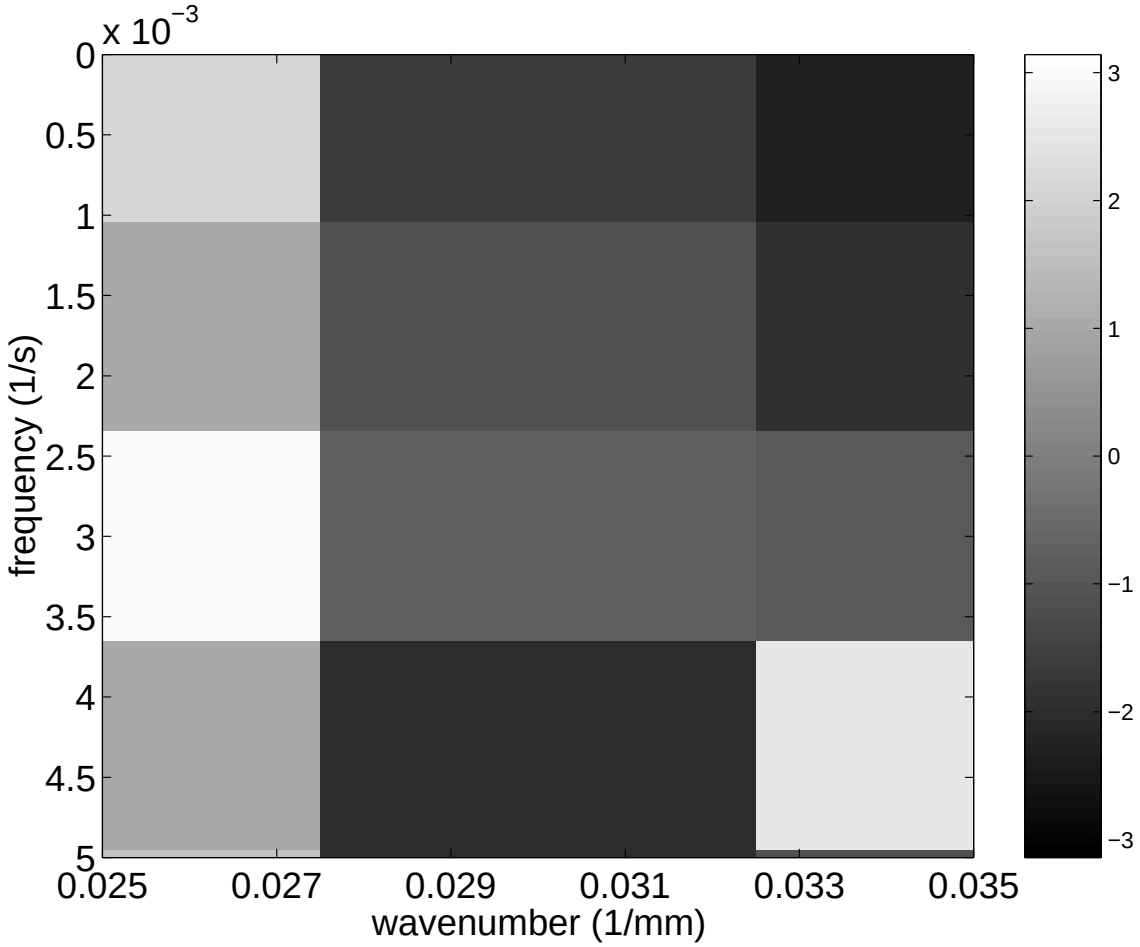

Figure 2.9: The phase angle of the area in the black box of the power spectrum shown in figure 2.8 calculated using Matlab's *angle* function.

In order to compare this data to a physical model [38, 39], we determined the wave speed and phase relationship between the dynamic angle and relative concentration fields. We accomplished this using the two-dimensional fast-Fourier power spectra of the evolving spatio-temporal fields from the space-time diagrams. Examples of two-dimensional discrete Fourier power spectra for the concentration and dynamic angle fields are shown in figures 2.8a and b respectively. First we fit a Gaussian to the upper-left and upper-right peaks in the power spectra. The wavenumber of the peak of the Gaussian gives the wavlength of the travelling wave pattern, the inverse of its wavenumber $(1/k)$. The frequency divided by the wavenumber yields the wave speed of the pattern. Matlab's *angle* function calculates the phase angle of the input discrete fft. This is shown plotted in figure 2.9 for the region corresponding to the boxed area in the power spectrum of the concentration field in figure 2.8a. The phase difference was taken to be the average of the absolute value of the angles located within the full-width half-maximum of the peaks in the power spectrum. We discuss in chapter 3 the implications of this data for the Aranson *et al.* model [38, 39].

2.4 Surface Video Imaging

The pioneering work of Choo *et al.* showed that by capturing video images at regular but short intervals, and essentially stacking them in time, one could observe dynamics of axial segregation that had not been observed before [35, 36]. These dynamics include a travelling wave transient and band merging events. This technique enabled them to measure the relevant length and time scales in the axial segregation process. We used this now standard technique to examine the coupling of the radial core with the relative surface concentration of grains, and the mixing of differently coloured but otherwise identical grains.

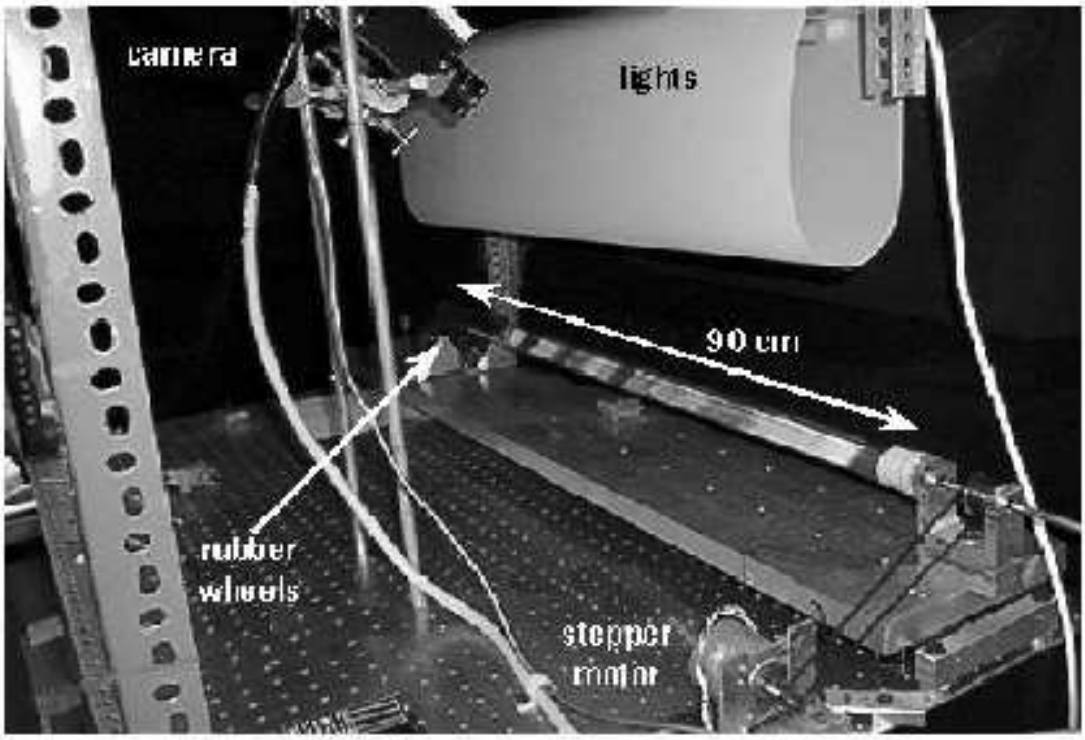

Figure 2.10: An image of the experimental apparatus used to investigate surface axial segregation. The drum is lit from above and the lights are covered by a Mylar sheet which acts as a light diffuser. The camera and stepper motor are computer controlled.

An image of the surface video imaging apparatus is shown in figure 2.10. A high speed CCD camera was mounted so that it viewed the grains perpendicular to the flowing granular surface and parallel to the drum. Typically this camera imaged a 20 cm portion of the drum, located at the midpoint of the drum. The overhead lights consisted of six 60 W incandescent light bulbs mounted above and parallel to the drum. The lights were covered in Mylar to reduce the reflected glare on the drum. The entire apparatus was enclosed in a black tent to isolate the experiment from variable background lighting. The controlling software was written in C and implemented on a computer with the QNX operating system by Z. S. Khan and W. A. Tokaruk. This software turned on the camera, rotated the drum at the input frequency, and controlled image acquisition. The images were taken at input intervals, typically five images per drum rotation, and were time stamped for the purposes of data analysis.

2.4.1 Data Analysis of Surface Video Images

Figure 2.11 shows a typical image taken of the rotating drum. The region of interest is highlighted by a grey box in the image. The format of the digital image is 8-bit black and white TIFF, the pixel intensity ranging from 0 (pure black) to 255 (pure white). Using Matlab's image processing software, the time-stamped digital images were input and converted to double format matrices. The region of interest was then subtracted from each image. Typically the length of this region was 20 cm located at the midsection of the drum. Longer regions of the drum were not generally examined due to the small diameter of the drum (2.85 cm); in order to capture more length the number of pixels spanning the width of the drum would have had to be descreased, and axial band dynamics would then be partially lost.

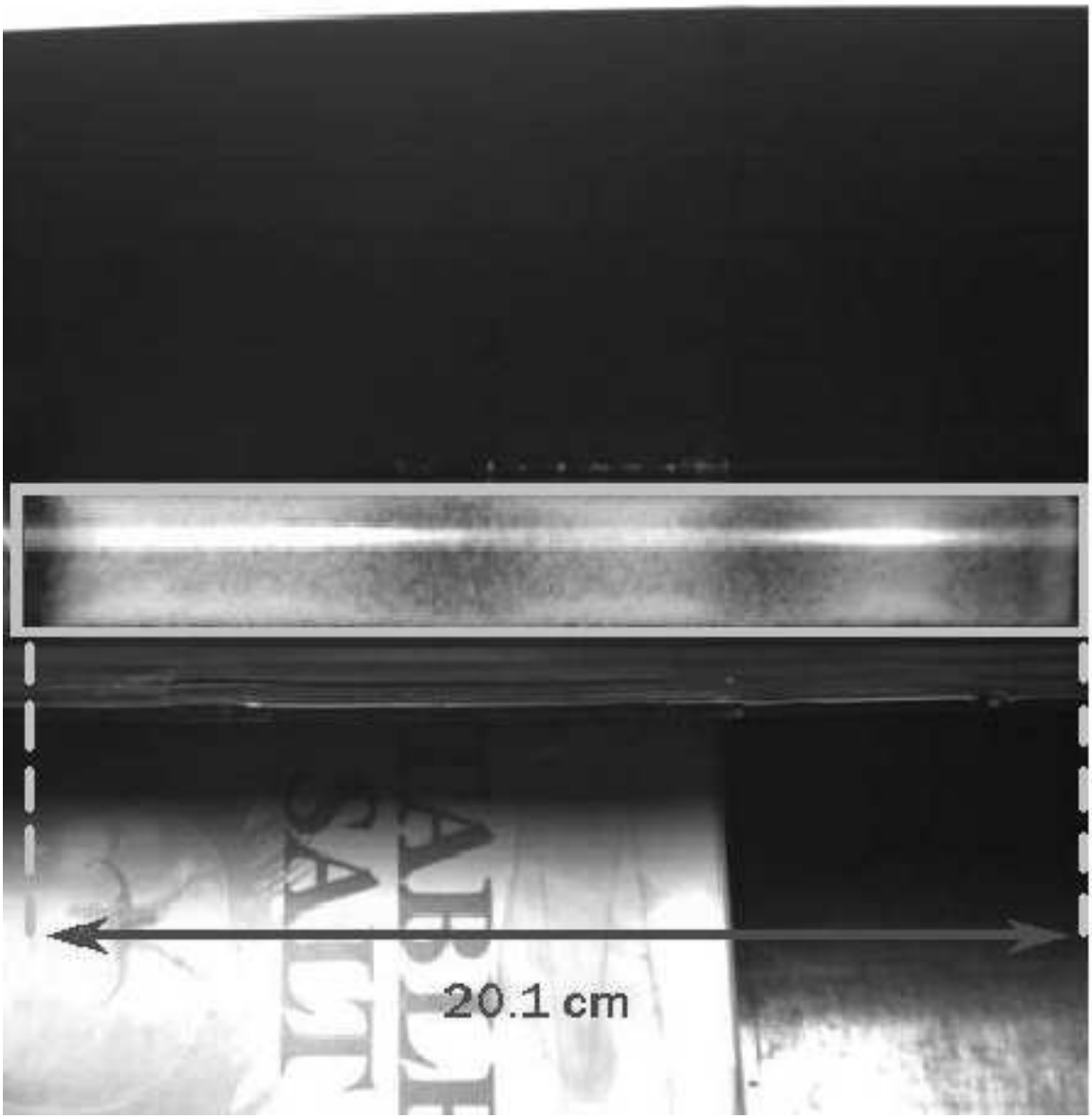

Figure 2.11: An image of the rotating drum containing a mixture undergoing axial segregation lit from above. The region of interest for image processing as described in the text is shown in a grey box

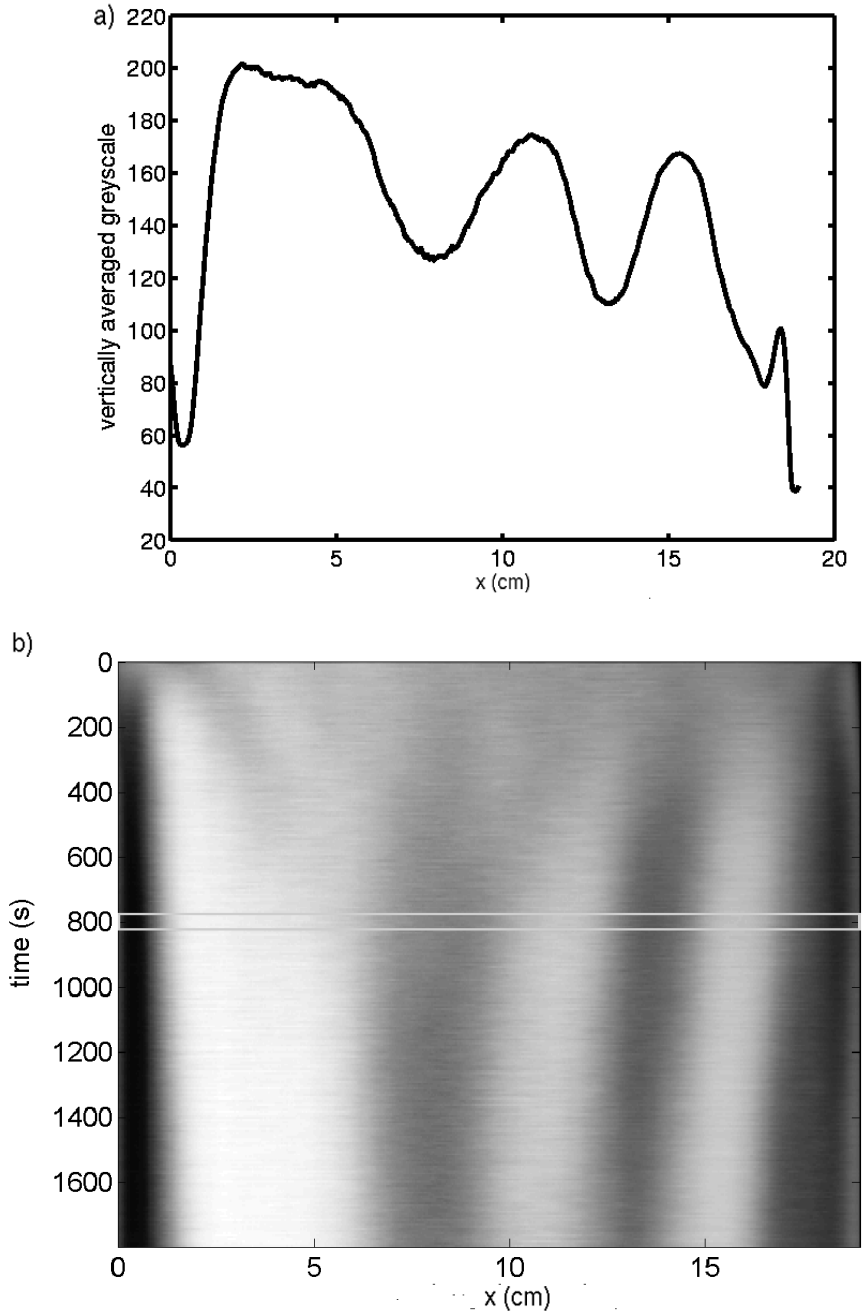

Figure 2.12: a) Vertically averaged greyscale values of an image of the rotating drum taken of the region of interest shown in figure 2.11. b) A space-time diagram constructed from vertically averaged greyscale values such as the one shown in (a). The region corresponding to (a) is enclosed in a grey box.

The digital images were taken at a rate of five per drum revolution, and averaged to produce a view of the drum at each revolution. Then the vertical greyscale average was determined by averaging row components for each column in the matrix (columns represent axial position). Figure 2.12a shows the vertical greyscale average of five images averaged at the drum revolution corresponding to figure 2.11. Averaging is performed over the full vertical extent of the drum because if the band is slightly wider at the top of the flowing layer than the bottom, the vertical average captures this information, whereas a horizontal line of pixels at some arbitrarily chosen location on the flowing granular surface does not. Due to the sharp colour contrast of the grains, the concentration of large to small grains was taken to be linearly proportional to the greyscale values [35, 36].

The average greyscale values, as shown in figure 2.12a were combined to create an m by n matrix. The m dimension refers to the number of averaged times taken; the five images per drum revolution were averaged to produce a mean view of the drum per revolution, and the five times stamped on these pictures were then averaged to determine the mean time. The n dimension refers to the axial position of each pixel along the drums axis. This matrix, when displayed as a black and white image, is a space-time diagram of the grain dynamics. The pixel colour corresponds to its value, and the pixel position corresponds to its time and position along the drum axis. Typically colour bars are not displayed for these space-time diagrams; the darkest regions correspond to regions of small black grains and the lightest regions correspond to regions of large white grains. The greyscale space-time values were used for more quantitative analysis, such as Fourier methods [35, 36]. An example of a space-time diagram is shown in figure 2.12b. The region of this diagram corresponding to the average greyscale values shown in figure 2.12a are at the center of the grey box. A detailed description of the Fourier methods used to determine the growth rate of the axial band pattern is given in section 2.5.1.

2.5 Bulk Visualization Technique

Many important and outstanding questions concern the role of the radial core in the axial segregation process. How are the radial and axial segregation modes related? Can the radial mode be taken to be the driving force of axial banding [43]? In an effort to elucidate answers to these questions, as well as questions about the radial core width and axial band coupling, a new bulk visualization technique was developed.

Since salt grains are translucent and sand grains are opaque, if a bright light is shone behind the rotating drum, one can observe the shadow of the radial core cast on the front face of the flowing granular surface. This was the basic idea behind the backlighting technique. The apparatus used for these backlit experiments is essentially identical to the one mentioned in section 2.4 with three important additions. A light fixture with bright 90 W incandescent light bulbs was mounted behind and parallel to the drum, and a mirror was placed beneath the drum at an angle in order to reflect light through the widest volume of grains in the drum. Finally, a light shield was mounted parallel to and behind the contact line between the grains and the back wall at the drum, to prevent the flooding of the CCD camera with the bright light, which would obscure the images. An image of this apparatus is presented in figure 2.13. Though this method only provides two-dimensional data, it poses an advantage over slower MRI methods since it is very fast. Five images per drum revolution were obtained and averaged to determine the evolution of the radial core. This method was combined with surface video imaging for some experiments, with the computer controlling both sets of lights via a triac-based switch developed by S. W. Morris. By sending a 5 V signal to the switch through a digital-analog-signal card, the lights were turned on and off, switching between the overhead lights described in section 2.4, and the back lights described here.

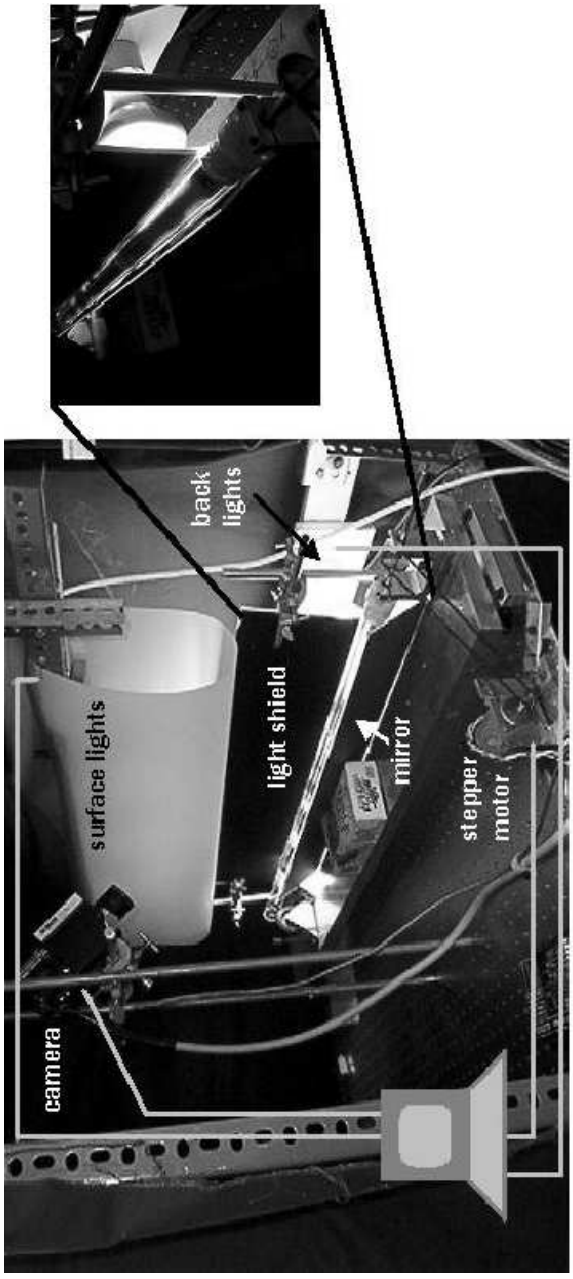

Figure 2.13: An image of the experimental apparatus used for the back-lit bulk visualization technique. The camera, surface lights, back-lights and stepper motor are computer controlled. A detailed image of the back-lights, light shield, drum and mirror are shown to the right, illustrating this methods' effectiveness in investigating subsurface phenomena.

A similar experimental technique has been used by Fiedor *et al.* [37]. In that work a bright light shone behind the drum filled with large transparent and small black glass spheres. The drum was filled with water which acts as an index-matching fluid to the large transparent spheres, so only the smaller black spheres comprising the radial core of this slurry mixture are visible. The techniques described here is better for the analysis of dry segregation because it eliminates the complicated interaction of the grains with the index-matching fluid and allows dry segregation to be studied. This technique was also used to examine the propagation of the radial core in mixtures containing glass spheres, as described in chapter 4.

2.5.1 Analysis of Bulk-Visualized Data

Figure 2.14a shows a typical image of the radial core shadow. This image was then subtracted from a background image of the drum filled only with large grains, that is, no sand grains present. This reduced noise effects on the data images, such as uneven lighting effects. Using Matlab's edge detection software package, the radial core height $h(x,t)$ was measured from background-subtracted data images as shown in figure 2.14b and expressed as a fraction of the full height of the material in the drum.

If we assume that any cross section of the three-dimensional structure of the radial core perpendicular to the axis of the drum is a fraction of a circular disk, then h^2, the fraction of the contents of the drum occupied by the radial core, is proportional to the concentration $C(x,t)$ of small grains contained in the radial core at each axial position x. We justify this assumption by noting that Ristow *et al.* [40] state that for their experiments in a half-full drum filled with small particles, the radial core occupies a half-circle in 2D axial cross sections of the drum. They further assume that for lower concentrations of small particles in the radial core, the small particles occupy regions in the shape of half-circles in axial cross-sections of the drum, albeit with a smaller radii, in order to calculate the concentration of small grains in the radial core. MRI images

of axial cross-sections of radial cores justify Ristow *et al.*'s assumption that the radial core in a half-full drum has a cross-sectional shape of a half circle [20]. Since we conduct experiments in an approximately 30 % full drum, we follow Ristow *et al.*'s argument and assume that the radial core occupies a 30 % fraction of a circle in axial cross-section of varying radius depending on the quantity of small grains within the radial core. We can then relate the concentration of small grains occupying the radial core with the fraction of the radial core h that we have measured, when we consider that h is the chord length of a circular segment, as shown schematically in figure 2.14c. The area of a 30 % fraction of a circular disk of radius r is $area = 0.3\pi r^2$. The chord length $h = 2r \sin\left(\frac{\theta}{2}\right)$ where θ is the central angle made by the chord. We then express the area of this circular segment to the chord length via $area = 0.3\pi h^2/4sin^2\left(\frac{\theta}{2}\right)$, which gives $C(x,t) \propto h^2$.

Figure 2.15a shows the time evolution of the x integral of h, which increases with time. Figure 2.15b shows that the x integral of h^2 is constant in time, as it should be for a conserved quantity. This supports our assumption about the core shape and demonstrates that h^2 can be used as a local concentration measure. The error in measurement of h^2 corresponds to an error in h of ± 2 pixels.

Our concentration profiles of small grains in the radial core then consisted of the values of h^2 for each spatial position and time for the course of the experiment. One such concentration profile is shown in figure 2.15c. These values of $h(x,t)^2$ were also used to construct space-time diagrams of radial core dynamics by creating a two dimensional image.

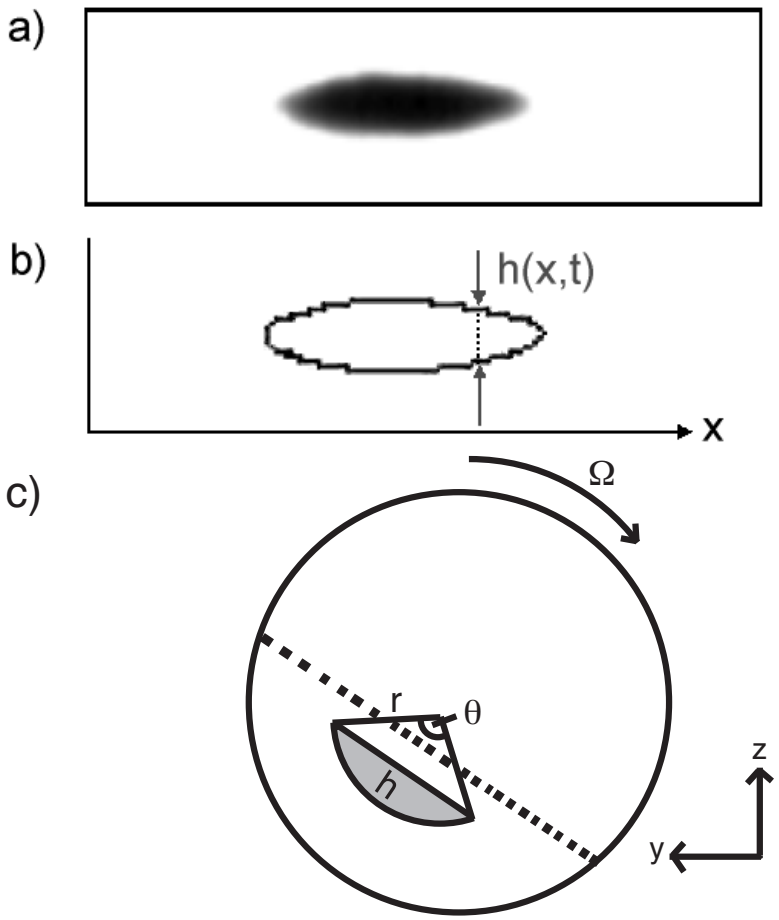

Figure 2.14: a) An example of data collected using the bulk visualization technique. This is a 1.5 mm presegregated pulse of black hobby sand in the size range of 177-212 μm spreading into surrounding salt grains in the size range of 300-420 μm. The drum rotation rate was 0.3 rev/s. b) An example of edge detection used on the image shown in (a). The fraction of the image occupying the radial core is denoted by $h(x,t)$ and is calculated for each axial position for each image taken with the time recorded on the image. c) An illustration of the radial core forming a circular segment shaded in grey, with a chord length h, making a central angle θ in a disk of radius r.

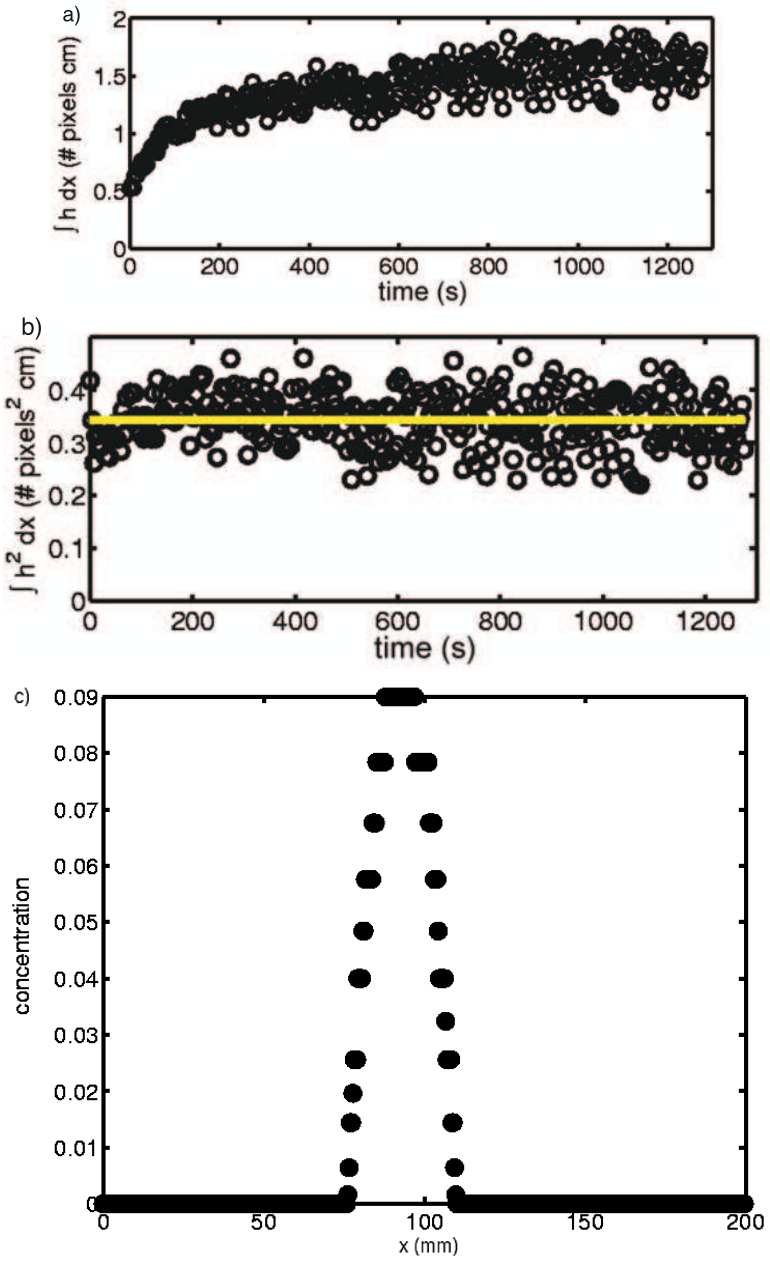

Figure 2.15: a) The x integral of h is not constant in time and is thus not proportional to the volume of small grains contained within the radial core. b) The integral of h^2 is constant in time and is assumed to be proportional to the desired concentration. c) A concentration profile corresponding to the data shown in figure 2.14a, it was calculated from h^2 at each axial position in the image.

Another example of data obtained with the backlit bulk visualization technique is shown in figure 2.16a. This image was taken of a mixture undergoing axial segregation in a mixture of 1/3 black hobby sand grains in the size range $177 - 212\ \mu m$ and 2/3 white table salt with sizes in the range $300 - 420\ \mu m$ in a 5.6 cm diameter drum. Figure 2.16b shows the fraction of the radial core squared or concentration of small grains measured at each axial position in figure 2.16a. A space-time diagram was constructed by creating an m by n matrix of these $h(x,t)^2$ values where the m-dimension corresponds to time and the n-dimension corresponds to the axial position x. Figure 2.16c shows a space-time diagram for the run from which image 2.16a was obtained.

In addition, for some experiments, growth rate measurements of axial bumps on the radial core were required [35, 36]. The growth rate was determined by taking a one-dimensional Fast Fourier Transform at each time step of axial pixels obtained at that time step and finding the largest bin which corresponds to the largest amplitude mode. Figure 2.17a shows a three dimensional plot for each time step of the 1D FFT for the space-time diagram shown in figure 2.16b. Then the logarithm of the power in the largest bin was plotted against time, and the early-time exponential growth was fit to a straight line to determine the growth rate as shown in Figure 2.17b.

In this chapter we described the experimental techniques used to produce the results we describe in the remainder of this thesis. Among the techniques common to research in this area are grain preparation and surface visualization methods, and digital image analysis. Our own original contributions to the methodology consist of the scanning profilometer and backlighting technique for bulk visualization. The scanning profilometer was used to establish the results discussed in chapter 3, which deals with our traveling wave experiments; the bulk visualization technique was instrumental in obtaining the results discussed in chapters 3 and 4; the latter outlines our investigation of subdiffusion in the axial transport of grains.

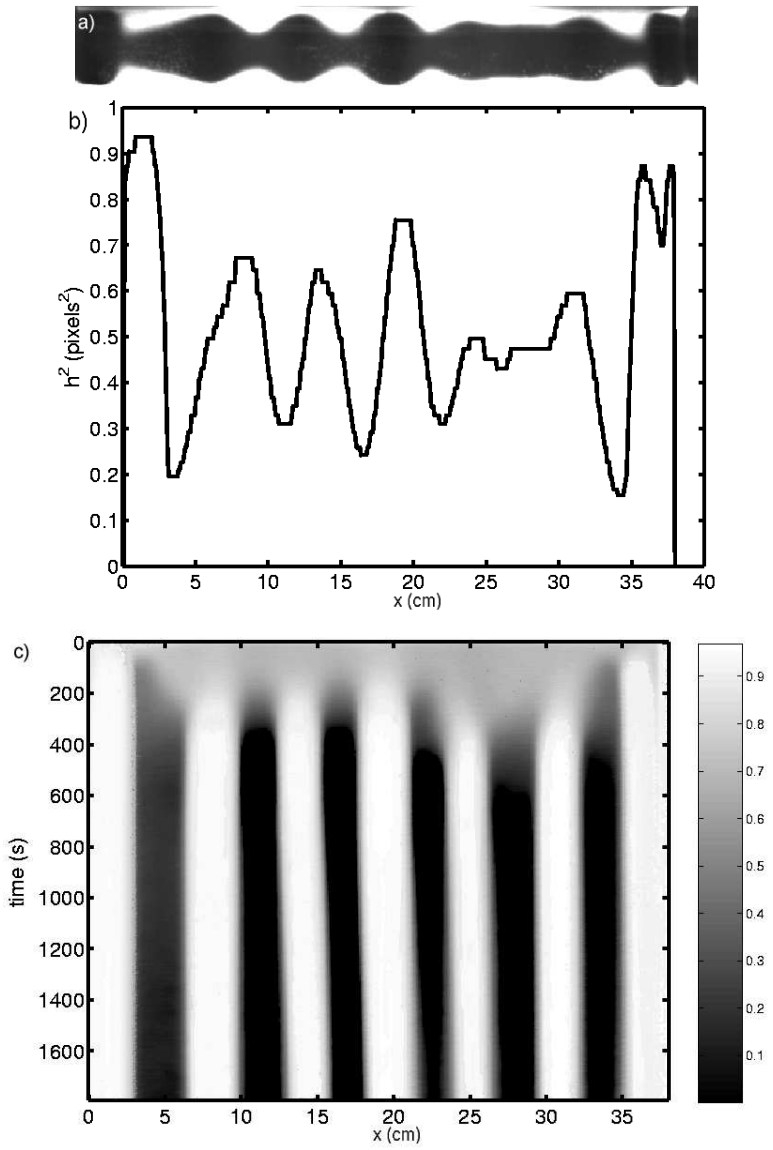

Figure 2.16: a) An example of data obtained using the bulk visualization technique described in the text. The mixture used in this run is composed of 1/3 sand in the size range 177-212 μm and 2/3 salt in the size range 300-420 μm with randomly mixed initial conditions. The drum rotation rate was 0.3 rev/s. This image was taken at t = 180 s. b) A concentration profile calculated from the radial core fraction squared $h(x,t)^2$ corresponding to the image in (a). c) A space-time diagram constructed from concentration profiles such as the one in (b) for the data run corresponding to (a).

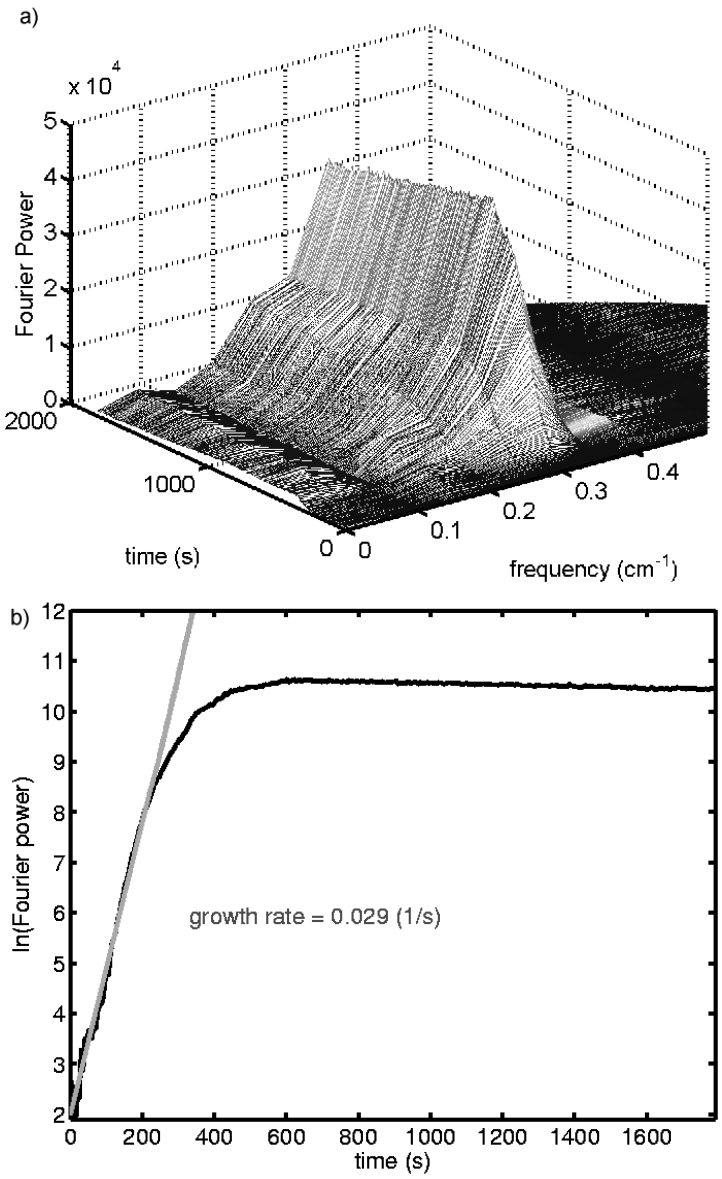

Figure 2.17: a) The power series of the spatial fft stacked in time for the space- time data shown in figure 2.16c). b) An example of the growth rate calculation for the axial segregation pattern shown in 2.16c). The logarithm of the power series for the largest bin in (a) is plotted in time, and early-time exponential growth is fit to a straight line.

Chapter 3

Traveling Waves; Experimental Results and Discussion

In 1997, Choo and co-authors discovered that a traveling wave transient can occur prior to axial band formation in a mixture of sand and salt grains [35, 36]. Using presegregated initial conditions with different wavelengths to study uniform regions of standing waves, they determined that the wave speed depended on wavelength, and that the standing waves ceased to propagate above an initial wavelength of 54 $\pm$ 1 mm. These intially segregated bands remained in a frozen state. With this data Choo *et al.* constructed a dispersion relation for the wave transient in their mixture.

This discovery falsified a detailed continuum model of axial segregation by Zik *et al.* [34], as described below, and prompted Aranson and Tsimring [38] and Aranson, Tsimring and Vinokur [39] to develop a new theory which models both axial segregation and the traveling wave transient. This chapter contains a discussion of both theories, including experimental tests of the predictions of the Aranson *et al.* model, and concludes with an examination of numerical simulations of axial segregation and how they are related to our experiments [30, 66]. We also discuss the observation of traveling wave dynamics in a bidisperse mixture of glass spheres by Fiedor *et al.* [37], and describe a more

recent attempt by Aranson and Tsimring [65] to theoretically model an oscillatory axial segregation transient found in ternary granular mixtures by Newey *et al.* [29].

3.1 An early theoretical model of axial segregation

The first detailed continuum model of axial segregation was proposed by Zik *et al.* [34]. This model was based on the dynamics of a thin mobile layer of particles flowing down the free surface of the grains in the drum; several experimental observations of segregation in mixtures of large glass and small sand grains provided the motivation. It was assumed that segregation is driven by an instability nucleated by concentration fluctuations due to the motion of the grains on or near the free surface, that bulk motion can be ignored, that the shape of the free surface plays a vital role, and that friction is essential to the occurrence of segregation.

The authors [34] elucidate the importance of friction between the different types of small and large grains by observing that the different frictional properties of the grains lead to different dynamic angles of repose. The *dynamic angle of repose* is defined as the angle of the slope of the free surface of grains in the drum as they are flowing continuously. It was also observed by the authors that the free surface often deviates from a flat surface to a more complicated S-shaped profile in experimental systems.

Zik *et al.* suggested that the variations in the dynamic angle of repose of the large and small grains provide the driving mechanism of axial segregation. They reasoned that if there is a local increase in the concentration of one type of particle with a larger angle of repose the local slope of the free surface at that location will be larger; typically the smaller grains have a larger angle of repose [32]. This will lead to a bump near the top of the free surface and a dip near the bottom. Since the particles tend to travel along the steepest path of descent, more particles with larger dynamic angles of repose accumulate in that location. The segregation instability develops from this.

The authors proposed the following continuum model

$$\frac{\partial c}{\partial t} = \frac{C}{\nu_T}(\tan\phi_g - \tan\phi_s)\frac{\partial}{\partial x}c(1-c)\left\langle (1+h_y^2)\frac{h_x}{h_y}\right\rangle \tag{3.1}$$

based on the conservation law for the fractional concentration of glass particles in a mixture of sand and glass particles,

$$c(x,t) = \frac{\nu_g}{\nu_g + \nu_s}$$

where ν_g and ν_s are the number densities of glass and sand respectively.

In the model, x and y are Cartesian coordinates along the axis of the drum and across the cross section of the drum, ϕ_g and ϕ_s are the dynamic angles of repose of glass and sand particles, $h(c,x,y,t)$ is a concentration-dependent function describing the shape of the free surface of the grains flowing in the drum, and $\nu_T = \nu_g + \nu_s$. $C = p_o^3/3\eta g^2$ is a constant related to the effective viscosity of the materials in the flowing layer and gravity, where Zik *et al.* consider the flowing layer to be a fluid with constant viscosity η, p_o is a constant pressure value, and g is the magnitude of the gravitational force. The term in the angled brackets denotes the axial flux of material averaged over the cross section of the drum.

In order to have axial segregation in this model, it is required that $\left\langle (1+h_y^2)\frac{h_x}{h_y}\right\rangle < 0$, in which case equation 3.1 becomes a diffusion equation with a negative diffusion coefficient, and so exhibits the segregation instability. The authors [34] also report that the term in the angled brackets vanishes for a straight free surface profile, $h_y = constant(y)$. This is due to their assumption that h_x changes sign in the middle of the drum, therefore the mixing and demixing processes cancel out. For the experimentally observed S-shaped free surface profile, Zik *et al.* determined that the instability condition, a negative diffusion coefficient is satisfied when the drum is more than 50 % full.

Experiments disagree with the predictions of this model, as axial segregation has been reported to occur in less than half full drums [27, 35, 36]. Furthermore, the report of a traveling wave transient which occurs prior to axial segregation [35, 36] invalidates this

model. Choo *et al.* showed that these waves are sufficiently linear at early times to form superposed standing wave patterns, and that the wave speed of left and right-going traveling waves is constant. This behaviour is unlikely to result from nonlinearity in a one dimensional diffusive PDE model which is first-order in time, as it cannot describe counter-propagating waves which obey superposition [35].

3.2 A model which reproduces the traveling wave transient

In order to account for the oscillatory transient preceding axial segregation found by Choo *et al.* [35, 36], Aranson and Tsimring [38], and Aranson, Tsimring and Vinokur [39], generalized Zik *et al.*'s model [34]. Aranson *et al.*'s assumption was that there is a slow variable involved, in addition to the relative concentration of grains $c = (c_A - c_B)/\langle c \rangle$, and this accounts for the oscillatory band dynamics [38, 39]. Here the grain type c_A has a larger static angle of repose and typically represents the smaller grain size, and the grain type c_B has a smaller static repose angle, and typically represents the larger grain size. The average concentration of particles over the entire length of the drum is represented by $\langle c \rangle = \langle c_A + c_B \rangle$. They conjectured that this slow variable is the dynamic angle of repose ϕ, which in contrast to Equation 3.1 is not slaved to the relative concentration of grains c, but is dynamically independent. Both c and ϕ are functions of the axial coordinate x and time t. The equations of the Aranson *et al.* model are:

$$\frac{\partial c}{\partial t} = \frac{\partial}{\partial x}\left(D\frac{\partial c}{\partial x} - g(c)\frac{\partial \phi}{\partial x} \right) \tag{3.2}$$

$$\frac{\partial \phi}{\partial t} = \alpha\left(\Omega - \phi + f(c)\right) + D_\phi \frac{\partial^2 \phi}{\partial x^2} + \gamma \frac{\partial^2 c}{\partial x^2}. \tag{3.3}$$

The first term on the right hand side of Equation 3.2 describes mixing due to diffusion, and the second term describes the differential flux of particles as a result of gradients in

the dynamic angle of repose. This incorporates Zik *et al.*'s observation that a concentration fluctuation results in a change in the dynamic angle of repose, as described in section 3.1. Aranson *et al.* use $g(c) = G_o(1 - c^2)$ where the constant G_o can be eliminated by rescaling the axial coordinate x by $x \rightarrow x/\sqrt{G_o}$. This term acts as a saturation mechanism for the segregation instability, since when there is a pure grain state, $|c| \rightarrow 1$ and $g(\pm 1) = 0$, so the segregation flux is eliminated.

The constant α in Equation 3.3 establishes the time scale for axial segregation, and is characterized by the ratio of the number of particles flowing within the thin surface layer to the number of particles transported in the bulk flow. For slowly rotating drums, particles are brought to the surface via solid body rotation, which results in $\alpha \sim 1$. The parameter Ω is the angular velocity of the drum, and $f(c)$ is the static angle of repose of the grains which has been reported to be an increasing function of the relative concentration of grains [67]. It has been observed that the angle of repose, as a function of concentration, changes within a small range of angles [21], thus Aranson *et al.* assume that $f(c)$ is linearly dependent upon c, $f(c) = F + f_o c$. The constant F can be eliminated by substituting $\phi \rightarrow \phi - F$.

The first term in Equation 3.3 describes the local dynamics of the dynamic angle of repose ϕ; increasing the angular velocity of the drum increases the dynamic angle, and $-\phi + f(c)$ incorporates the concentration dependence of the dynamic angle of repose. The second term in the equation, $D_\phi \frac{\partial^2 \phi}{\partial x^2}$, describes the relaxation of the angle of repose due to axial diffusion. In order to determine if variations in the dynamic angle were relaxed due to diffusion in the absence of concentration gradients, we placed monodisperse salt grains in the rotating drum, and scooped out a portion of the grains, creating a region with a smaller static angle of repose, since less grains were present in that location. When the drum was rotated, the axial transport of grains quickly filled that region, and the dynamic angle of repose relaxed to a uniform value throughout the drum. The last term in Equation 3.3, $\gamma \frac{\partial^2 c}{\partial x^2}$, represents the lowest order contribution from an inhomogeneous dis-

tribution of the relative concentration of grains which results from the coupling between the bulk flow and axial diffusion. This term is the source of the transient oscillatory dynamics in a two-component or binary mixture of grains. When γ was set to 0 in the simulation code provided by the authors [57], traveling wave dynamics did not occur.

Aranson *et al.* [38, 39] show that linear stability analysis of this model about a homogeneously mixed state, $c = c_o$, $\phi_o = \Omega + f_o c_o$, gives for $g_o f_o > \alpha D$ a long wavelength perturbation which is unstable. If $g_o \gamma > (D_\phi - D)^2/4$ short wavelength perturbations oscillate and decay. The dependency of oscillation frequency on wavenumber was shown to agree quantitatively with experimental values measured by Choo *et al.* [35].

The results obtained by numerical simulations of Equations 3.2 and 3.3 are shown in figures 3.1a and b. The simulation code was provided by the authors [57]. The code was run for a dimensionless presegregated wavelength in the traveling wave regime. Figure 3.1a shows the concentration field exhibiting oscillatory band dynamics, and figure 3.1b shows the corresponding dynamics in the dynamic angle of repose field.

A crucial feature of this model is that these two essentially diffusive fields are coupled in such a way that they oscillate $\pi/2$ radians out of phase during the traveling wave transient. The two order parameters have a conjugate relationship, like position and momentum in a mechanical oscillator. Such a relationship is a generic feature of coupled position-momentum models. It is shown below that the concentration of grains and dynamic angle of repose do not have the required phase relationship and are in fact slaved, falsifying this model [28]. When we assume that the dynamic angle of repose ϕ is slaved to the concentration c in the above model via a linear relationship, $\phi = Ac + B$ where A and B are constants, we obtained a steady-state solution from equations 3.2 and 3.3, where the concentration field does not evolve in time.

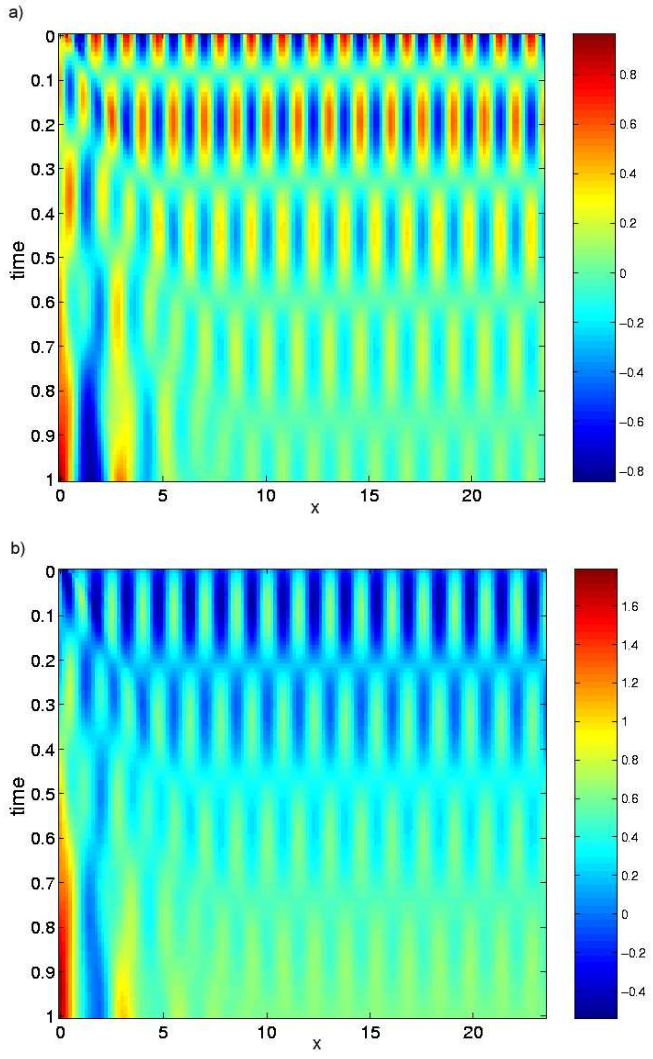

Figure 3.1: a) A simulated run of the travelling wave transient using the simulation code from Refs. [38, 39]. In this graph, the space and time dimensions are calculated in dimensionless units. Here the concentration values range from -1 (pure large grains) to 1 (pure small grains). b) The simulated dynamic angle dynamic angle field corresponding to a). The units of dynamic angle are presented in radians. For this run, presegregated initial conditions were used. The decaying oscillations in the concentration and dynamic angle fields are out of phase during the oscillatory transient, and are in phase for axially segregated bands, such as the one which has formed near the lower left corner of the space-time diagram.

3.3 Experimental measurements of dynamic angle and concentration.

The scanning profilometer device described in chapter 2 was used to simultaneously measure the dynamic angle and surface concentration of grains in a rotating drum. In order to study uniform regions of standing waves; presegregated initial conditions were used. Figure 3.2 shows the results for an initial wavelength of 30 mm. Decaying left and right travelling waves pass through each other to form a standing wave until they are absorbed into nearby axial bands. Figure 3.2a shows the relative concentration measurements and figure 3.2b shows the corresponding dynamic angles. Traveling waves do not occur for wavelengths above a cut-off, which was previously reported to be 54 ± 1 mm [35, 36]. Above the cut- off wavelength, presegregated bands were reported to remain frozen at their initial position. We have studied the relationship between the concentration and dynamic angle in numerous runs using presegregated wavelengths above and below the cut-off as well as with random initial conditions.

To verify that we have experimentally reproduced Choo *et al.*'s original result, and to check that these mixtures are devoid of any systematic errors in their preparation which might produce similar wave transients but not identical to the ones described by Choo *et al.* [35, 36], we plotted the wave speed dependence on wavelength for both the concentration and dynamic angle fields, shown in figure 3.3a. The wave speeds were calculated by fitting a Gaussian to the power spectrum of the 2D FFT of the space-time diagrams. The wave number divided by the frequency of the peak yields the wave speed, and the error in the wave number and the frequency were taken as the half-width of the Gaussian at half-maximum. This data closely resembles Choo's original data presented in figure 2 of Reference [35]. Figure 3.3b shows the difference of the wave speeds of concentration and dynamic angle as a function of wavelength. This figure shows that the wave speed data for both fields are experimentally indistinguishable.

Examining figures 3.2a and b, it is clear that the phase difference between the concentration and dynamic angle of repose fields must be close to a multiple of π radians. This is most apparent from the temporal nodes, which occur at nearly the same time for both fields. In order to determine the phase difference between the two fields, we analyzed the two-dimensional Fourier spectra of their space-time evolution. The phase difference for each peak was taken to be the average of the absolute value of the angles located within the full-width half-maximum of the peaks in the power spectrum. The error for each run was taken as the sum of the squares of the standard deviation of the absolute value of the angles located within the full-width half-maximum and the deviation between the values of each peak. The phase difference is shown in figure 3.4a, as a function of the presegregated wavelength. In all cases, the standing waves are π out of phase, within the uncertainties, including those above the cut-off wavelength. Note that our anti correlation (the phase difference of π) is merely a consequence of our conventions about concentration, that is, it is the same as measuring a phase difference of 0. Thus, high concentration of the larger, white salt component is directly correlated with small dynamic angles of repose, while black sand concentration is correlated with large dynamic angles. This is the case both during the oscillatory transient and for the fully segregated bands.

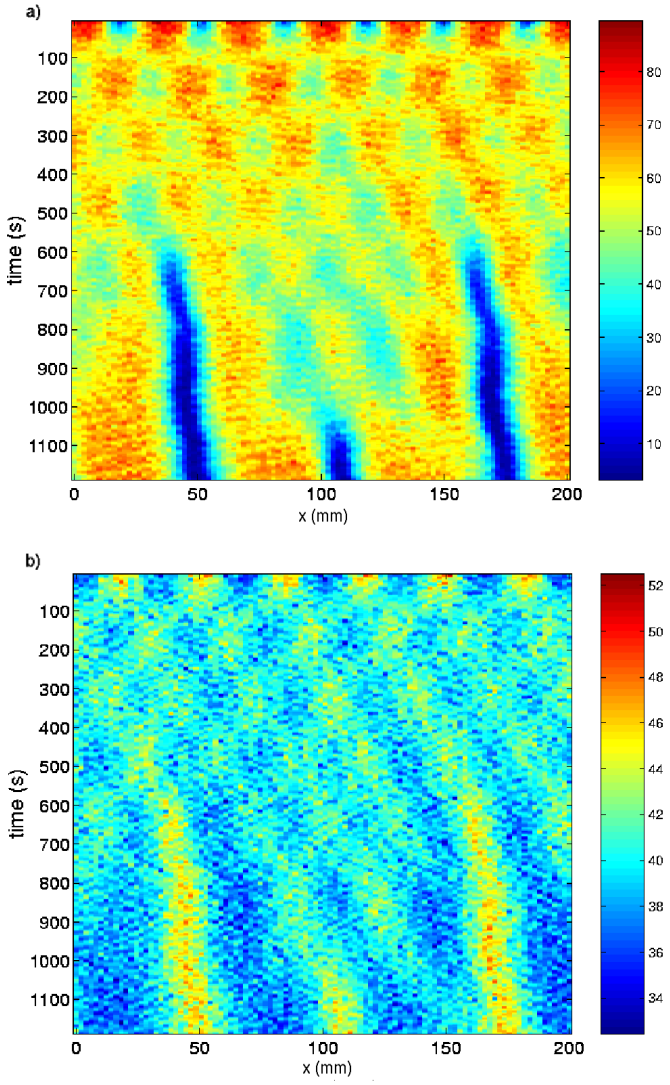

Figure 3.2: (a) Space-time plot of relative concentration for a mixture with a 30 mm presegregated wavelength initial condition. (b) The corresponding space-time plot of dynamic angle of repose. The maximum amplitude of the standing wave in concentration corresponds to the minimum amplitude of the standing wave in the dynamic angle, and vice versa, thus the two fields are π out of phase throughout the oscillatory transient. It is also apparent that the saturated axial bands in both fields maintain this phase relationship.

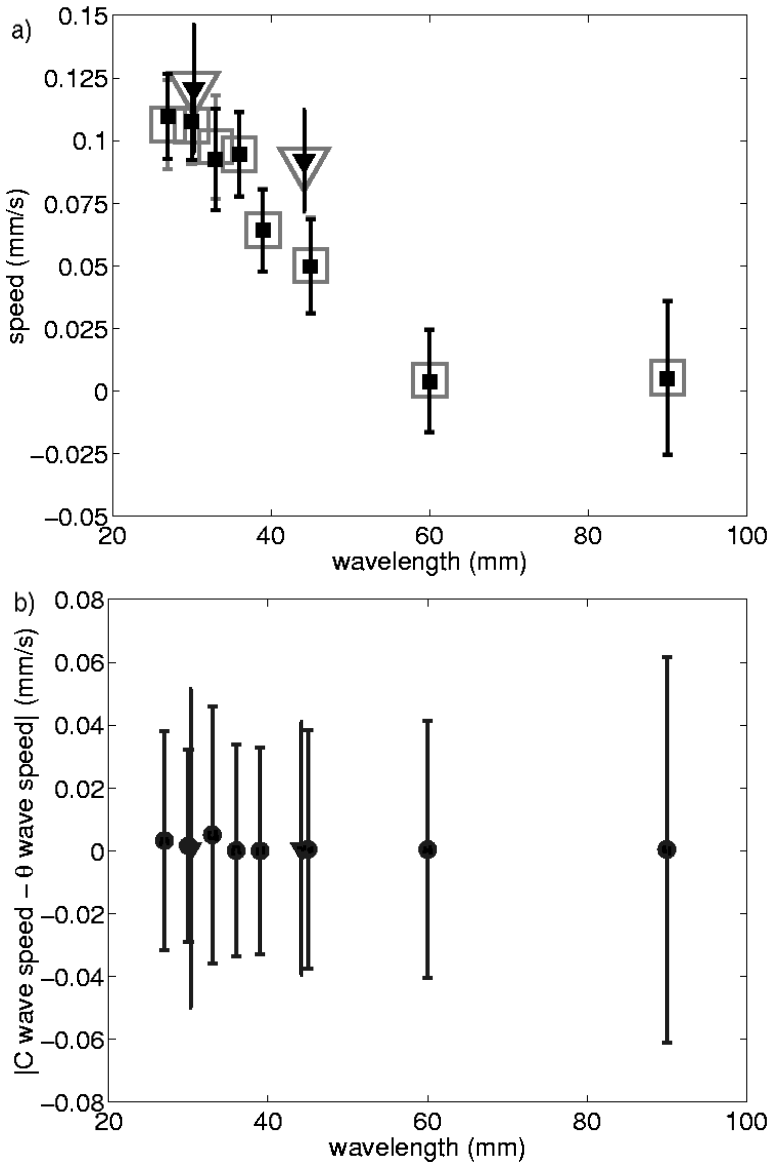

Figure 3.3: a) Velocity dependence of wavelength for the concentration (small solid symbols) and dynamic angle (large open symbols) for mixtures with presegregated initial conditions (squares) and randomly mixed initial conditions (triangles). b) The difference of wave speeds for dynamic angle and concentration as a function of wavelength for mixtures with presegregated intial conditions (circles) and random initial conditions (triangles).

These results dramatically contradict the predictions of theory [38, 39]. In order to compare them directly, we ran the full nonlinear simulations described in [38, 39, 57] for presegregated initial conditions. Figures 3.1a and b shown in section 3.2 are an example of these simulated runs, which are output in the same format as the experimental data. We analyzed these results using the same procedure as for the actual data. Figure 3.4b shows the absolute value of the phase difference for the simulated runs; below the cut-off the phase difference is $\pi/2$, and the two fields are out of phase as one expects for conjugate order parameters. For initial wavelengths above the cut-off, zero phase difference is found. This clear contradiction with experiment demonstrates that the dynamic angle of repose is not the order parameter conjugate to the surface concentration. Since no other superficial feature appeared likely to be an independently evolving slow field, we turned our attention to subsurface phenomena.

3.4 Subsurface phenomena

The radially segregated core, which is ignored in continuum models [34, 38, 39], has long been suspected of being involved with the mechanism of axial segregation. Observations using MRI imaging [20, 21] suggest that axial bands begin as subsurface bumps on the core which only become visible when they break the surface. Thus, a possible candidate for the second order parameter would be the local thickness of the core. In this view, the waves are caused by the periodic exchange of material between the surface and the core. We know that such a core is present in our sand and salt mixtures from excavating the segregated mixture after the experiments, and from observations through a window forming the end of the drum.

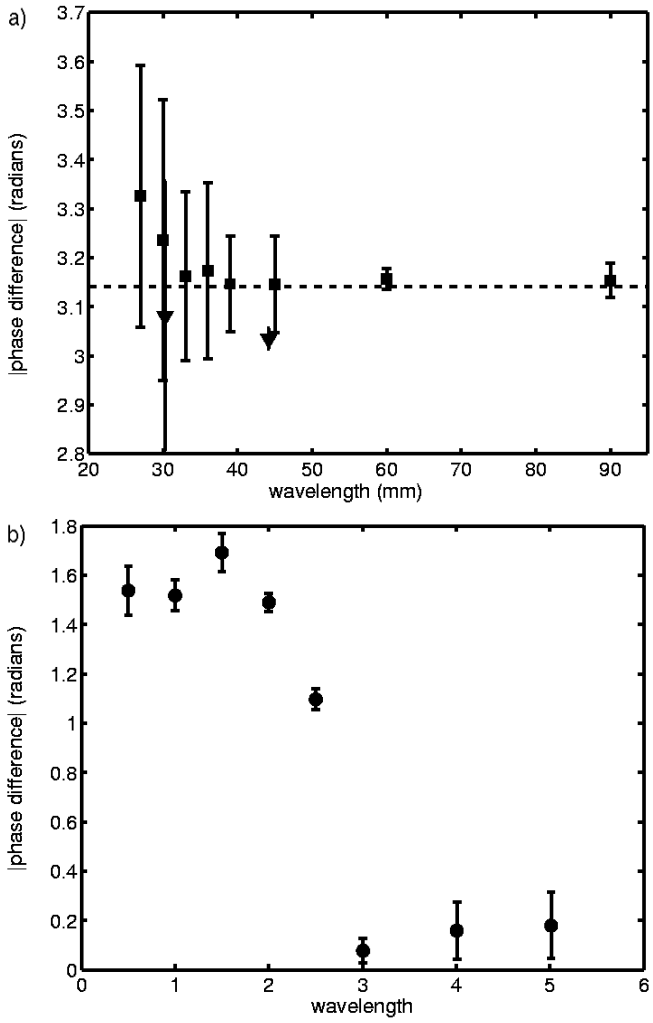

Figure 3.4: a) The absolute value of the phase difference between the experimentally measured concentration and the dynamic angle of repose fields as a function of wavelength for presegregated initial conditions (squares) and random initial conditions (triangles). The dashed line serves as a visual aid, demarcating the value of π radians. The data indicates that the two fields have a constant phase difference of π radians. b) The absolute value of the phase difference between the concentration field and dynamic angle of repose as a function of wavelength for the theoretical simulation used in Refs. [38, 39]. The simulated wavelength values are dimensionless units. The phase relationship between these two fields as predicted by the theory is in direct disagreement with the experimental values shown above.

In order to quantitatively investigate the role of the radial core, we developed the bulk visualization technique as described in chapter 2. Since the salt grains are translucent and sand grains are opaque, we found that positioning a bright light source behind the rotating drum casts a shadow of the radial core on the front face of the mixture. The shadow is in effect a two dimensional projection of the core. No index-matching interstitial fluid is required [37]. By alternately illuminating the drum from above and behind, we collected images of both the surface concentration and the projected core as a function of time using a stationary camera.

Figures 3.5a-i show the actual core projections at different times through the transient. From these images it is apparent that the transient is a result of an oscillatory radial core instability, where the thickness of the core oscillates between the axial bands. Using edge detection, the radial width of the shadow of the core was measured and expressed as a fraction of the full width of the material in the drum. Figure 3.6 shows the space-time evolution of a mixture with a 30 mm presegregated initial wavelength. The oscillatory transient can be clearly seen in both the surface concentration and the core width. We can see from figure 3.6 that, as in the case of the dynamic angle of repose, the width of the radial core and the surface concentration are not $\pi/2$ out of phase; they are oscillating in phase with one another. Thus, a simple order parameter based on the width of the core also fails to satisfy the requirements of an order parameter conjugate to the surface concentration.

Another possible mechanism of the traveling wave transient is static charging of grains due to frictional contact with the drum walls or inter-grain frictional charging. It has been observed by others that a variety of wave patterns are found to form in thin layers of sand rotating in a glass drum at a constant rotation rate. In these experiments, the sand coating the drum forms a standing wave pattern, where the peak of the waves form cusps [50]. The coating of the grains was likely due to electrostatic forces and the grains rearranged themselves into spatial patterns in response to forces exerted between

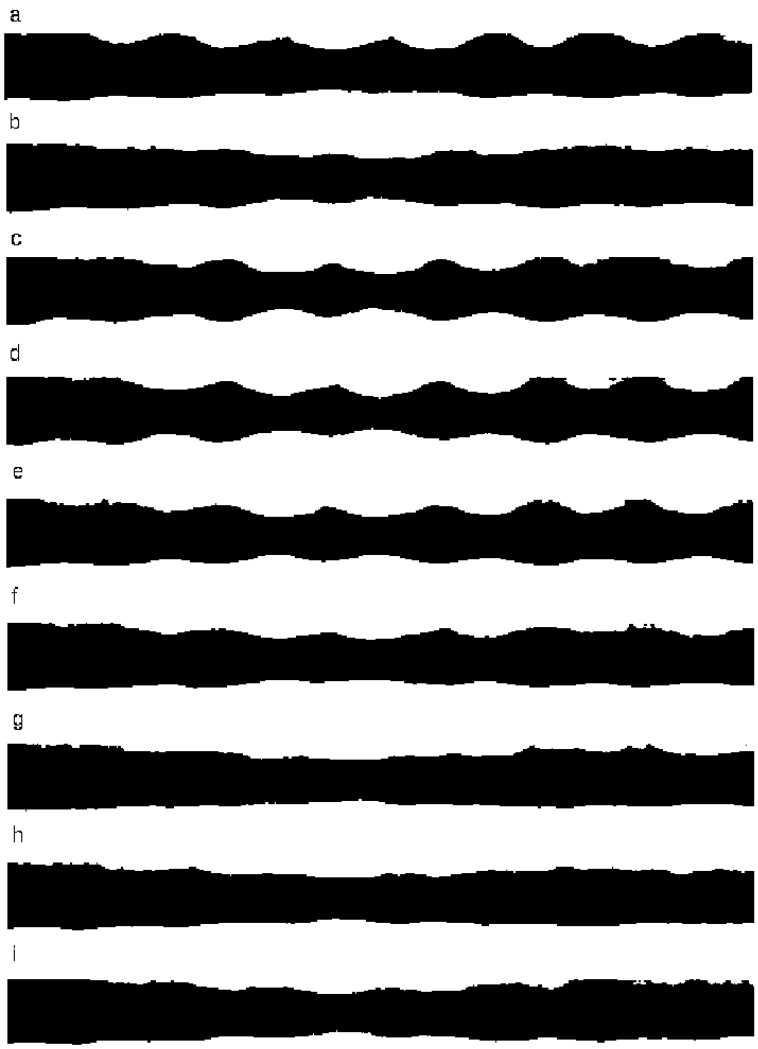

Figure 3.5: Axial projections of the radial core at: a) 66 seconds, b) 88 seconds, c) 111 seconds, d) 133 seconds, e) 156 seconds, f) 178 seconds, g) 201 seconds, h) 223 seconds, and i) 246 seconds. For this run, the drum was approximately 30 % full, with a 3.0 cm presegregated initial wavelength. The drum rotation rate was 0.76 rev/s. Here we can see that the transient results from an oscillatory radial core instability.

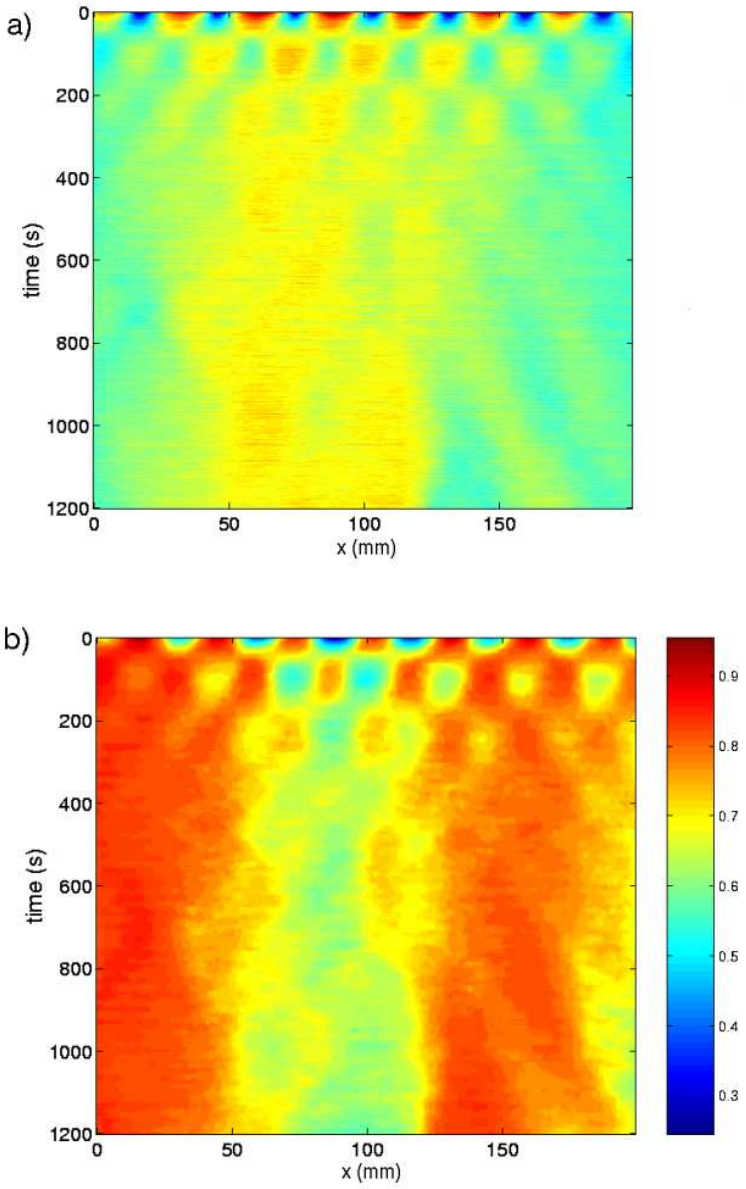

Figure 3.6: (a) Space-time plot of greyscale surface measurements for a mixture with a 30 mm presegregated wavelength initial condition. (b) The corresponding space-time plot of the fraction of radial core from axial projections of the radial core. The maximum amplitude of the surface measurements corresponds to the minimum amplitude of the fraction of radial core, and vice versa, thus the two fields are π out of phase throughout the oscillatory transient.

neighbouring grains [51]. Note that in our own experiments static was controlled, as described in chapter 2.

In order to test the possibility of static charging forming the second field in the Aranson *et al.* model of the traveling wave transient, we performed a number of stopping experiments in which the drum was halted and then restarted after a variable delay time. The delay ranged from a few seconds to over an hour and in all cases was sufficiently long that all grain motion ceased. Figure 3.7 shows space-time diagrams from stopping experiments, the location of the thick black line on the space-time diagram shows when the experiments were stopped and restarted. Figure 3.7a shows data from a run that was stopped for five seconds, figure 3.7b was from a run that was stopped for one minute, and figure 3.7c was from a run that was stopped for one hour. We observed that some of the decaying oscillations continued after any delay, even when the drum was stopped at a temporal node line. These oscillations continue to the left and right of axial bands, in all three of the cases studied. This suggests that the memory of the pattern does not reside in static electric charge effects, which we would expect to diffuse away with time. In addition, it is not clear how simple static charge effects due to inter-grain friction would account for oscillatory traveling-wave transients in a mixture of glass spheres of two different sizes [37]. It is possible that inter-grain friction could result in an exchange of electrons in a mixture of sand and salt, but this is unlikely to occur in a mixture of spheres of the same material. Nor is it obvious how static charge effects between the grains and the drum walls would result in an oscillatory radial core instability, where the radial core is buried below the flowing surface layer. The experiments described above appear to prove that the memory of the oscillatory instability resides in the three dimensional configuration of the grains, not in momentum or charge effects.

3.5 Simulation results in the literature

Parallel to the experimental and theoretical studies of the dynamics of axial segregation, molecular dynamics simulations have also been performed by Rapaport [66] and Taberlet *et al.* [30]. These simulations allow researchers to explore the role of material parameters by modeling the force laws for each grain interaction, and the interactions between the grains and the walls of the drum. Some of the parameters that are explored in these studies are grain roughness and cylinder roughness; these parameters are more difficult to explore experimentally than in a simulated environment. Below we discuss their results; for details about the implementation the interested reader can see the cited publications.

In one molecular dynamics study, Rapaport [66] performed a systematic study of the role of inter-particle and particle-wall friction separately. It was found that if the large particle and cylinder wall friction coefficient was greater than the smaller particle and cylinder wall friction coefficient, axial segregation always occurs regardless of the ratio of the large and small inter-particle friction coefficients. It was also found that if the large and small grain particle-wall friction coefficients are equal, axial segregation occurs if the large grains have a higher inter-particle friction coefficient than the smaller grains.

This simulation study also revealed the presence of randomly oscillating segregated bands along the axis of the drum, however this was attributed to the periodic boundary conditions of those drums lacking longitudinal stability. In addition, views of the small grains and large grains alone in the drum revealed that a radial core of the larger grains was present when axial segregation occurred. This does not correspond to experimental observations, where the radial core is composed of small grains [20, 21, 28].

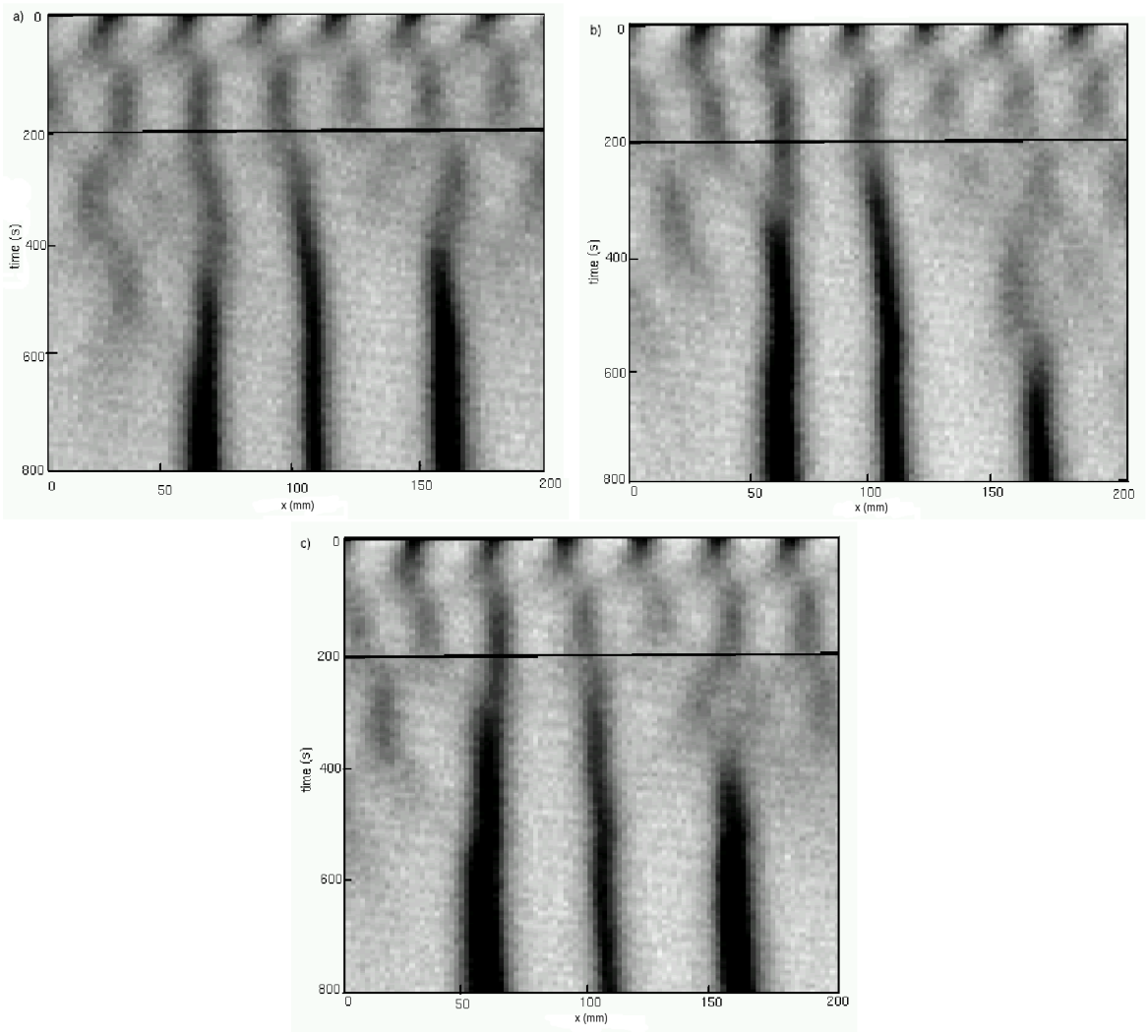

Figure 3.7: Space-time diagrams of the travelling wave transient where the drum is stopped and restarted after: a) 5 seconds, b) 60 seconds, and c) 3600 seconds. The space-time diagrams were constructed from surface-imaged data and the horizontal line at 200 seconds in the space-time diagram indicates where the drum was stopped. The time axis does not reflect the time delay in the stopping of the drum, only the length of time for which the drum was rotated. In all of these space-time diagrams, oscillations continue to the left and right of axially segregated bands which were formed at the center of the drum

Taberlet *et al.* [30] used molecular dynamics simulations of collisions between soft frictional spheres to study axial segregation in a mixture of grains with two different sizes, when the friction coefficients of the large and small grains were equal. When the friction coefficients of the large and small grains were different, rapid axial oscillatory motion of the small-grain bands occurred. It is not clear how these results are related to experimental observations and measurements of oscillatory band motion as the period of these simulated oscillations is on the order of several drum rotations, and the period of experimentally observed oscillations is typically several hundred drum rotations [28, 29, 35, 36, 37]. Additionally, oscillatory axial band motion has been observed in mixtures of glass spheres differing only by size [29, 37], thus the different frictional properties of the small and large grains are unlikely to be the mechanism of these oscillations as proposed by Taberlet *et al.*.

3.6 Observations of traveling waves in a binary mixture of glass spheres

A series of segregation experiments were performed by Fiedor *et al.* using mixtures composed of 1/2 small black glass spheres with a diameter of 300 μm and 1/2 large transparent glass spheres with a diameter of 900 μm in a circular and a square tumbler with a 6.35 cm inner diameter and inner side length respectively. They observed that at low rotation rates, from 10-15 rpm, the randomly mixed grains formed axial bands which remained frozen in time for 2500 drum revolutions, at a faster rotation rate of 20 rpm they observed band merging dynamics, and for a rotation rate of 25 rpm, they observed that axial bands displayed traveling wave dynamics. They also reported that traveling waves were observed in a square tumbler for a rotation rate of 10 rpm, and above this rotation rate band merging dynamics were seen. When Fiedor *et al.* added water as an index-matching fluid to these granular mixtures, the traveling wave dynamics no longer

occurred.

In order to directly compare Fiedor *et al.*'s observations in a circular tumbler with the traveling waves observed by Choo *et al.* [35, 36] and those reported here, we calculated the Froude number of each of these systems. The Froude number is the ratio of the centrifugal force of rotation to gravity, and is defined as $Fr = \Omega^2 R/g$, where Ω is the angular speed of the drum, R is the radius of the drum, and g is acceleration due to gravity. This dimensionless number can be used to characterize flows in the rotating drum system, where $Fr \ll 1$ corresponds to the avalanching regime, where the flow consists of discrete avalanches, and as the rotation rate increases, inertial effects become more important. The regime of smoothly streaming flow corresponds to $Fr < 1$, and the critical speed for centrifuging occurs at $Fr = 1$ [15]. While we do not expect experiments performed with different physical parameters such as drum diameter or grain size to scale with the Froude number, this balance of the relevant forces does allow us to compare experiments performed at different scales. For Fiedor *et al.*'s results described above, axial bands are frozen in time at $Fr = 9 \times 10^{-4} - 8 \times 10^{-3}$, band merging was observed at $Fr = 1 \times 10^{-2}$ and traveling waves were observed at $Fr = 2 \times 10^{-2}$. Choo *et al.* [36] report that traveling waves are robust and have little dependence on rotation rate in the range of 15-42 rpm, which corresponds to $Fr = 7 \times 10^{-3}$ to 7×10^{-2}. The traveling waves reported by Choo *et. al* persist for a larger range of Froude numbers, and it is unknown if Fiedor *et. al*'s traveling waves have a dependence of wave speed on wavelength, thus it is unknown how closely the two systems are related.

3.7 Axial band oscillations in ternary mixtures

Newey *et al.* [29] conducted a study of axial segregation using combinations of differently sized glass spheres, all dyed different colors. They found that under certain conditions, when they had a mixture with three non-overlapping sieve cuts or size distributions,

bands oscillate axially. In these experiments, the width of axial bands of small particles oscillate and the width of larger particle axial bands stay constant. Eventually the axial bands merge and this oscillatory transient decays. In contrast to Choo *et al.*'s oscillatory axial segregation transient which can be described as a periodic mixing and demixing of axial bands as viewed from the surface of the flowing granular material, Newey *et al*'s oscillatory transient in ternary mixtures is in the form of periodic band displacements as viewed from the surface .

Aranson and Tsimring [65] proposed the following set of phenomenological equations to describe the oscillation of axial bands in ternary grain mixtures. They define concentration differences $C_A = c_1 - c_2$ and $C_B = c_2 - c_3$ where $c_{1,2,3}$ are the individual concentrations of the components of the ternary mixture. By analogy with their previous model, Equations 3.2 and 3.3, they write a system of coupled equations for the concentration differences linearized near a homogeneously mixed state:

$$\frac{\partial C_A}{\partial t} = D_A \frac{\partial^2 C_A}{\partial x^2} + \mu_A \frac{\partial^2 C_B}{\partial x^2} \tag{3.4}$$

$$\frac{\partial C_B}{\partial t} = D_B \frac{\partial^2 C_B}{\partial x^2} + \mu_B \frac{\partial^2 C_A}{\partial x^2}$$

When the cross-diffusion terms $\mu_{A,B}$ have opposite signs, the concentration differences $C_{A,B}$ will exhibit space-time oscillations. The authors state that this mechanism is intrinsic to granular mixtures with three distinct size components or ternary mixtures, but in experimental systems there may be no clear distinction between ternary and polydisperse granular mixtures of grains. As well, it is unclear how closely the oscillatory band dynamics observed by Newey *et al.* [29] relate to the dynamics studied by Choo *et al.* [35, 36] and Khan *et al.* [28], since no study was made of wave speed dependence on wavelength in ternary mixtures which exhibit the oscillatory instability.

To recapitulate, in this chapter we have examined the development of several theories which try to explain the occurence of axial segregation in a rotating drum. At

the time when Zik *et al.* developed their model [34], the phenomenon had been reported on, and detailed images and descriptions of the final segregated state were availble [17, 18, 23, 24, 31, 32]; however, no spatio-temporal data was available on the dynamics of band formation or segregation transients. Later experiments performed by Choo *et al.*, using digital video imaging techniques not available to previous generations of researchers, showed that oscillatory transients occured prior to axial segregation [35, 36]. The discovery of these traveling waves invalidated Zik *et al.*'s theory, prompting Aranson *et al.* to generalize the Zik theory to account for the new dynamics [38, 39]. This promising theory agreed quantitatively well with Choo's detailed measurements, but an additional slow variable, the dynamic angle of repose, was needed to account for oscillatory dynamics, and this implied that the concentration and dynamic angle of repose fields would have a conjugate phase relationship. The present author, in her masters research, developed an experimental technique to test this implication [64], but in the course of further experimentation found that these two fields are in fact slaved [28]. Hence the Aranson *et al.* theory was also invalidated. This has led us finally to investigate other candidate slow variables; upon consideration of various alternatives we are led to believe that there is no independently evolving second surface field. Examination of the dynamics of the radial core using a new bulk visualization technique provides evidence that axial segregation and oscillatory dynamics of axial bands are a subsurface phenomenon. Detailed investigations of the dynamics of the radial core in the absence of oscillatory dynamics is the topic of the next chapter.

Chapter 4

Radial Core Dynamics: Models and Experiments

Subsurface visualization of axial segregation in a rotating drum using MRI techniques [20, 21, 43] and optical techniques [28, 29] gave rise to the view that axial bands may result from a radial core instability that widens and narrows the core at roughly periodic spatial intervals. This key aspect of axial segregation has long been of interest to experimentalists [20, 21, 43], though it has been virtually ignored theoretically [33, 34, 38, 39, 41]. In this thesis, we investigate this phenomenon with the backlighting bulk visualization technique described in chapter 2. We focused on one aspect of this problem, which was a natural extension of our previous work on the coupling betwwen the radial core width and surface concentration described in chapter 3: the axial transport of grains in the radial core. We investigated how the transport process depends on physical parameters such as drum rotation rate, grain size, surface roughness and drum diameter. These parameters are easily varied and are physically relevant to the axial segregation phenomenon [27].

In this chapter we discuss two models of the axial transport of grains in the radial core, a one dimensional diffusion equation [47] and a one dimensional diffusion equation with a nonlinear diffusion coefficient [40]. We present our experimental tests of these

models and find that these previously proposed models do not describe our data well. We instead find that the radial core of small grains evolving from a small pulse initial condition spreads slower than diffusion, or *subdiffusively*. We propose two models which describe subdiffusive transport processes. We also report on investigations of how the growth of the axial segregation pattern depends on drum diameter and grain size ratio, and how varying these parameters affects the radial core dynamics. We conclude this chapter with an investigation of the self-mixing of identical grains differing only in colour, and find that this mixing process is also subdiffusive.

4.1 Previous studies of the axial transport of grains

Work dating from 1962 by Hogg *et al.* investigated the mixing of identical grains differing only in colour [47]. These measurements were performed by mixing yellow and transparent glass spheres in the size range of 75-105 μm from a two-band initial configuration in a 4 inch diameter and 16 inch long drum which was approximately 60 % full, and then at regular intervals, removing grains and counting their proportions. This sampling was done at thirteen locations along the length of the drum, and only a few such measurements were performed over several thousand drum rotations. The authors reasoned that the mixing of the grains in the axial direction can only result from inter-particle collisions and will be completely random. As a consequence the authors considered the process of the mixing of identical grains to be analogous to diffusion in gases or liquids, and they modeled their data using the one-dimensional diffusion equation integrated over the cross-section of the drum

$$\frac{\partial C(x,t)}{\partial t} = \frac{\partial}{\partial x}\left(D\frac{\partial C(x,t)}{\partial x}\right). \tag{4.1}$$

Here $C(x,t)$ is the relative concentration of the mixture at time t from the beginning of drum rotation and a distance x from the center of the drum, the location of the original interface, and D is the diffusion coefficient. In this case, since the grains are identical the

diffusion coefficient D was assumed to be concentration independent. Taking this into account and replacing the time t with the number of drum revolutions N, Hogg *et al.* write [47]

$$\frac{1}{D}\frac{\partial C(x,N)}{\partial N} = \frac{\partial^2 C(x,N)}{\partial x^2} \tag{4.2}$$

where the diffusion coefficient D is expressed in the units of in^2/rev. The initial conditions used were

$$C(x,0) = \begin{cases} 0 & \text{if } -\frac{L}{2} \leqslant x < 0, \\ 1 & \text{if } 0 < x \leqslant \frac{L}{2}, \end{cases} \tag{4.3}$$

to correspond to the two-band initial condition. Neumann boundary conditions were employed because there is zero axial flux at the boundaries due to the presence of end caps:

$$\begin{aligned} \left.\frac{\partial C}{\partial x}\right|_{x=-L/2} &= 0 \\ \left.\frac{\partial C}{\partial x}\right|_{x=L/2} &= 0. \end{aligned} \tag{4.4}$$

Equation 4.2 can be solved analytically for the initial and boundary conditions given above, and the solution is

$$C(x,t) = \frac{1}{2} + \frac{2}{\pi}\sum_{k=1}^{\infty}\frac{1}{2k-1}\exp\left(\frac{-(2k-1)^2\pi^2 DN}{L^2}\right)\sin\left(\frac{(2k-1)\pi x}{L}\right). \tag{4.5}$$

In Ref. [47] Fig. 8, Hogg *et al.* superimposed their experimental data on theoretical concentration curves determined from equation 4.5, using the average value of the diffusion coefficient determined for several different numbers of drum revolutions. The authors determined that there was excellent agreement between this theory and their experimental data. We have found instead that the self-mixing of indentical grains is subdiffusive, using higher spatial and time resolution digital imaging techniques, as described below.

Nakagawa *et al.* [44] investigated the mixing of differently-sized particles from a two-band initial condition. These experiments were conducted in a 6.9 cm diameter, 27.5 cm long acrylic drum rotating at 15 rev/min. The drum was designed so that it could be separated into top and bottom parts for the setup of a two band initial condition. This

also facilitated sample removal, where 12 dividers were placed into the bottom part of the drum and the contents of each of these 13 sections of the drum were examined. The grains used in these experiments were pharmaceutical particles which contain a liquid core of vitamin oil, with 1 mm, 5 mm, and 3 mm outer diameters. For these experiments, two grain sizes were set up in a two band initial condition, and the radial core transport was determined by weighing the portion of small spheres and large spheres in each of the 13 drum sections at different times.

The authors found that a radial core composed of small particles forms at the interface between the band of large and small particles, and that it advances along the axis of the drum. Removing the grains from the drum and counting them, they produced concentration profiles for the advancing radial core. They found that their concentration profiles were similar to the predictions given by diffusive front spreading for small numbers of drum rotations, but that deviations from symmetric concentration profiles were observed for large numbers of drum rotations.

The axial advance of the radial core of small particles was also studied using non-invasive MRI techniques by Ristow and Nakagawa [40]. In this study, a 10 cm long and 7 cm diameter drum filled with small (1 mm diameter) and large (4 mm diameter) pharmaceutical grains containing vitamin oil was rotated, stopped, and inserted into the MRI bore to obtain concentration profiles of large particles evolving from a two-band initial condition. The drum was rotated at a constant rate of 11.4 rpm, and measurements were taken after 0, 15, 30, 45, 60, 75, 90 and 600 seconds of rotation. The authors observed that the concentration profiles were slightly asymmetrical; they reasoned that this is due to the presence of more voids in the cascading layer for the smaller particles to move into, since the smaller particles advance more easily into the region occupied by larger particles. The authors also observed that the larger particles traveling on the surface reached the opposite end cap before the smaller particles; they argued that this is what leads to a radially segregated core in these experiments.

The authors assumed random particle motion in the axial direction, so they also used the diffusion equation, equation 4.1, to describe the interface of their two-component system, where in this case $C(x,t)$ denotes the relative concentration by volume of the smaller grains and D is the diffusion coefficient of the smaller grains. Ristow and Nakagawa used the two-band initial condition and the no-flux boundary conditions shown above as equations 4.3 and 4.4 respectively [40]. For a constant diffusion coefficient the authors solve equation 4.1 analytically for the specified initial and boundary conditions,

$$C(x,t) = \frac{1}{2} + \frac{2}{\pi}\sum_{k=1}^{\infty}\frac{1}{2k-1}\exp\left(\frac{-(2k-1)^2\pi^2 Dt}{L^2}\right)\sin\left(\frac{(2k-1)\pi x}{L}\right). \tag{4.6}$$

They noted that with a constant diffusion coefficient the model shown above always leads to symmetric concentration profiles. The authors also showed that the front advancement of the radial core is underestimated when the propagation of large particles from equation 4.6 is plotted with the experimental data. This motivated the authors to investigate the effects of a concentration dependent diffusion coefficient on the particle motion. They investigated two linear dependencies of the form

$$D_{\pm} = D_0 \pm D_0\left(C - \frac{1}{2}\right) \tag{4.7}$$

which fulfill the condition

$$\langle D\rangle = \int_0^1 D_{\pm}dC = D_0. \tag{4.8}$$

They used the concentration dependent diffusion coefficient above in equation 4.1 and solved this equation using a standard finite difference procedure with a value of D_0 that is identical to the one they previously used for the constant diffusion coefficient D. They determined that there is better agreement with their experimental data using the above model than with a constant diffusion coefficient.

In order to understand more fully Ristow and Nakagawa's choice of concentration dependent diffusion coefficients in equation 4.7 above, we constructed and ran simulations of equation 4.1 using equation 4.7 as they described in reference [40] using a forward time

centered step finite differencing scheme with a spatial step size of 0.05, a time step size of 0.01, and $D_0 = 0.02$. This is the value of D_0 used by Ristow and Nakagawa. We ran this simulation using two different initial conditions: a two band initial condition as was used in the experiments described above, and a narrow symmetrical pulse of small grains.

Figure 4.1a shows the simulation results for a concentration dependent diffusion coefficient with a positive sign, and figure 4.1b shows the results for a coefficient with a negative sign; both are evolving from a two band initial configuration. It is clear both positive and negative signs lead to non-symmetric concentration profiles; the choice of a positive sign results in large grains diffusing into the small grain rich area more quickly, while the choice of a negative sign results in small grains diffusing into the large grain rich area more easily. Figures 4.2a and b show the simulation results for a diffusing small pulse with a positive and negative sign respectively. Here, the pulses drift to the left or to the right depending on the sign. This asymmetry is obvious from the symmetry of the equation, but it violates the symmetry of the general physical situation. While the small grains may spread more easily into the larger ones, this model does not reflect this situation for arbitrary initial conditions. In effect, Ristow *et al.* have built the asymmetry of the evolution of a two-band initial condition into the dynamical equation. For this reason, we abandoned the model developed by Ristow *et al.* [40] as a candidate model of the axial transport of grains within the radial core. In the next section we describe our own axial transport experiments starting from a two-band initial condition.

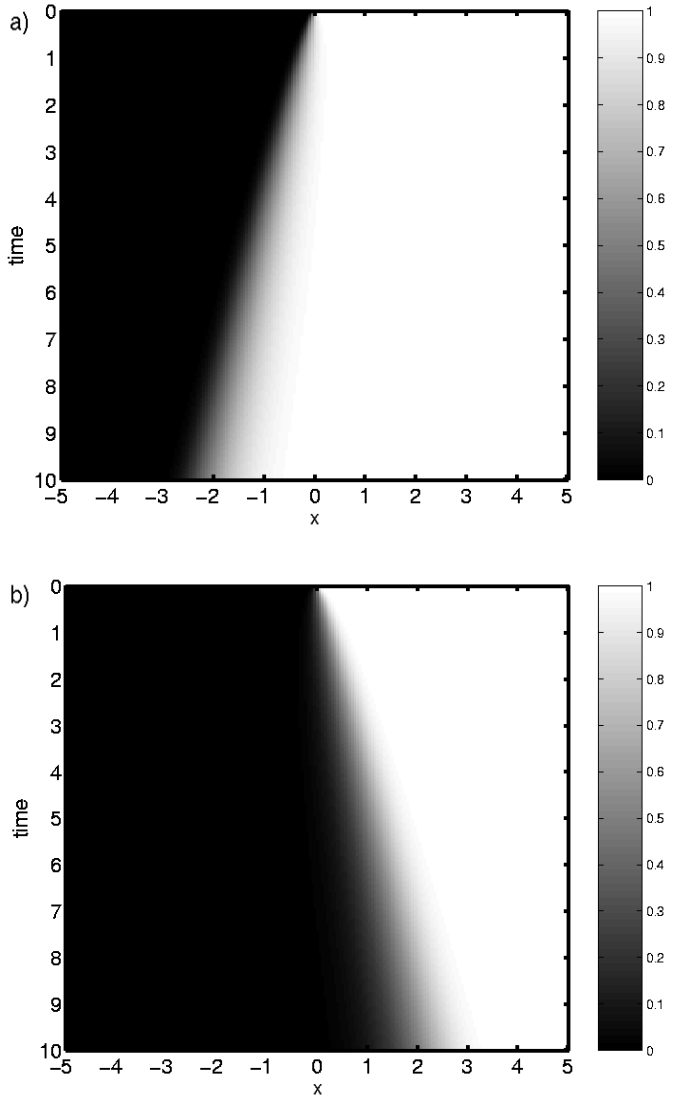

Figure 4.1: Finite-difference simulation results of equation 4.1 with a concentration dependent diffusion coefficient given in equation 4.7 and a two band initial configuration. (a) shows the results for a positive sign choice D_+ and (b) the results for a negative sign choice D_-. The simulation details are provided in the text, the colour bar indicates the relative concentration of large grains.

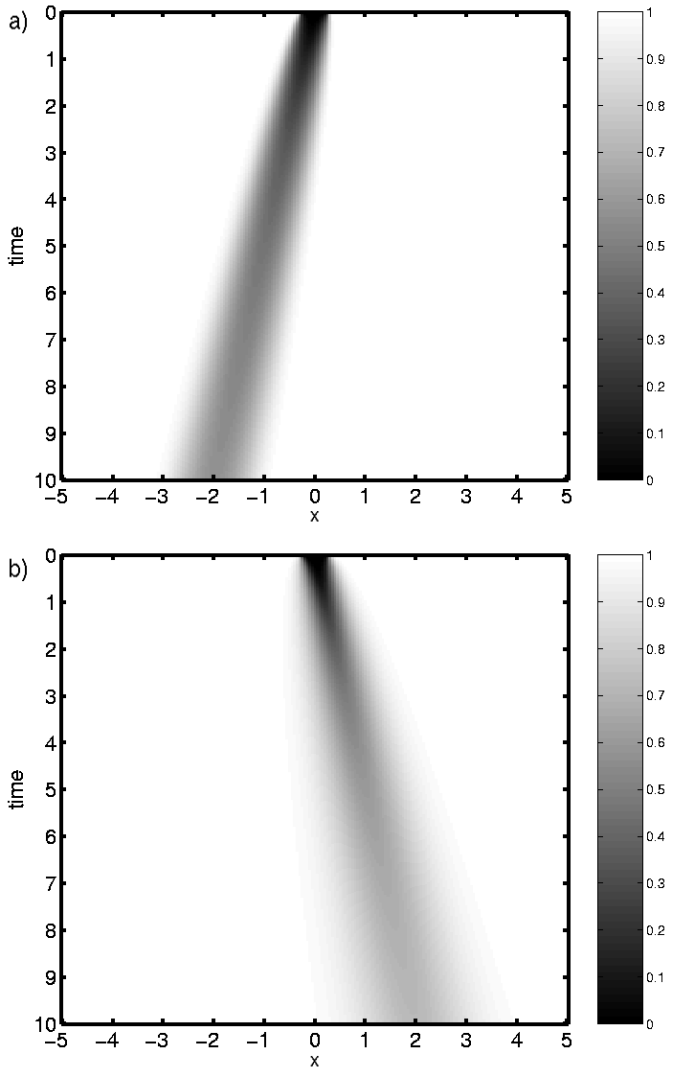

Figure 4.2: Finite-difference simulation results of equation 4.1 with a concentration dependent diffusion coefficient given in equation 4.7 and a 0.5 spatial unit pulse initial condition of small grains. (a) shows the results for a positive sign choice D_+ and (b) the results for a negative sign choice D_-. Here the colour bar indicates the relative concentration of large grains. Note the presence of drift in both cases.

4.2 Experiments on axial transport within the radial core

The axial migration experiment described above lends itself easily to the bulk visualization technique detailed in chapter 2 and chapter 3, since a two-band initial condition could be easily set up with our presegregation method. Using opaque small grains and translucent large grains one can observe the radial core growing from a two-band initial condition. The axial transport of grains was studied using a two-band initial condition, with a sharp interface between the band of small and large grains. The small grains were black hobby sand grains in the size range of 177-212 μm and the large grains were white table salt grains in the size range of 300-420 μm. The drum used in all experiments described below had an inner diameter of 2.85 cm, and it was rotated at three different rates within the smoothly streaming regime: 0.36, 0.5 and 0.63 rev/s. The backlighting bulk visualization technique was used to obtain data. The majority of small grains comprising the core did not actually mix into the bulk of large grains, instead a radial core advanced into the large grains beneath the flowing surface layer. The relative concentration of small grains was determined as described in chapter 2, the fraction of the radial core occupying the drum was determined at each axial position in the digital image via edge detection, and the concentration of small grains was expressed as this fraction divided by the height of the materials in the drum squared. The justification for this approach is provided in section 2.5.1. This produces a concentration data point which depends on axial position and time and ignores the structure of the radial core, but simplifies analysis, so that comparisons to one-dimensional transport equations could be done more simply. This method has been used extensively by other authors [40, 44] and we do not break with this convention in the description of work to follow.

Figure 4.3 shows data collected from a run where the drum was rotated at 0.375 rev/s. We fit this data to the solution of the one dimensional diffusion equation, Eqn.

4.1, with $C(x,t)$ being the relative concentration by volume of the small particles and D a constant diffusion coefficient. The initial conditions for a two-band configuration were used, as shown in equation 4.3, and Neumann boundary conditions as described in equation 4.4, because there is no axial flux of grains due to the presence of end caps. This equation can be solved analytically for the initial and boundary conditions specified above, as shown above in equation 4.6.

We fit experimental data such as that shown in figure 4.3a to equation 4.6 with the sum over k truncated to N using a nonlinear Levenberg-Marquardt fitting scheme, with the diffusion coefficient D being the fitting parameter. The order N used in the fit was 50, and this was chosen to reduce the Gibbs phenomenon. The Gibbs phenomenon occurs when one fits a partial sum of a Fourier series, such as the one described above, to a jump discontinuity, like the two-band initial condition. Gibbs showed that this partial sum always overshoots the jump by about 9 %. The width of the overshoot goes to zero as $N \rightarrow \infty$ but the extra height remains at 9 % at the top and bottom of the discontinuity [81]. We used as high an N value as possible to have a reasonable fit to early time data where the jump discontinuity is present, and to make computations feasible. The measurement error used for the fit was the concentration error corresponding to $\pm$ 2 pixels from the width of the radial core, and the corresponding error bar was 0.12.

Figure 4.4a shows a space-time diagram of this fit. Examining the experimental data in figure 4.3, one can observe that the radial core of small grains spreads more quickly into the volume of large grains, that the growth of the interface is asymmetrical as described by Ristow and Nakagawa [40], and that any fit to a diffusion equation with a constant diffusion coefficient will not capture this transport property. Based on the commonly accepted practice that a typical value of χ^2 for a moderately good fit is on the order of the number of degrees of freedom, we can say the calculations fit the data reasonably well [58]. Here, the value of χ^2 obtained for this fit is 0.0125 and the number of degrees of freedom are 50,687. However, the residuals of this fit all lie on the evolving interface

between the sand and salt grains, as opposed to being scattered normally, as shown in figure 4.4b. When the residuals in a fit are skewed or clustered in a non-normal way this indicates that the model being fit to does not quite describe the data, though it may be usable as an approximation within a limited range. Presumably Nakagawa *et al.* [44] and Ristow *et al.* [40] were able to obtain reasonable fits to the diffusion equation because their data was based on far fewer measurements. Our calculations, based on denser space-time data, led us to look beyond the diffusion equation with a constant diffusion coefficient as a model for the system.

Our calculation of concentration profiles used in these fits depends on certain assumptions about the shape of the radial core, namely that the concentration of small grains in the radial core $C(x,t)$ is proportional to the fraction of the radial core squared, or h^2, as described in chapter 2. Our conclusion that the diffusion equation does not model these experiments well is robust, however, in that no assumptions are needed to observe that the radial core of small grains penetrates more quickly into the large grains resulting in the growth of an asymmetrical interface between the two species of grains. If the concentration profiles had a different functional form, the majority of the residuals of the fit to the diffusion equation would still lie on the evolving interface between the small and large grains.

In order to pursue this further, we experimented with initial conditions involving a symmetric narrow pulse of small grains, as outlined in the next section. The two-band initial condition is, in fact, a poor choice to test models of axial transport, because all of the important variation is concentrated near the interface. Any model of diffusion is likely to correctly fit the constant concentration values at $x = \pm\infty$, especially if the experiments are not run for a very long time. A single symmetric pulse initial condition is a better test of models because its evolving profile can be examined for symmetry, as described in the following section.

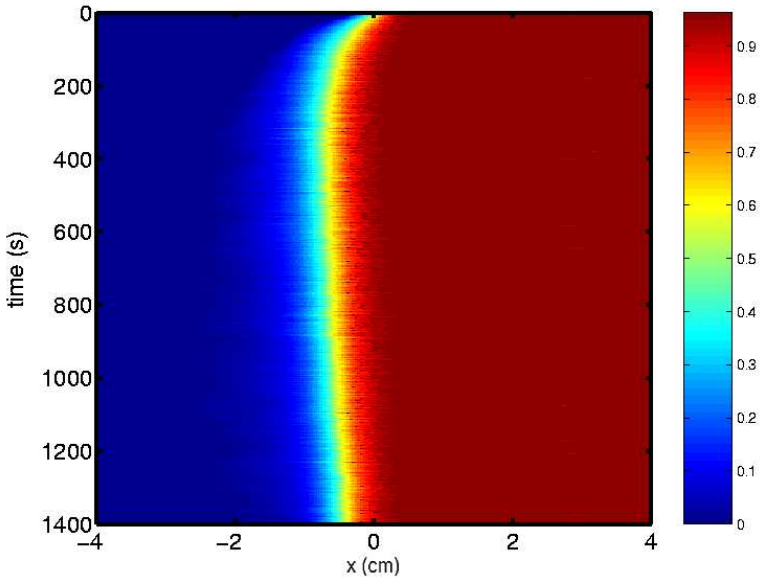

Figure 4.3: Space-time plot of the advancement of the radial core from a two-band presegregated initial condition. The small black hobby sand grains used were in the size range of 177-212 μm, and the large white table salt grains had sizes in the range of 300-420 μm. The drum rotation rate was 0.375 rev/s. Our bulk visualization technique was used to aquire data, the colourbar shows the relative concentration of grains within the radial core.

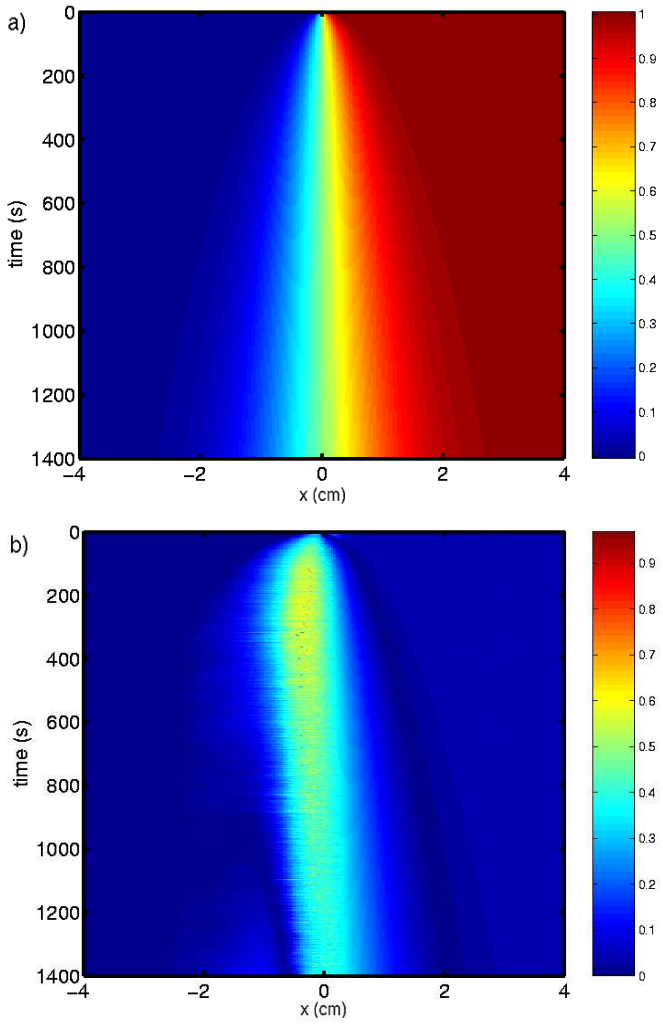

Figure 4.4: (a) A fit of the data shown in figure 4.3 to the solution of the one-dimensional diffusion equation, equation 4.6. Details of the fitting method are provided in the text. (b) A space-time diagram of the residuals of the fit shown in (a).

4.2.1 Narrow pulse experiments

Having ruled out the most frequently used model in the literature to determine the axial transport of small grains within the radial core, we needed to employ physical insight to determine a more appropriate model. Models of the more complex axial segregation phenomenon do not provide any clues; even the most sophisticated of them [38, 39] assumes that the axial transport of grains is a diffusive process. However, a very important insight is that the diffusion equation possesses a similarity under scaling: given a symmetric initial condition such as a delta function, the solution at any later time can be rescaled in the spatial and time variables to collapse to the initial condition. For normal diffusion this scaling is given by the transformations $x \rightarrow xt^{-1/2}$ and $C \rightarrow Ct^{1/2}$. In other words, concentration values (say the peak concentration) decay with a $t^{-1/2}$ power law, and the width of the symmetric pulse evolving from a delta function initial condition grows with a $t^{1/2}$ power law [52].

In the words of G. I. Barenblatt, "scaling laws are not merely some particularly simple cases of more general relations. They are of special and exceptional importance; scaling never appears by accident. Scaling laws always reveal an important property of the phenomenon under consideration: its self-similarity"[53]. The search for a power law scaling in concentration profiles of the small grains comprising the radial core seemed to be a reasonable starting point for additional axial transport experiments; by using a narrow symmetric pulse of small grains as the initial condition and by measuring the expansion of the radial core of small grains, we could determine if power-law dependencies are present in the evolving concentration profile shape, and perform data collapse to definitively determine if this system is governed by diffusion. If no power law scaling is present in the data we have narrowed the field of potential governing equations considerably, and if a power law scaling is present which differs from the one due to diffusion, then we have narrowed the field even further.

The drum used in the experiments described below was 60 cm long with an inner

diameter of 2.85 cm, rotated within the smoothly streaming regime at 0.31 rev/s or 0.62 rev/s. The larger grains were white table salt and had a size range of 300-420 μm. The smaller grains were irregularly shaped black hobby sand, with a size range of 177-212 μm. An initial condition consisting of a 1.5 mm pulse of small grains was made using the presegregation technique described in chapter 2. As described in chapter 2, we used edge detection of bulk visualized data to determine the fraction of the drum occupied by the radial core, h, and assume that the concentration of small grains $C(x,t)$ is proportional to h^2.

Figure 4.5a shows a space-time diagram of the expanding radial core of small grains from a 1.5 mm pulse initial condition. Figure 4.5b shows concentration profiles taken at different times from this run. By plotting the maximum concentration value against time on a logarithmic scale we obtained a power law relation between concentration and time, shown in figure 4.6a with triangle markers. This power law was $C \propto t^{-\beta}$, where $\beta = 0.38 \pm 0.03$. Additionally, by plotting the full width at half-maximum concentration on the logarithmic scale, we obtained a power law relation between the evolving pulse width and time. This is also shown in figure 4.6a with circular markers. Here the power law we measured was width $\propto t^{\alpha}$ where $\alpha = 0.37 \pm 0.02$. This already suggests that this transport process is subdiffusive, because $\alpha < \frac{1}{2}$. It should be noted that the peak concentration decrease power law depends on our assumption that $C(x,t) \propto h^2$, while our conclusion that the width of the axial pulse grows as t^{α} where $\alpha < \frac{1}{2}$ does not, as the width of the evolving pulse is measured directly from our data.

This analysis, however, only determines the power-law time dependence of one arbitrarily chosen dimension of a pulse and not the whole pulse shape, assuming that $C(x,t) \propto h^2$. For a symmetric initial condition, data collapse can test the scaling of the entire pulse. Figure 4.6b shows collapsed data corresponding to the concentration profiles in 4.5b, where the axial length scale was transformed as $x \rightarrow xt^{-\alpha}$ and the axial concentration of small grains $C(x,t)$ was transformed as $C \rightarrow Ct^{\alpha}$. The pulse width

increases at the same rate as the pulse amplitude decreases, thus the spreading process is self-similar. This implies that the integrated concentration is constant and that no grains are lost from the core. The collapse parameter determined for this run was $\alpha = 0.37 \pm 0.02$. The best data collapse parameter α was determined using a brute-force search method. A wide range for α was input, and fluctuations about the mean rescaled C values were determined for each rescaled x value. The best α value was the one with the least scatter about the mean rescaled C value. The average collapse parameter for large salt grains and small sand grains with a drum rotation rate of 0.62 rev/s was found to be 0.37 ± 0.03, averaged over ten runs. This parameter α was determined for ten runs using our brute-force search method and averaged to produce the value given in table 4.1. The error is half of the difference of the maximum and minimum α value determined for these runs. This data, along with the power-laws for evolving pulse width, rule out diffusion as the mechanism for the axial transport of grains within the radial core, and shows that a subdiffusive process is responsible for this phenomenon.

In order to determine how generally applicable this result is, we conducted runs where we systematically varied drum diameter, grain size ratio, grain material, and rotation rate. The first set of experiments performed checked different grain types and rotation rates within the smoothly streaming regime using the same sizes of large and small grains and drum diameter as in the experiments described above. Here we found that the subdiffusive and self-similar nature of the transport process was preserved. When drum diameter and grain size ratio were varied, we found that the transport was subdiffusive but no longer self-similar; these experimental results are discussed in section 4.3.

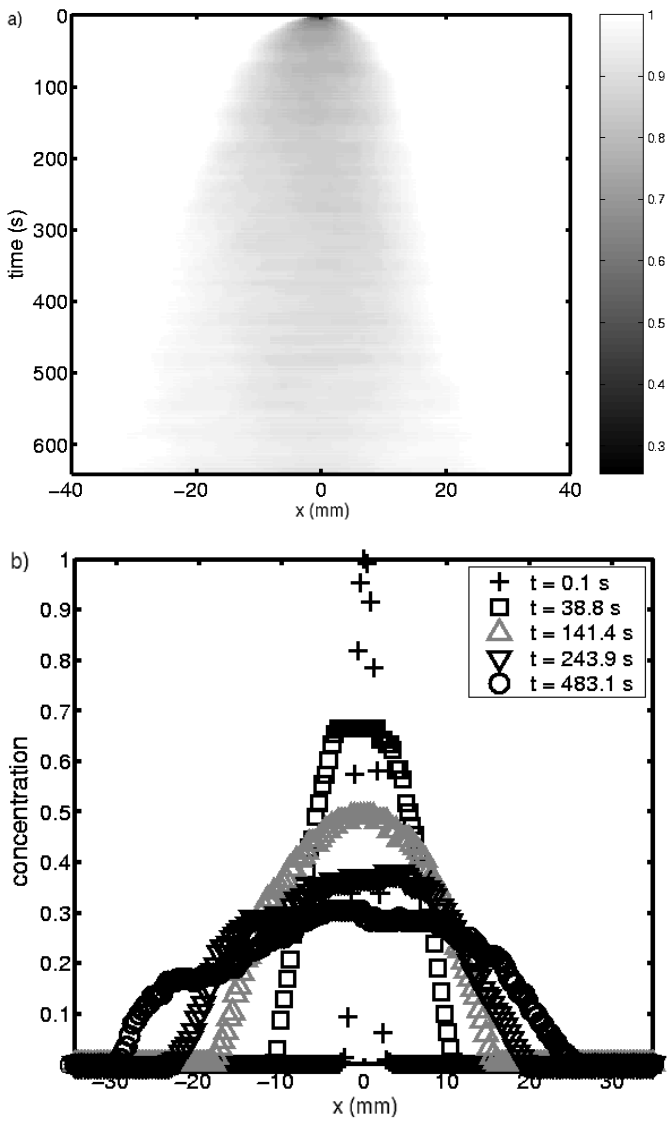

Figure 4.5: a) Space-time diagram of the evolution of a 1.5 mm pulse initial condition. The drum rotation rate was 0.62 rev/s and the drum inner diameter was 2.85 cm. The small grains are black hobby sand grains with sizes in the range of 177-212 μm and the large grains are table salt grains with sizes in the range of 300-420 μm. This space-time diagram is shown is contrast-enhanced, the colour bar indicates the relative concentration of large salt grains throughout the depth of the drum at each axial position. b) Concentration profiles of small grains within the radial core taken at different times corresponding to the space-time diagram shown above.

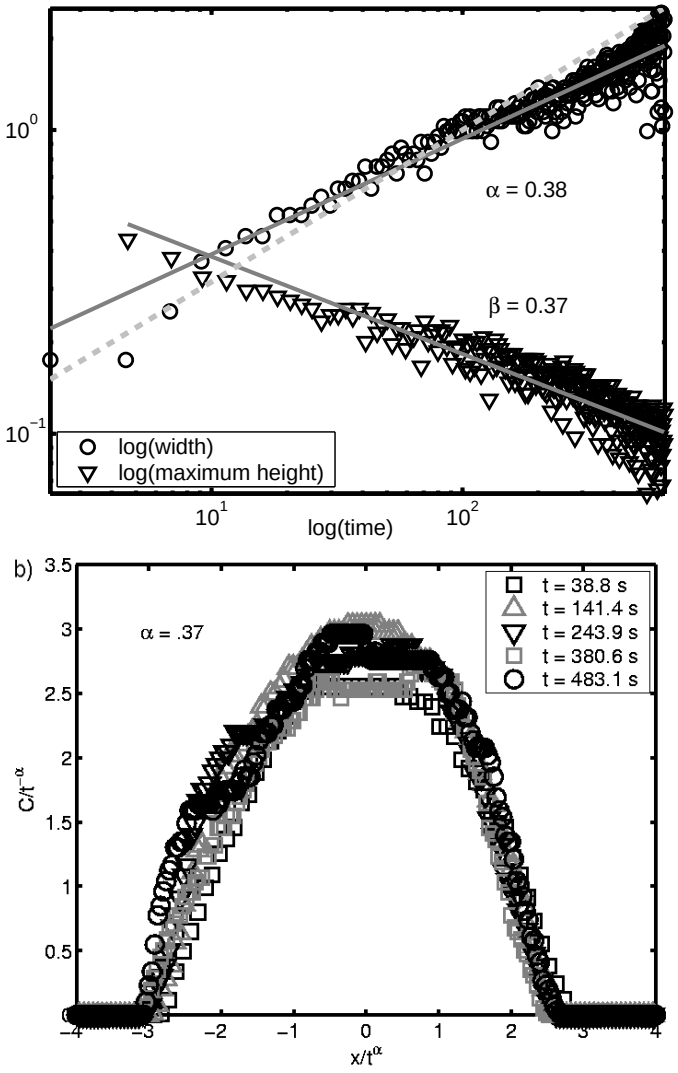

Figure 4.6: a) The FWHM (circles) of the evolving pulse shown in figure 4.5 plotted against time on logarithmic scales. The linear fit shows that the pulse width evolves with the power law width $\propto t^{0.38}$. The maximum concentration profile height is also plotted against time (triangles) and the linear fit shows that pulse concentration decays with the power law peak concentration $\propto t^{-0.37}$. The dotted line has a slope of 1/2, for comparison with the power laws we obtained from the data. b) Collapsed concentration profiles of the radial core pulse corresponding to figure 4.5a. The collapse parameter is $\alpha = 0.37 \pm 0.02$.

One would think that rough grains such as sand and salt could have different transport properties than smooth spherical grains, such as glass and bronze spheres. Also, the transport properties could also be affected by the drum rotation rate. We repeated the small pulse experiments using glass spheres in the size range of $300 - 420$ μm and bronze spheres with sizes in the range $177 - 212$ μm at the drum rotation rates of 0.31 and 0.62 rev/s. These experiments were also repeated for sand and salt grains with a drum rotation rate of 0.31 rev/s, all results are shown in table 4.1. These experiments confirmed that the axial transport within the radial core is a subdiffusive front spreading process. We conclude that cores of small grains spread axially as t^α where $\alpha \sim 1/3 < 1/2$, independent of the grain types we used and drum rotation rate within the smoothly streaming regime [26].

Large grains 300-420 μm	Small grains 177-212 μm	Rotation rate (rev/s)	α
salt	sand	0.31	0.38 ± 0.03
salt	sand	0.62	0.37 ± 0.03
glass	bronze	0.31	0.31 ± 0.04
glass	bronze	0.62	0.29 ± 0.01
glass	sand	0.31	0.35 ± 0.03

Table 4.1: Collapse parameters for the self-similar spreading of radial cores in various grain types and rotation frequencies. The drum diameter for all experiments was 2.85 cm.

4.2.2 One dimensional subdiffusive models

The temporal scaling of pulse width was determined to be less than 1/2, which indicates that the mixing process is slower than diffusion and hence is subdiffusive. In addition to

examining the temporal scaling of the pulse, we also measured in detail the functional shape of the scaling solution, assuming that $C(x,t) \propto h^2$. Here is it possible to distinguish between different subdiffusive processes, if our assumptions about the radial core shape are correct. We have investigated two candidate models for radial core spreading; the the porous medium equation (PME) and fractional diffusion equation (FDE) .

The porous medium equation,

$$\frac{\partial}{\partial t}C(x,t) = D\frac{\partial^2}{\partial x^2}(C(x,t)^2) \tag{4.9}$$

is a nonlinear model which describes the spreading of a compact groundwater mound, and has the property that for a narrow pulse initial condition the width grows as $t^{1/3}$ and the scaling solution has a parabolic profile [53]. This parabolic model becomes degenerate when $C(x,t) = 0$, so the non-zero portion of the solution, $\{C(x,t) > 0\}$, moves with a finite propagation speed. As a result, the PME is often regarded as a better model of spreading than the linear diffusion equation which predicts an infinite propagation speed [52].

The fractional diffusion equation was formulated as an initial value problem by W. R. Schneider and W. Wyss [54];

$$\frac{\partial^\gamma}{\partial t^\gamma}C(x,t) = D\frac{\partial^2}{\partial x^2}C(x,t) \tag{4.10}$$

with initial data

$$C(x,0) = f_0(x). \tag{4.11}$$

Here $\gamma = 2\alpha$ denotes the order of a fractional time derivative [54, 55]. The solution to the initial value problem is

$$C(x,t) = \int dy G_0^\gamma(|x-y|,t,D) f_0(y) \tag{4.12}$$

where $G_0^\gamma(r,t,D)$ is the Green's function for this initial value problem, and can be expressed in terms of Fox's H function [54]:

$$G_0^\gamma(r,t,D) = (1/\gamma)(1/\sqrt{\pi})(1/r)H_{12}^{20}\left[(2\sqrt{D})^{-\frac{2}{\gamma}} r^{\frac{2}{\gamma}} t^{-1}\Big|_{(\frac{1}{2},\frac{1}{\gamma}),(1,\frac{1}{\gamma})}^{(1,1)}\right] \tag{4.13}$$

and the value of this Green's function for the input values of $D, r = |x - y|, t$ and γ are given by the series expansion of Fox's H-function [55],

$$H_{pq}^{mn}\left[z\Big|_{(b_1,B_1),(b_2,B_2),\ldots,(b_q,B_q)}^{(a_1,A_1),(a_2,A_2),\ldots,(a_p,A_p)}\right] = \sum_{h=1}^{m}\sum_{\nu=a}^{\infty}\frac{\Pi_{j=1,j\neq h}^{m}\Gamma(b_j - B_j(b_h+\nu)/B_h)}{\Pi_{j=m+1}^{q}\Gamma(1-b_j+B_j(b_h+\nu)/B_h)} \tag{4.14}$$

$$\times\frac{\Pi_{j=1}^{n}\Gamma(1-a_j+A_j(b_h+\nu)/B_h)}{\Pi_{j=n+1}^{p}\Gamma(a_j+A_j(b_h+\nu)/B_h)}\times\frac{(-1)^{\nu}z^{(b_h+\nu)/B_h}}{\nu!}.$$

Solutions of this linear equation have the property that the width of a narrow pulse initial condition grows as t^{α}, where $\alpha \leq 1/2$. If $\alpha = 1/2$ the solution reduces to normal linear diffusion. This model is often used to describe processes which occur in spaces where there are temporal or spatial constraints, such as the flow of tracers through porous media [56].

We fit radial core concentration data collapsed with α to the series solution of the FDE, and data collapsed with $\alpha = 1/3$ to a numerical solution of the PME, as shown in figure 4.7a and b respectively. For both fits, the initial data was taken from the first series of averaged images of the radial core spreading, and the fit parameter was the constant diffusion coefficient D. We found that while both solutions model the collapsed concentration profiles reasonably well within experimental error, the PME has a smaller systematic discrepancy since the profiles are better described as parabolic. The FDE solution has exponential wings and inflection points that are not obvious in the data. We note, however, that our projection visualization technique may simply be too insensitive to detect these tails. We also performed fits to ordinary diffusion with $\alpha = 1/2$ which were poor, as shown in figure 4.7c. It can be easily seen that the solution to the diffusion equation does not fit the data when the concentration of small grains approaches zero. The uncertainty in each concentration data point is 0.12, corresponding to a loss or gain of one pixel at the top and bottom of the radial core at each axial position. The tails of the solution to the diffusion equation at those positions miss the collapsed data points by twice the experimental error. It should also be noted that the collapse of the data with $\alpha = 1/2$ has twice as much spread as the collapse when α values are closer to 1/3.

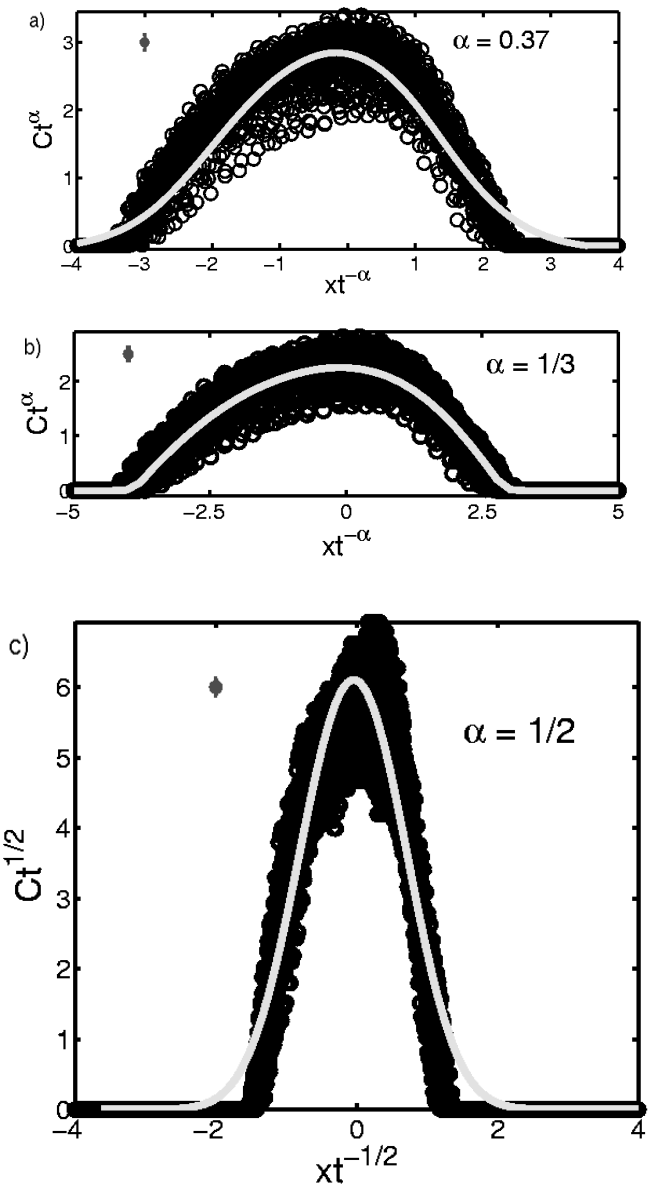

Figure 4.7: Collapsed concentration profiles of a black sand radial core in salt grains fit to: a) the fractional diffusion equation (grey line) and b) the porous medium equation (grey line) and c) the diffusion equation (grey line). The uncertainty in each concentration data point is 0.12 which corresponds to a loss or gain of one pixel at the top and bottom of the radial core at each axial position.This corresponds to the size of the error bar on the dark grey plotting symbol at the upper left corner of each graph. Each of these graphs are constrained to have the same vertical scale.

4.3 Drum diameter and grain size experiments

Previous studies by Choo *et al.* show that arrays of axial bands in the rotating drum exhibit a reasonably well-defined and quasi-stable emergent wavelength. Figure 5 of Reference [36] shows that the Fourier spectrum of the space-time diagram of the axial segregation pattern prior to saturation reveals a strong low-wavelength cutoff and a sharp peak with a long tail to higher wavelengths. After a longer time of rotation, it has been reported that either complete segregation occurs [68] or a smaller number of bands evolve via coarsening effects [22, 29, 37]. From these studies, several obvious questions of pattern scaling present themselves. First, how does the emergent wavelength of the axial segregation pattern scale with other simple length scales in the experimental system, such as the drum diameter? Second, how does the growth rate of the axial band pattern depend on physical parameters? Although axial segregation has been the subject of many experimental studies, as discussed in chapter 1, its scaling behaviour has not been systematically explored. A recent study by Alexander *et al.* [25] of the existence of axial banding as a function of the ratio of drum diameter to average grain size suggests that a scaling approach could be fruitful. In particular, this study finds that there is a critical drum diameter to average grain size ratio below which axial segregation never occurs, which implies that there is functional dependence between the growth rate of axial segregation and drum diameter. This motivated Charles *et al.* to investigate in a systematic way the dependence of the axial segregation pattern on drum diameter [27]. These results are described below.

4.3.1 Axial band pattern scaling

Charles, Khan and Morris performed a systematic study of the scaling of axial segregation patterns as a function of drum diameter [27]. In these experiments, equal volume mixtures of large black glass spheres 750 μm in diameter and small transparent glass spheres with

diameters in the range of 297-420 μm were rotated in nine drums with diameters in the range of 2.85 cm to 11.5 cm at a constant rotation rate of 0.8 rev/s. No segregation was observed for a drum diameter of 1.9 cm after several hours of rotation, and for a 2.35 cm diameter drum, segregation was irregular and incomplete for rotation times of less than 2 hours, but long-term segregation was observed after 15 hours of rotation.

Figure 4.8a shows the average wavelength λ plotted against drum diameter D. A linear fit does not intercept the origin, indicating that the wavelength is not directly proportional to the drum diameter. Figure 4.8b shows the ratio λ/D versus D for the same data. For large drum diameters, λ/D tends towards a constant value, equal to the slope of λ versus D shown in figure 4.8a. Figure 4.9 shows growth rate measurements for six drum diameters where axial segregation occurred. Our method of determining growth rates from space-time diagrams of axial segregation patterns is described in Chapter 2. It was determined from this data that the growth rate of axially segregating bands is an increasing function of drum diameter [27].

Continuum models of axial segregation [19, 34, 38, 39, 41, 49] do not appear to account for this observed scaling behaviour. In general the models are scaled so that all lengths are expressed in units of the drum diameter, and, for constant parameters, they apparently predict a linear proportionality for the wavelength as a function of drum diameter. Also, these continuum models do not show an explicit scaling with the mean particle size, and studies such as this one and Alexander *et al.* [25] show that the drum diameter to average grain size should be incorporated into continuum models of axial segregation.

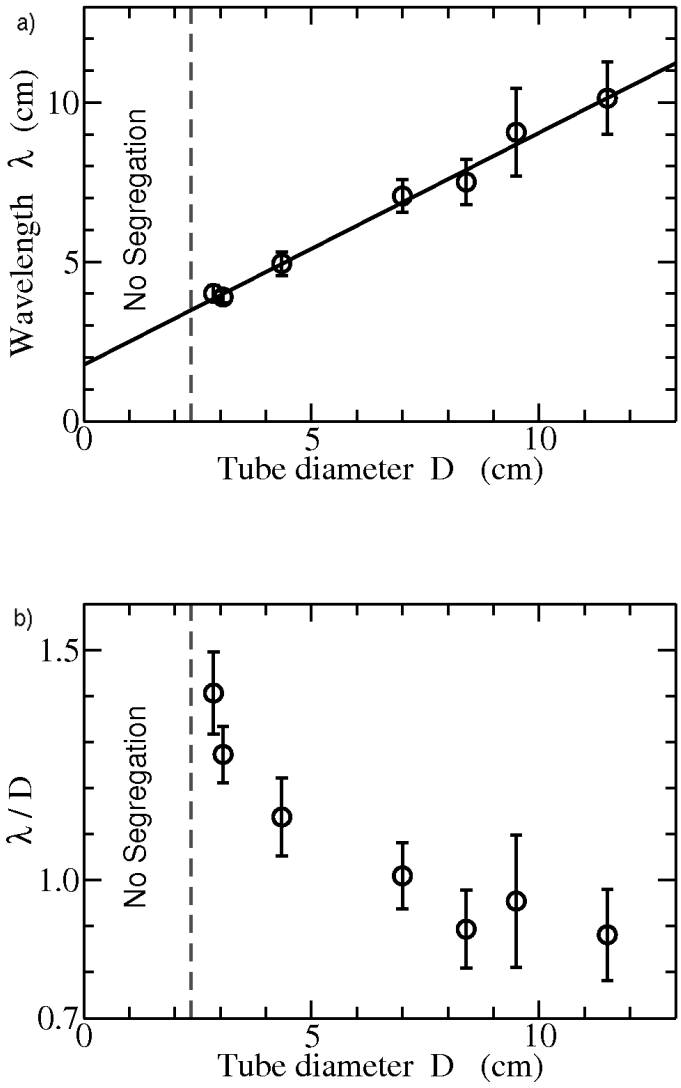

Figure 4.8: Axial segregation results showing (a) λ vs. D and (b) λ/D vs. D for segregation experiments performed with a mixture of small glass spheres with diameters in the range of 297-420 μm and large black glass spheres 750 μm in diameter rotated at a constant rate of 0.8 rev/s. No segregation was observed for drums smaller than $D = 2.35$ cm. From reference [63].

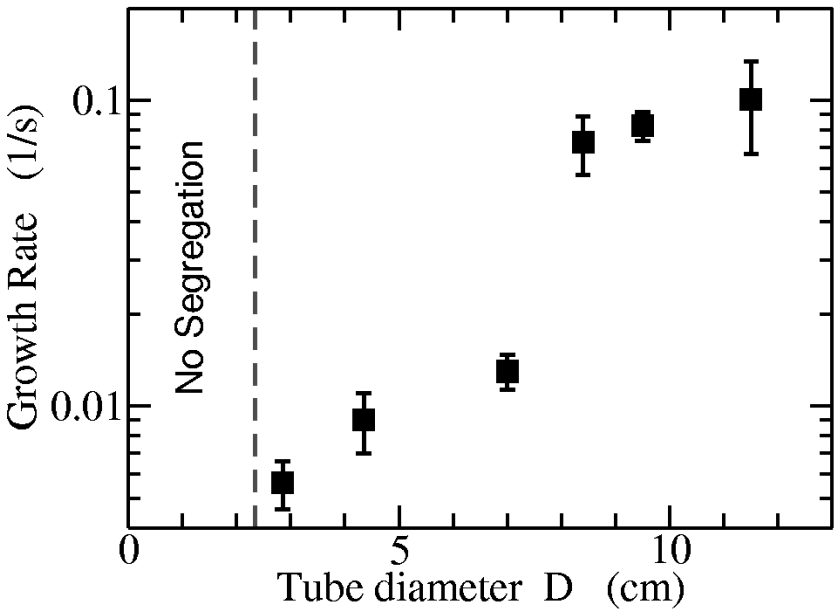

Figure 4.9: Growth rates for six drums as a function of drum diameter. No segregation, hence a zero growth rate, is found for drums with a diameter smaller than 2.35 cm. From reference [63].

In order to investigate possible connections between the dynamics of grains in the radially segregated core and scaling relationships between segregation and drum diameter, the experiments described above were reproduced in mixtures of sand and salt. This enabled us to use our bulk visualization technique to measure the growth rate of bumps on the radial core, as well as compare pulse transport data with axial segregation data as a function of the parameter values. We also investigated growth rate scaling as a function of grain size ratio by increasing the larger grain size and keeping the smaller grain size fixed. This research was motivated by a report in the literature that when the ratio of the large to small grains is below a critical value of 1.2 axial segregation does not occur [31]. The implication is that the axial band pattern growth also depends on grain size ratio.

We measured the growth rate of axial bands in the same manner as Charles *et. al* and Choo *et. al* [27, 36] as described in chapter 2. We loaded the drums with a mixture of 1/3 sand with sizes in the range of 177-212 μm and 2/3 salt with sizes in the range 300-420 μm in drums with inner diameters of 2.85, 4.4 and 5.6 cm. For all experiments described here the aspect ratio (drum length/drum diameter) was 7, and in all cases studied and the drum rotation rate was 0.31 rev/s. The backlighting bulk visualization technique was used to acquire data.

We found that the growth rate of axial bands increases as a function of drum diameter, and the results are show in table 4.2. We also measured the growth rate as a function of relative grain size ratio by loading the 2.85 cm diameter drum with mixtures of 1/3 sand with sizes in the range of 177-212 μm and 2/3 salt with sizes in the ranges of 420-500 and 500-600 μm, and measuring the axial segregation pattern with our bulk visualization technique. These results are also shown in table 4.2. The growth rates shown in table 4.2 were determined by averaging the growth rate for five runs at each parameter value. The error in the growth rate was estimated by dividing in half the difference in the maximum and minimum growth rates measured. From this additional

Drum diameter cm	Large grain size μm	Growth rate $1/s$
2.85	300-420	0.0018 ± 0.0004
2.85	420-500	0.0045 ± 0.0002
2.85	500-600	0.0081 ± 0.0002
4.4	300-420	0.008 ± 0.002
5.6	300-420	0.014 ± 0.003

Table 4.2: Growth rates for the formation of axial bands in mixtures with varying large grain sizes and drum diameters. In all cases the small grain size is 177-212 μm and drum rotation rate is 0.31 rev/s.

data we also found that the growth rate of axial segregation increases as a function of grain size ratio in the parameter range studied. The particular values we calculated for the growth rates in these experiments do depend on our assumptions about the radial core shape. However, the trend that we observed here, that bumps on the radial core grow faster as a function of drum diameter and increasing grain size ratio, remains unaffected. In the next subsection, we discuss the effect of changing drum diameter and grain size ratio on the axial transport of small pulses.

4.3.2 Additional axial transport experiments

Having determined that the growth rate of axial bands increases as a function of drum diameter and grain size ratio in mixtures of sand and salt, we examined the axial spreading of small pulses to determine if axial transport properties differ in situations where axial banding of the radial core is less strongly damped by the motions of the larger grains. The experiments reported in section 4.2 dealt with the radial spreading of small pulses whose grain sizes and drum diameter correspond to the case shown in table 4.2

with the smallest growth rate of axial bands.

Figure 4.10a shows the radial core concentration profile at different times, for a mixture of 177-212 μm sand grains, 300-420 μm salt grains in a 5.6 cm diameter drum. Plotting the full width half-maximum of the concentration profile against time as well as the maximum height of the concentration profile against time, we determined their respective power law dependencies, as shown in figure 4.10b. Note that these power law dependencies are no longer similar, $1/2 > \alpha > \beta$, thus the pulse evolution is no longer self-similar, while remaining subdiffusive. Testing the power law dependence of the whole pulse shape, we performed data collapse of the concentration profile by transforming the axial length scale as $x \rightarrow xt^{-\alpha}$ and the axial concentration of small grains $C(x,t)$ as $C \rightarrow Ct^{\beta}$ where $\alpha \neq \beta$. Figure 4.11a shows the collapsed data corresponding to the concentration profiles shown in 4.10a; we see that the pulse amplitude decreases more slowly than the width expands. The concentration decrease power law and loss of self similarity that we have measured depends on our assumptions about the shape of the radial core, however the amplitude of the pulse in the vertical direction does decrease more slowly than the case studied in section 4.2, corresponding to the case of the smallest growth rate of axial bands. A possible explanation for this is that large grains are intruding into the radial core, increasing its amplitude. Figure 4.11b shows that the integral of $h(x,t)^2$ for the pulse shown in figure 4.10a increases in time, indicating that our measure of the radial core volume increases. These experiments were repeated in a 4.4 cm diameter drum; the results are summarized in Table 4.3. It was found in this case as well that the pulse evolution is no longer self-similar under our assumptions, and that mixing may possibly be present in the radial core.

Pulse evolution experiments were also performed varying grain size ratio by keeping the small sand grain sizes fixed at a range of $177-212$ μm and using large salt grain sizes in the ranges of $420-500$ μm and 500-600 μm in a 2.85 cm inner diameter drum. Figure 4.4a shows the power law scaling of the full width half-maximum and peak concentration

with time of a mixture with 500-600 μm salt grains. It was determined that in this case, the concentration profile height decreases more rapidly than the width increases, $\beta > \alpha$, while $\alpha < 1/2$. These values for β depend on our assumptions, but the amplitude of the pulse does decay more quickly than in the previous cases studied. This could occur if small grains become relatively scarce at the interface of the radial core with the larger grains and can no longer be detected by our optical technique. Figure 4.4b, where the integral of $h(x,t)^2$ is plotted against time, shows that our measure of the volume of the radial core is decreasing, possibly because small grains are being lost from the radial core.

Table 4.3 shows the width parameter α and the height parameter β for the experiments described above. The values of the collapse parameters α and β were determined by averaging over five runs at each parameter value. The error corresponds to half the difference of the maximum and minimum values obtained. From this, we can see that α does not depend on drum diameter or relative grain size, but β does. While the values for β depend on our assumption that concentration depends on h^2, our observation that pulse amplitude decreases as a function of drum diameter and increases as a function of grain size ratio remains intact. As a result of this observation, we postulate that mixing is enhanced in the radial core as drum diameter and relative grain size ratio increases. From table 4.2 we also observe that the growth rate of axial bands increases as a function of these parameters. From this evidence, we conclude that axial pulse spreading is a subdiffusive process, however mixing may occur within the radial core. While we do not have conclusive evidence that mixing is occurring, we believe that this possibility deserves future study using 3-D bulk imaging techniques.

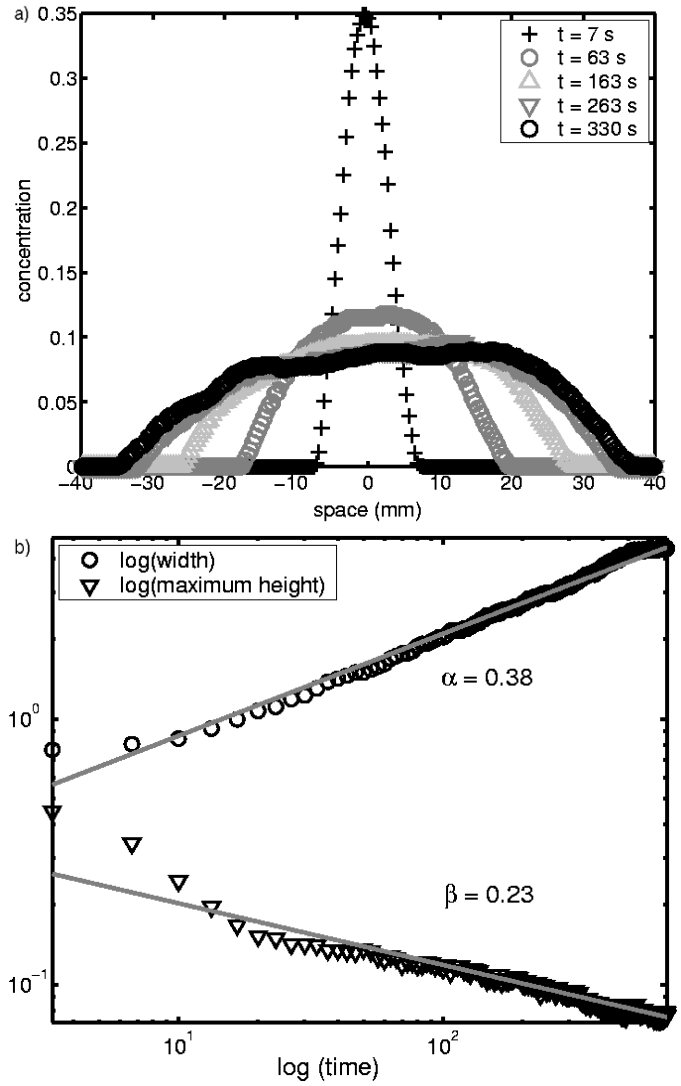

Figure 4.10: a) Concentration profiles at various times of a spreading pulse of sand grains 177-212 μm large within salt grains $300 - 420$ μm large in a drum with diameter 5.6 cm. b) Power law scaling of the FWHM and peak concentration value . From the linear fits (grey lines) we find that the width $\propto t^{0.38}$ and peak concentration $\propto t^{-0.23}$.

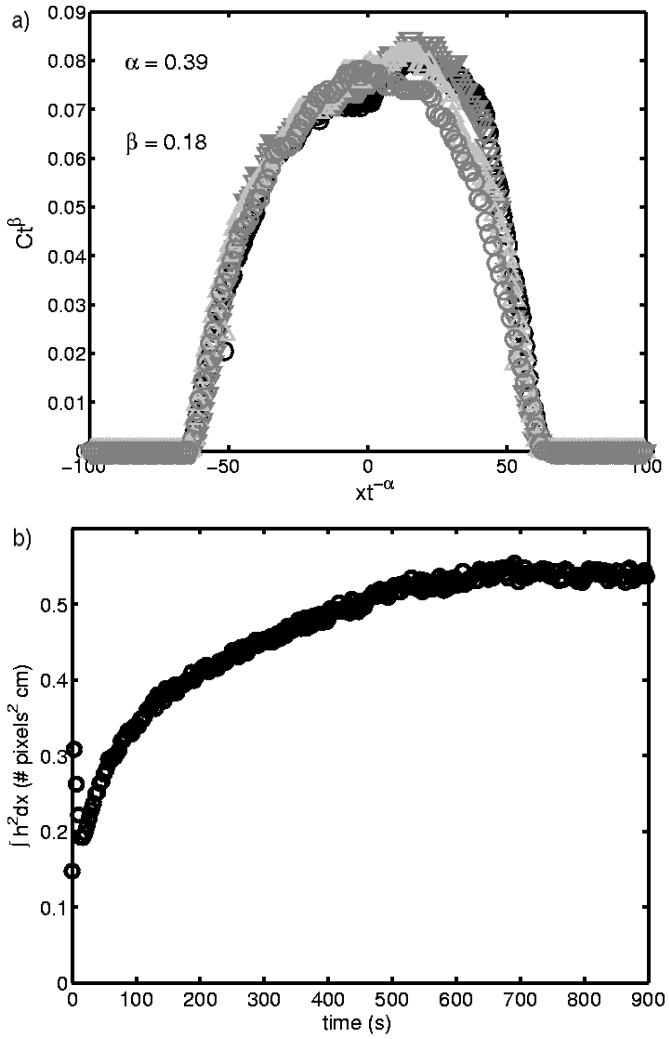

Figure 4.11: a) Collapsed concentration profiles of the radial core pulse corresponding to figure 4.10a. The collapse parameter for pulse width is $\alpha = 0.39$ and for pulse concentration is $\beta = 0.18$. b) The integral of h^2 for the pulse corresponding to figure 4.10a is increasing in time, the apparent volume of the radial core is not conserved.

Drum diameter cm	Large grain size μm	α	β
2.85	300-420	0.38 ± 0.03	0.38 ± 0.03
2.85	420-500	0.29 ± 0.05	0.48 ± 0.08
2.85	500-600	0.33 ± 0.04	0.57 ± 0.05
4.4	300-420	0.32 ± 0.03	0.25 ± 0.05
5.6	300-420	0.38 ± 0.07	0.19 ± 0.05

Table 4.3: Collapse parameters for the spreading of radial cores for various grain size ratios and drum diameters. In all cases the small grain size is 177-212 μm and drum rotation rate is 0.31 rev/s.

4.4 Axial Self-Diffusion of Monodisperse Grains

We also investigated the self-mixing of monodisperse grains. Historical evidence from Hogg *et al.* indicates that the mixing of identical grains is a diffusive process [47]. Our ability to measure the dynamics of the grains in the drum with high speed digital cameras lends a distinct advantage to repeating these self-diffusion measurements [59] since we can measure the relative surface concentration of grains to a much higher degree of spatial and temporal resolution. Unfortunately, our measurement technique does tend to have a higher degree of systematic error than the method employed by Hogg *et al.* since counting is in principle exact and our method does not probe beneath the surface of the flowing layer. However, our faster method lends itself to repeatability, thus all measurements were repeated 5 to 10 times. We used surface imaging techniques to acquire data for all of the non-segregating experiments described below, thus no assumptions were needed about the shape of the radial core.

In order to study the self-diffusion of the larger grains alone, a portion of table salt grains in the size range of 300-420 μm were dyed black with water-based India ink. Also, glass beads in the same size range were also dyed black with a mixture of black acrylic paint and Sunlight dish soap. In order to be sure that the grain properties of dyed and un-dyed grains were identical, their angles of repose were measured in a Hele- Shaw cell, and found to agree within error.

The black salt grains were loaded into a 1.5 mm small pulse initial condition surrounded by otherwise identical white salt grains. The pulse evolution was observed using surface visualization techniques as described in section 2. Figure 4.13a shows a space-time diagram of an evolving small pulse self-diffusion experiment. Data was obtained by subtracting images of the pulse of dark salt grains from background images of white table salt flowing in the drum. This was done in order to correct for uneven lighting conditions. Figure 4.13b shows the corresponding concentration profiles of the dyed grains mixing at selected times. We determined power law dependencies by performing data collapse as described in section 4.2. Figure 4.14 shows the resulting data collapse for the concentration profiles shown in figure 4.13b. Table 4.4 shows the collapse parameter α for self-diffusion averaged over five runs for both salt grains and glass beads in the size range $300 - 420$ μm, and both results are consistent with a subdiffusive mixing process [26].

In order to compare the functional form of the non-segregating self-diffusion case to the axial spreading of the radial core, we fit the non-segregating self-diffusion of the large grains to both the FDE and PME models and found that the FDE gives a qualitatively better fit because in this case the concentration profiles have tails within experimental resolution while the parabolic PME solution does not. Examples of these fits to collapsed concentration profiles of mixing salt grains are shown in figures 4.4a and b.

Since increasing drum diameter and relative grain size ratio had a measurable effect on the transport of small grains in the radial core, the self-diffusion experiments were

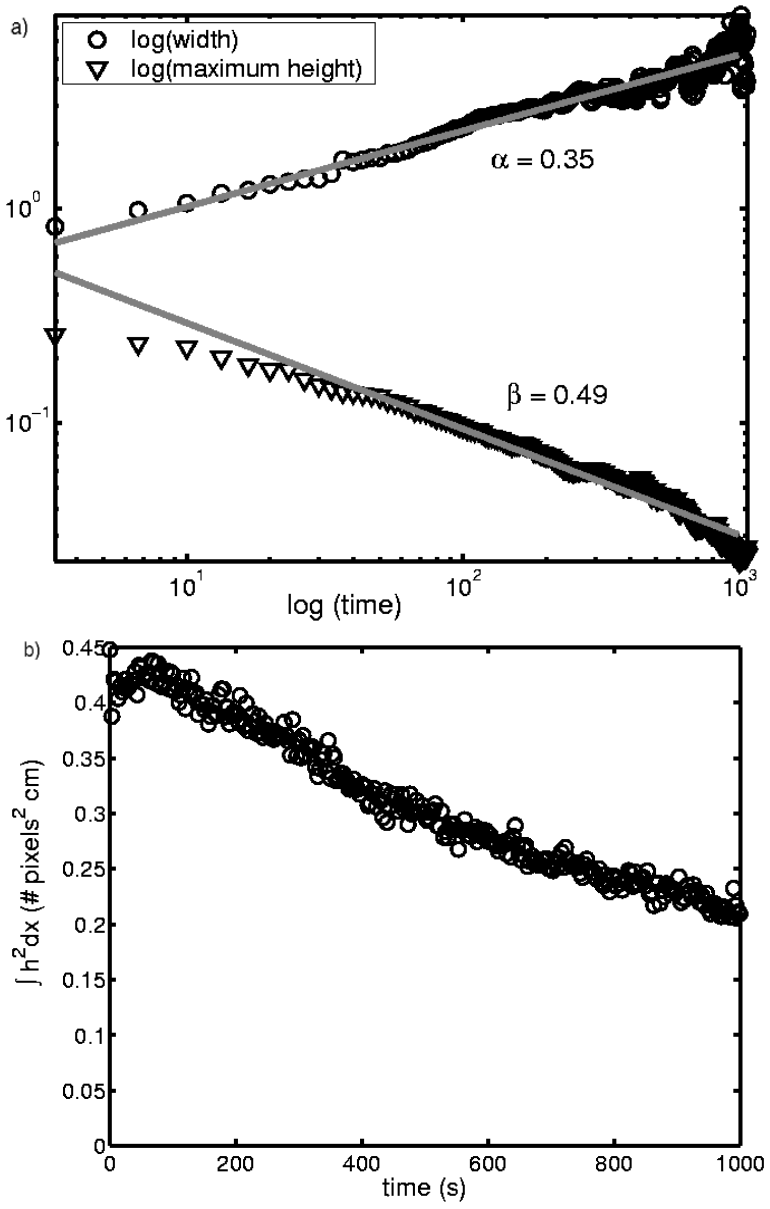

Figure 4.12: a) Power law scaling of the FWHM and peak concentration value for a pulse of sand grains with sizes in the range 177-212 μm expanding into salt grains in the size range 500-600 μm . From the linear fit (grey line) we find that the width $\propto t^{0.35}$ and peak concentration $\propto t^{-0.49}$ b) The integral of h^2 for the pulse corresponding to (a) is decreasing in time, the volume of the radial core is not conserved.

repeated in these cases. For drums with 4.4 and 5.6 cm inner diameters, salt grains in the size range $300-420$ μm were used. For the 2.85 cm diameter drum, the self-diffusion runs were repeated with salt grains in the size range of $420-500$ μm and $500-600$ μm. The temporal exponent α for all cases was determined using data collapse on the data sets. The results are summarized in table 4.4, and it should be noted that the temporal exponent α for all these cases are consistent within error. From this we conclude that the mixing of the large grains alone with no small grains present is subdiffusive, with no significant dependence on drum diameter, grain size, or grain roughness.

Drum diameter cm	Grain size μm	Grain type	α
2.85	300-420	glass	0.34 ± 0.04
2.85	300-420	salt	0.29 ± 0.01
2.85	420-500	salt	0.29 ± 0.05
2.85	500-600	salt	0.31 ± 0.04
4.4	300-420	salt	0.27 ± 0.05
5.6	300-420	salt	0.30 ± 0.04

Table 4.4: Collapse parameters for the mixing of small pulses of dyed salt grains and glass spheres with otherwise identical grains. The parameters we varied were grain size and drum diameter. In all cases the drum rotation rate is 0.31 rev/s.

To summarize, we performed a systematic survey of the axial transport of grains and varied grain size ratio, drum diameter, grain type and drum rotation rate. Our finding was that in all cases studied, we found that the axial transport of grains is subdiffusive and that the width of an evolving pulse possesses power-law scalings. Some, but not all, have the additional property of self similar evolution, employing assumptions about the radial core shape. While these results differ significantly from historic work on this system, it should be noted that our ability to resolve temporal changes in the system within seconds, and our ability to repeat the experiments due to the ease in obtaining measurements, are paramount to determining dynamical properties of this system.

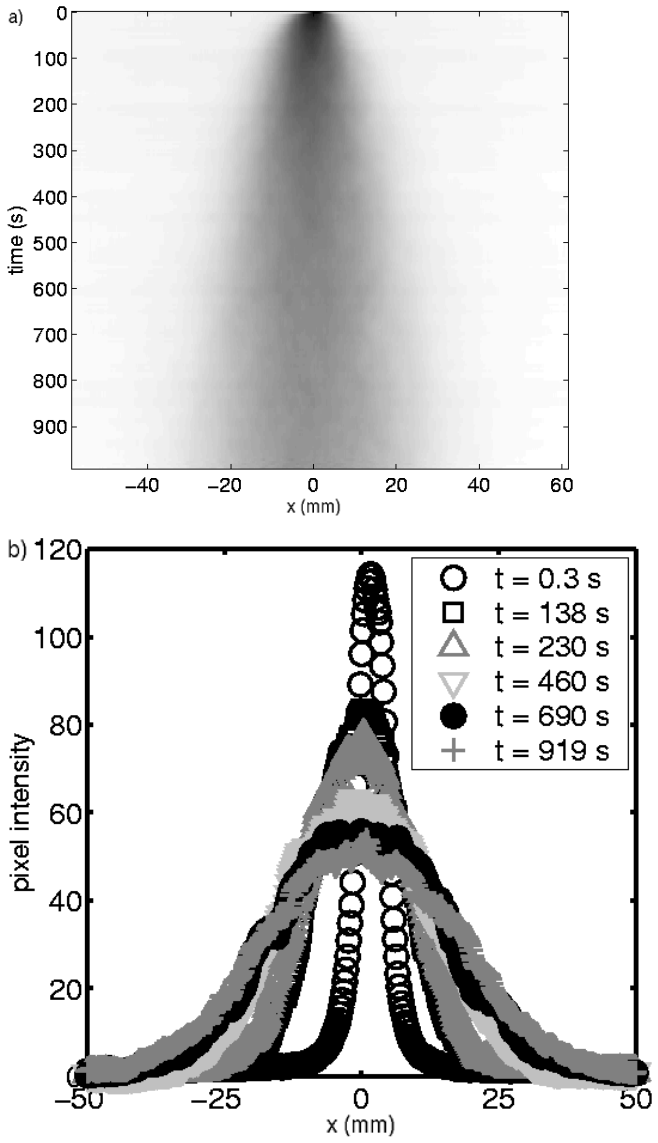

Figure 4.13: a) A space-time diagram of a mixing pulse of dyed black salt grains surrounded by un-dyed white salt grains in the size range of 300-420 μm. The drum diameter was 2.85 cm and the drum rotation rate was 0.62 rev/s. b) Concentration profiles of a mixing pulse of dyed black salt grains surrounded by white salt grains corresponding to (a).

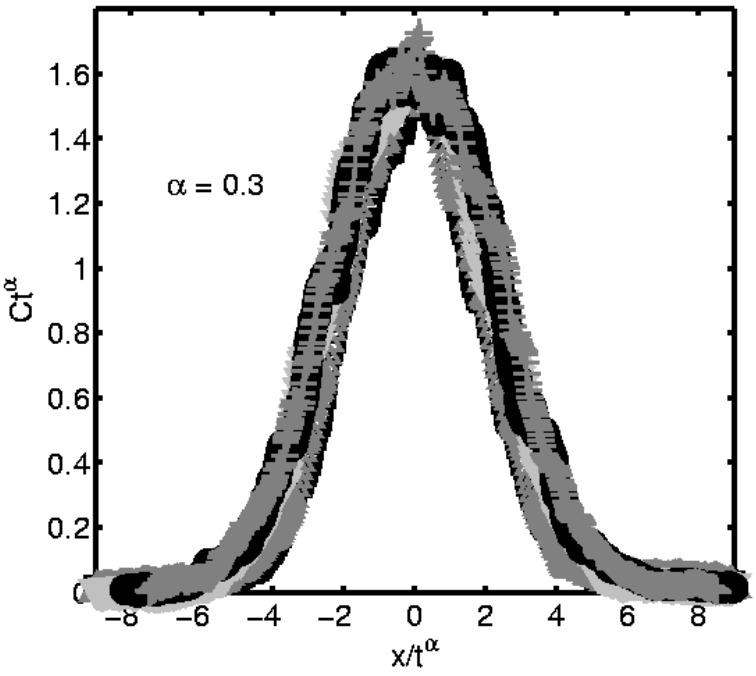

Figure 4.14: Collapsed concentration profiles corresponding to figure 4.13a. The collapse parameter is $\alpha = 0.3$.

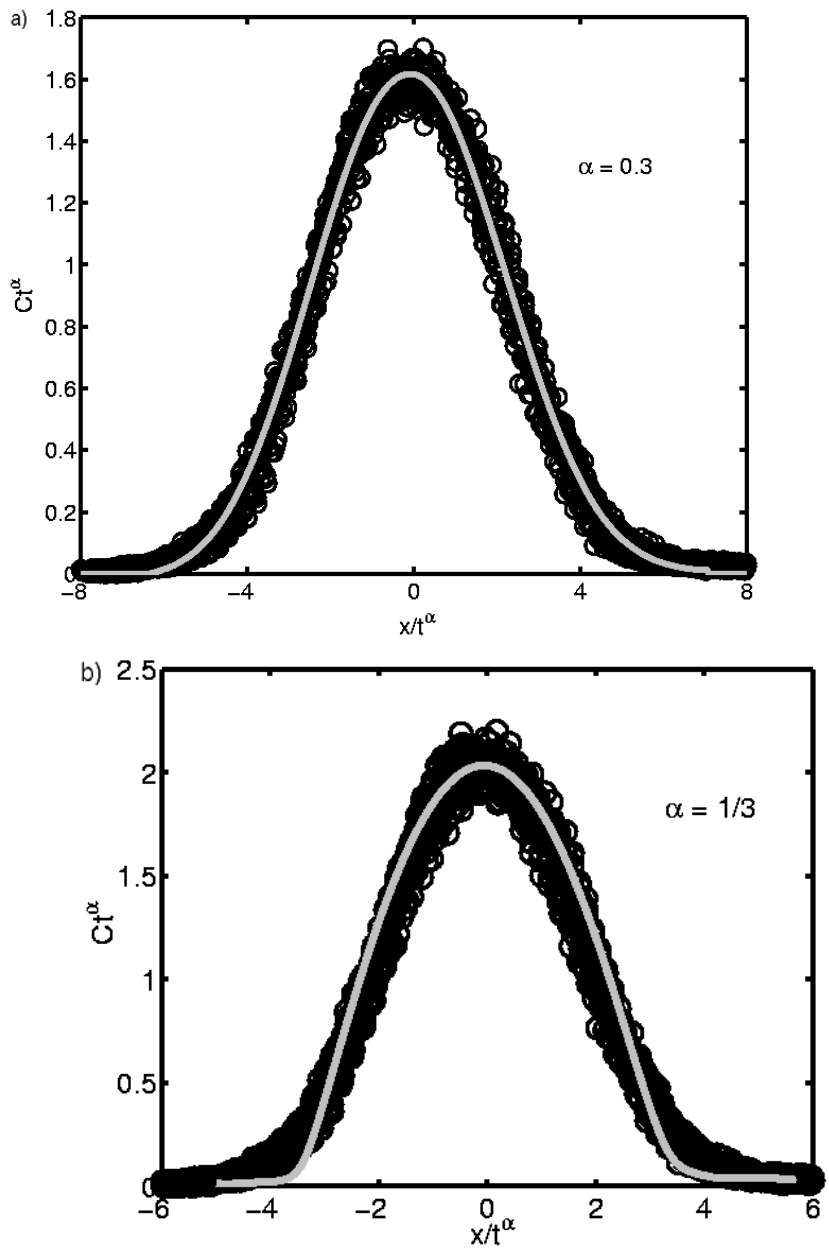

Figure 4.15: Collapsed concentration profiles of mixing dyed black salt grains fit to: a) the fractional diffusion equation (grey line) and b) the porous medium equation (grey line).

Chapter 5

Theoretical Outlook

In this thesis, we report on a number of experimental results which each individually falsify all of the currently existing PDE models of axial segregation. Recall that the first model, proposed by Savage [33], was based on the diffusion equation. This model was further developed by Zik *et al.*, who based their description of the dynamic instability on that of phase separation in spinodal decomposition [34]. Choo *et al.*'s discovery of the traveling wave transient invalidated this model, since a simple diffusion equation cannot describe oscillatory dynamics [35, 36]. To remedy this deficiency, Aranson *et al.* generalized the Zik *et al.* model as a two field reaction-diffusion system of equations [38, 39]. This elegant model, which agreed quantitatively with Choo *et al.*'s experimental data, was in turn invalidated by the present author's experiments which showed that the postulated second field, the dynamic angle of repose, did not evolve as predicted. In addition, subsequent experiments did not reveal any obvious choice for the second field. For details, the reader is referred to chapter 3.

Subsequent research pursued for this thesis presented findings that must be accounted for in any future theoretical model. To begin, the dynamics of axially transported grains in the smoothly streaming flow regime is subdiffusive, at least in every region of parameter space that we have investigated. Hence any future attempt to model this system

must either assume subdiffusive behaviour everywhere or account for its presence in the particular region we have investigated, if not elsewhere. Furthermore, it was determined that the growth rate of axial bands increases as a function of drum diameter and grain size ratio. This indicates that there must be a functional dependence on these quantities incorporated into or explained by any future model. Next, it is fairly obvious from experiments that axial bands grow from undulations on the radial core. As we have seen from figure 3.5, we have reason to believe that traveling waves result from a periodic mixing and unmixing of the radial core, since the traveling waves were shown to result from an oscillatory radial core instability. These last two findings imply that a description of the structure and behaviour of the radial core is fundamental for any future theory.

We acknowledge that while the theories of Zik *et al.* and Aranson *et al.* were invalidated, they were instrumental in guiding experimental research up to and including work done for this thesis. However, with the body of experimental data accumulated thus far, it is questionable whether this particular direction, i.e. developing a diffusive model based on analogy with phase separation in spinodal decomposition, can be pursued fruitfully. What are the alternatives? There are as yet no good candidates for a new model that incorporates all of the experimentally observed features; any future ad-hoc models that do so will likely be much more complex than the recently invalidated theories, and hence require a great deal of time to develop. They will still be vulnerable to falsification in the portion of parameter space that has yet to be explored. For the time being, the best approach would be to explore three directions in parallel. First, we do need to verify experimentally that the findings mentioned in the previous paragraph extend to the rest of parameter space of the rotating drum, and if not, determine where the transitions are. Second, given the current state of the theory, we can try to implement simulations of the rotating drum system that agree quantitatively with known experimental results, thereby adding to our understanding of the phenomenon, as well as hopefully allowing us to make predictions which can guide future experiments. And third, work on a new

model should proceed, but it is best to do so starting from first principles, whether those principles are specific to the rotating drum system or apply to granular media in general.

In the remainder of this chapter we will look at two first-principles theoretical approaches developed for granular systems other than the rotating drum, and discuss their applicability to this system. Following that, we will consider simulation methods, and examine two which have already been directly applied to the rotating drum system.

Any first principles approach, whether by theory or simulation, has to contend with the following facts: In granular systems ordinary temperature plays no role [69]; in contrast to gases, the energy scale k_BT is at least 10^{12} times smaller than the potential energy scale mgd of a grain of mass m raised by one diameter d in the Earth's gravity g. Because of this, the usual thermodynamics arguments do not apply. In fact, without the role of temperature in fluids providing a microscopic velocity scale, the only velocity scale present in granular media is imposed by the macroscopic flow. Typically, the interactions between grains are dissipative because of frictional and inelastic collisions, so in each collision energy is lost. Because of this, approaches based on elastic interactions between particles or energy conservation methods do not apply.

The two theoretical approaches we discuss below are the hydrodynamics approach to granular gases as outlined by Goldhirsch, among others [69, 72, 74], and Edwards' statistical mechanics approach for dense slowly evolving granular systems [76, 77, 78, 79]. It should be noted that these different conceptualizations tend to be applicable to different experimental regimes. The discrete simulational methods described are a molecular dynamics simulation which reports diffusive axial transport of grains due to Taberlet *et al.* [70] and Yanagita's implementation of a cellular automaton model of axial segregation [71].

5.1 Hydrodynamics of granular gases

Granular gases, previously denoted by the term "rapidly sheared granular flows", became an object of investigation among the granular community in the early 1990's with the work of Goldhirsch, Walton, Pöschel, and others [69]. The idea is that driven granular gases can display fluid dynamical properties such as surface wave patterns [5], so one might expect them to obey hydrodynamic equations [72]. Under gravity, collections of grains can be fluidized by strong forcing such as vibration or shear. The grains interact by nearly instantaneous collisions, reminiscent of the classical picture of a molecular gas; this is why fluidized grains are referred to as a "granular gas".

Despite the intuitive analogy, granular systems, even ones that are highly fluidized, differ from molecular gases in notable ways. To begin with, grains are obviously much bigger than molecules; furthermore, one cannot just assume that granular gases are macroscopic realizations of classical gases with the same equations of motion on a larger scale. Also, grain collisions are typically inelastic. This is the result of energy loss upon grain impacts, so any theory of granular gases would need an energy sink term. And because thermal temperature plays no role in granular systems, the temperature field must defined differently, typically in terms of fluctuating velocities of grains.

The starting point for defining the hydrodynamic fields in the theory of granular gases is the single particle distribution function $f(\mathbf{v}, \mathbf{r}, t)$defined at a point $\mathbf{r}$ and time t. This is equal to the number density of particles having a velocity in the interval between $\mathbf{v}$ and $\mathbf{v}+d\mathbf{v}$ at $\{\mathbf{r}, t\}$. The number density n, the velocity field $\mathbf{V}$, and the granular temperature T can be expressed as averages with respect to the single-particle distribution function f [72], where the number density n is

$$n(\mathbf{r}, t) \equiv \int d\mathbf{v}\ f(\mathbf{v}, \mathbf{r}, t)$$

the velocity field V is

$$\mathbf{V}(\mathbf{r}, t) \equiv \frac{1}{n(\mathbf{r}, t)} \int d\mathbf{v}\ \mathbf{v} f(\mathbf{v}, \mathbf{r}, t)$$

and the granular temperature T is

$$T(\mathbf{r},t) \equiv \frac{1}{n(\mathbf{r},t)} \int d\mathbf{v}\ (\mathbf{v}-\mathbf{V})^2 f(\mathbf{v},\mathbf{r},t).$$

The equations of motion for granular fluids follow from continuum mechanics and are very general [72]. For the case of monodisperse grains with mass normalized to unity, the equation of mass continuity is

$$\frac{Dn}{Dt} + n\frac{\partial V_\alpha}{\partial r_\alpha} = 0$$

where $\frac{D}{Dt} \equiv \frac{\partial}{\partial t} + \mathbf{V}\cdot\nabla$ is the material derivative, Greek indices denote Cartesian vector components, and summation is assumed. The momentum density is expressed as

$$n\frac{DV_\alpha}{Dt} + \frac{\partial P_{\alpha\beta}}{\partial r_\beta} = n\mathbf{g}$$

where $\mathbf{P}$ is the stress tensor, $\mathbf{g}$ is acceleration due to gravity, and granular temperature is

$$n\frac{DT}{Dt} + 2\frac{\partial V_\alpha}{\partial r_\beta}P_{\alpha\beta} + 2\frac{\partial Q_\beta}{\partial r_\beta} = -r\Gamma$$

where $\mathbf{Q}$ is the granular heat flux, and Γ represents the energy sink due to the inelasticity of collisions.

These equations are derivable from the Boltzmann equation, and describe ensemble-averaged fields. The hydrodynamic description is complete when constitutive relations through which $\mathbf{P}$, $\mathbf{Q}$ and Γ are expressed in terms of hydrodynamic fields established. In order to derive constitutive relations from the Boltzmann equation, one needs to find an approximation for the single-particle distribution function through application of the Chapman-Enskog expansion [65, 72].

This theory has been succesfully used to model instabilities in small-scale flows, including the flow of dilute grains past an obstacle [73] and patterns formed in vibrating layers of grains [74]. Also, some researchers report that this approach can be used to model phenomena such as segregation in shaken grains when driven at a high shaking

amplitude [75]. It should be noted, however, that one might expect this theory to be more applicable to highly fluidized shaker experiments than to systems with denser flows. The granular gas theory cannot describe force chains which transmit stress via persistent contacts in dense granular flows, or account for coexisting solid and fluid states such as the flow down the front face of a heap of grains [65]. In the rotating drum experiment, for example, we have a wide range of densities: the flowing granular surface may be highly fluidized, but next to it are tightly packed regions moving in solid-body rotation with the drum, and grains constantly make transitions between these regions [20]. It does not seem likely that a theory based on granular gases can be directly applied to the rotating drum system.

5.2 A statistical mechanics approach for dense flows

A more directly first-principles approach, and one starting from the opposite end of the flow spectrum, is Mehta and Edwards' granular statistical mechanics, which was first proposed in the late 1980's [76]. This formalism addresses fundamental issues concerning dense granular flows by considering granular packings i.e. the circumstances under which granular materials act more like a solid than a liquid.

Depending on the filling method, a random configuration of spherical grains can be packed in a range of volume fractions from 0.55-0.64 [69]. Often, when we have grains in a container force chains caused by static friction keep the grains in a metastable state between these volume fraction limits, and so prevent the grains from collapsing. Since thermal energy plays no role in this system, it can only sample other configurations by external disturbances such as vibration or tapping. This led Edwards and others to propose that it is possible in principle to develop an analogue of thermodynamics for jammed states in dense granular packings [76, 77, 78, 79].

In this formalism the energy is neglected because the particles have no interactions

aside from hard-sphere repulsion [77]. Internal energy is replaced with volume, and a volume functional takes the place of the hamiltonian and is given by the distribution of contacts between grains. The temperature is given by the compactivity, $\frac{\partial V}{\partial S}$ of the material, where the entropy S is the logarithm of the number of ways one can fit a powder into a volume V . External vibrations change the packing, thus the volume and compactivity change, allowing the system to explore phase space.

It has been shown experimentally that external vibrations of grains lead to a slow approach of the packing density to a steady-state value [80]. Depending on the initial packing and shaking acceleration, the system can move reversibly between steady-state values of packing density or become irreversibly trapped in a metastable state. The Edwards theory qualitatively describes these branches of configurational phase space [78, 79].

While this theory has had some success in describing some granular systems, such as the tapping experiment above, its applicability to the rotating drum system and segregation phenomena in general appears as yet to be limited. The statistical mechanics approach is most suited to systems with slowly evolving and static packings, so it focuses on structural characteristics as opposed to dynamics, and assumes spatially homogenous arrays of grains. As such we do not know how it could immediately be brought to bear on the dynamics of axial transport or radial segregation. In this theory, segregation is due to the tendency of the system to reduce the configurational entropy, and the dynamics only serves to rearrange the microstates.

It should be noted that since the statistical mechanics method and the hydrodynamics method discussed in the last section approach granular materials from opposite directions, it is very difficult to make a direct comparison with respect to applicability to our system of interest, the rotating drum. For obvious reasons, experiments designed to test the theories and predictions made by the theories have been for either highly fluidized or fairly static systems. Recently, tentative proposals have been made on both sides to

account for segregation effects in some granular systems, but so far neither theory has been directly applied to axial or radial segregation in a rotating drum. At this point there is no clear reason to prefer one of the theories over the other with respect to the results presented in this thesis, and since both theories are more like general frameworks than fully worked out models, and it would require a not insignificant amount of time and effort to apply either of them to the rotating drum or other granular systems in the dense flow regime. Until these theories have been developed further, therefore, we think that the best way to proceed is via the simulational approach discussed in the next two sections.

5.3 Molecular dynamics simulations

Even before the falsification of the Aranson *et al.* model, simulation was the most popular approach to theoretical study of the rotating drum system. In general, simulations are very useful because they allow researchers to efficiently explore the effects of varying many physical parameters which are not easily accessible to experiment, either separately or simultaneously. This allows one to fine tune phenomenological pictures and models of the system being explored even when a fully developed theoretical model is not available. With respect to the rotating drum, the two most frequently used simulation techniques are molecular dynamics and cellular automata [1]. Of the two, molecular dynamics is more explicitly grounded in physics, while cellular automata models generally require less computational resources and are simpler to implement.

Molecular dynamics or the discrete element method for granular systems is based on the molecular dynamics method for the study of liquids and gases [15]. There are a couple of different methods of implementing this approach; the method that is applied depends on the density and flow regime of the system of interest.

Rigid-particle models are used for low-density rapid flow regimes such as for shaken

granular fluids [15]. In this method there is no interpenetration or deformation of the particles during each impact, which is considered to be infinitely brief. The loss of linear momentum is captured via the coefficient of elastic restitution, while the rotation of the particles is neglected [1]. The method of simulation is event-driven with every collision being calculated.

Soft-particle methods are used to model high density slow-flow regimes such as the rotating drum experiment [30, 66, 70]. In this method friction and elastic restitution are implemented by having spheres penetrate into each other, with the magnitude of the interaction depending on the penetration depth [1]. The flow is characterized by lasting contacts, and particle trajectories are determined by explicitly solving Newton's equations of motion for linear and angular momentum for each particle. The forces acting on each particle are the gravitational force and interparticle collision forces which are applied normal to or tangent to the line of contact between grains. The accuracy of this method depends on the choice of contact forces. In contrast to the hard-sphere method, particle trajectories are updated at each time step [15].

5.3.1 A molecular dynamics simulation of the axial transport of grains

Recently Taberlet *et al.* employed a soft-particle molecular dynamics scheme to investigate the axial transport of grains in a rotating drum. This study found that the radial core of small grains spread diffusively, and that the self-mixing of the monodisperse grains was a diffusive mixing process [70].

In this study, the normal force between grains in contact was modeled using the dashpot-spring model and the tangential force with the regularized Coulomb solid friction law. Particle wall collisions are treated like inter-particle collisions but with the wall treated as a particle with infinite mass and radius. They report that varying the coefficient of restitution from 0.4 to 0.9 had little influence on the diffusion process. The

equations of motion were integrated using the Verlet method with a time step of $\frac{\Delta t}{30}$ where $\Delta t \backsimeq 10^{-3}$ s is the duration of a collision. They typically run their simulation for 10^7 time steps, or a few hundred drum rotations. For grains, small particles with a 5 mm diameter and large grains with a 10 mm diameter were used. The drum length for their self-diffusion runs was 300 mm and diameter was 200 mm, with an average filling fraction of 37 % and a rotation rate of 0.5 rev/s.

Taberlet *et al.* report that for these simulations both the axial transport of small grains within the radial core and the self-diffusion of monodisperse grains are simply diffusive processes. They claim that this is in direct disagreement with the results reported here and in reference [26]. That the self-mixing was diffusive was determined by examining the mean-squared displacement of individual grains from one run of small grains and one run of large grains. The authors also note that the ratio of drum diameter to average grain diameter was 26 for the simulation, while the experimental ratio is closer to 100. In other words, far fewer and larger grains were used in this simulation than in our experiments, described in this thesis and in reference [26]. To give an idea of scale, if the particles in the simulation were the same size as those used in the experiments, the drum would be the size of a thimble, with only about 6 or 7 layers of grains in it. Hence we do not consider the simulation results to directly disagree with our experimental results, since they cannot be directly compared.

Molecular dynamics is certainly a promising approach to the study of dense-flow granular systems. There are, however, things that must be considered before going further. The validity of the simulation is entirely dependent upon the choice of force laws and adjustable parameters used, and the values assigned to those parameters. If any relevant parameter is not included in the implementation, or the parameter value is not physically justified, then the results of the simulation cannot of course be quantitatively trusted. This puts a constraint upon implementing idealized models or simplifying assumptions, or using estimated values for parameters; before doing so one needs to at least validate

the simulation by direct comparison to experimental results. Unfortunately, simplifying assumptions, idealizations, and similar expedients are often necessary to make the computations involved feasible. For example, a rough estimate for the number of particles in a one-third full rotating drum experiment such as described in this thesis is about 700,000. Since each time step requires updating or at least checking every particle, a realistic molecular dynamics simulation of a real-life experimental setup run for a reasonable length of time would require massive computational resources. While we might expect that future technological developments will make this possible at some point, for the time being molecular dynamics simulations of the rotating drum system must work on rather limited time or spatial scales.

5.4 Yanagita's cellular automaton model

In 1999 Yanagita proposed a three dimensional cellular automaton model (CAM) in which particles of two different frictional properties randomly slide down a sloped collection of grains confined to a rectangular box [71]. His model is based on the assumption that axial segregation is driven by differences in the dynamic angles of repose of the two types of grains, so he neglects the motion of particles in the bulk. Compared to Molecular Dynamics simulations, cellular automata do not require detailed knowledge of grain interactions, such as tangential and normal forces, therefore computational time is greatly reduced. Surprisingly, this model apparently reproduces many of the features of axial band formation, such as radial core formation and axial bands growing from modulations on the radial core [29, 71]. For this reason, we implemented Yanagita's CAM as described in reference [71] to see if the self-mixing of one grain species in this model was a subdiffusive process, and initial results indicate that this is so.

Yanagita's CAM uses a three-dimensional simple cubic lattice to model a drum, (x, y, z) where x is the axial coordinate, y is the depth coordinate and z is the verti-

cal coordinate. Each site has a discrete field variable $\sigma(x, y, z)$ whose value is taken from the set $\{0, 1, 2\}$ corresponding to empty, particle A, or particle B respectively. Following Zik *et al.*'s reasoning [34], Yanagita assumes that segregation is entirely due to the particle motion on the free surface; thus the updating rules for the CAM only consider sliding surface particles and not the particles in the bulk. The dynamics of the field variable σ is comprised of two steps: (1) A surface particle $\sigma(x, y, h(x, y))$ is chosen randomly, where h is the height from the bottom of the drum to the surface at the position (x, y). (2) The selected particle slides down to a randomly selected site, chosen from neighbouring sites $(x + \Delta x, y + \Delta y, h(x + \Delta x, y + \Delta y) + 1)$, where Δx and Δy are random variables with values taken from the following sets $\Delta x = -1, 0, 1$, $\Delta y = 0, 1$ with uniform probability. (3) The sliding motion outlined above is accepted if the height difference between the two positions $\Delta h = h(x, y) - h(x + \Delta x, y + \Delta y)$ is larger than the "effective" friction F acting on the particle; that is, Yanagita only considers the case where grain types A and B only differ by frictional properties. The effective friction F is simply the sum of the local frictions arising from the interaction with adjacent particles, f_{AA}, f_{AB}, and f_{BB}, which leads to the interaction rule

$$F = \sum_{\delta x=0,-1} \sum_{\delta y=-1,0,1} \sum_{\delta z=0,-1} f[\sigma(x, y, h(x, y))\sigma(x + \delta x, y + \delta y, h(x, y) + \delta z)]$$

where f is defined as a local map $f : (0, 1, 2, 4) \to (0, f_{AA}, f_{AB}, f_{BB})$. (4) The procedures above are applied r times, where the rotational frequency ω is proportional $1/r$. Yanagita then introduces the rotation of the drum: the rectangular lattice is divided into a lower (L) region and a higher (H) region separated by the vertical plane $y = N_y/2$. The H side is slid upward and the L side downward by one cell, and the bottom layer of the L side is turned over and attached to the H side, which is illustrated in figure 5.1. This creates a stepwise height difference at $y = N_y/2$. Particles at this stepwise difference then slide down, creating a propagating collapse, and after a few rotations the front face of the mixture is smooth. The steps (1)-(4) described above define one cycle of the

dynamics. Yanagita used fixed boundary condition, with the friction at positions $x = 0$ and $x = N_x + 1$ the same as that of the B particles. The particles at $y = 1$ are constrained not to move in the y direction.

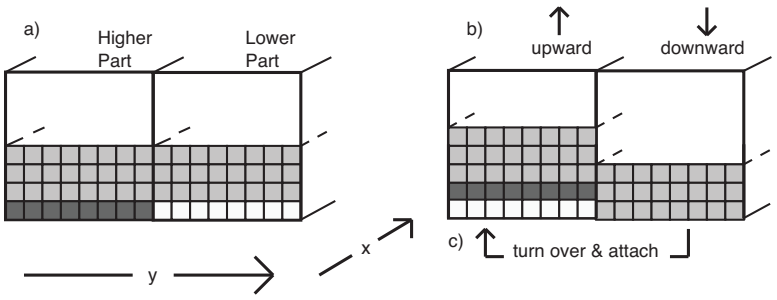

Figure 5.1: Yanagita's schematic explanation of the rotation procedure implemented in his cellular automaton model. In part (a), the region is divided into the lower (L) and higher (H) sides. In (b), the H side is slid upward and the L side is slid downward by one cell. In (c), the bottom layer of the L side is turned over and attached to the bottom of the H side.

Starting with a half and half mixture of particles A and B with random initial conditions, and frictional values $f_{AA} = 0.4$, $f_{AB} = 0.44$, and $f_{BB} = 1.0$, Yanagita obtains a radial core made up of the higher friction particle B after a small number of drum rotations. After approximately 50 drum rotations axial bands appear, and after several hundred rotations axial bands merge and coarsened bands appear. Yanagita also reports that the time scales of the rotation and axial transport of particles are quite different, thus band coarsening shows slow dynamics. This CAM was modified by Newey *et al.* to model the segregation dynamics of ternary mixtures by incorporating a third particle type into the rules described above. They found that the automata reproduced experimentally observed band-in-band segregation, and a radial core composed of the highest friction grains in the center surrounded by the particles with an intermediate friction value. The coarsening process in the simulation was also consistent with what they had observed experimentally [29].

We implemented the rules outlined above, for a grid sized with 150 sites in the axial direction, 40 sites in the vertical direction and 10 sites wide, with the drum being half full. We applied the sliding procedures 11000 times, which resulted in approximately 3000 successful slides, per cycle. One drum rotation is considered to be 40 cycles with the values we used above. We examined the self-mixing of identical grains by setting the frictional properties to be identical, $f_{AA} = f_{AB} = f_{BB} = 0.44$, and our initial condition was a pulse of grain B two grains wide located at the center of the drum, surrounded by the otherwise identical particle A. This enabled us to track the motion of the B grains throughout the simulation length, which corresponded to 100 drum revolutions. Figure 5.2a shows a space time diagram of B particles self-mixing with A particles, evolving from a small pulse initial condition as described above. Figure 5.2b shows the power-law dependencies of pulse width and height on time, we find that these power laws are consistent with self-similar subdiffusive self-mixing found experimentally. Figure 5.3 shows concentration profiles for various times from the run shown in figure 5.2 and figure 5.3b shows that those concentration profiles collapse with a parameter $\alpha = 0.39$.

It should be noted that Yanagita's model, however simplified and non-cylindrical, is in rough qualitative agreement with the basic phenomenology of what happens in a rotating drum i.e. a flowing surface layer and a static bulk rotating with the tube, as for example given by Hill *et al.* [20]. Hence we may be able to explain observed phenomena in the real-life system by working backwards from the rules implemented in the simulation. In the automaton, particles can only move axially when they are on the surface, and every particle that comes to rest in the L region must eventually be recycled into the H region, where it is trapped in the bulk until it again reaches the surface. This means that the motions of the particles are constrained and thus not Brownian, so one would expect that analysis of the simulation data would show that axial transport in the absence of segregation effects was subdiffusive. Given that our own experimental data showed subdiffusion, and given the real-life rotating drum's phenomenology, this

bulk trapping/surface freeing could quite plausibly be the mechanism for the slower than diffusion axial movement of grains.

The cellular automata approach seems to be quite promising as an avenue of research into the rotating drum system. It is easy to implement and modify, and in comparison to molecular dynamics is much less computationally intensive. Hence it is feasible to validate by comparison to real-life experiments. This is of course necessary since the rules we chose are somewhat arbitrary; the only criterion is whether the automaton mimics the real phenomenon successfully in the first place. When a set of rules has been found that does replicate the phenomenon, it is sometimes possible to work back from these rules to an actual explanation or mechanism, as outlined in the above paragraph. There is indeed no guarantee that this can be done or that a plausible explanation generated in this way is the correct one. We think, however, that this is not a major drawback in comparison with the advantages of this method, and that for now CAM has the most potential for further understanding of the rotating drum system.

With regards to the Yanagita model in particular, there are modifications that would need to be made if one were to pursue this as future research. To begin, one would want to explicitly include rules that distinguish particles by size, in order to check whether size segregation and radial core formation occur. Once this has been implemented, the first test would be to see if mixtures of multiple grain types or sizes, in analogy to the travelling wave mixtures used in experiments, will result in oscillatory band dynamics. If this does not turn out to be the case then clearly the Yanagita model would require further modification. On the other hand, if travelling waves were replicated it would be very a meaningful result, implying a simple underlying mechanism.

In this chapter we have examined some of the theoretical possibilities which could guide future experimental work on the rotating drum. We began by evaluating the diffusion-based theories that were current when the research for this thesis started, and which were invalidated by the experimental results presented here. Our conclusion was

that modifying or fixing these theories in order to account for new experimental data was not likely to be very fruitful. We then looked to a couple of general approaches that have been put forward to deal with granular systems in different phenomenological regimes, and discussed their applicability to our own system. While both these approaches, one a hydrodynamical theory and the other a statistical mechanics based theory, have had success in dealing with their specific regime of granular flow and may have potential applications elsewhere, neither currently is in a position to address the rotating drum. Lastly we considered the possibilities implicit in two simulational approaches, molecular dynamics and cellular automata models. While both have their drawbacks they both seem to have more potential then any current theoretical framework. Cellular automata, for the moment at least, have one undeniable advantage in that for them simulating real-life systems is not too heavily constrained by issues of computationally feasibility. Thus in our opinion this seems to be the most promising avenue for theoretical progress in the near future.

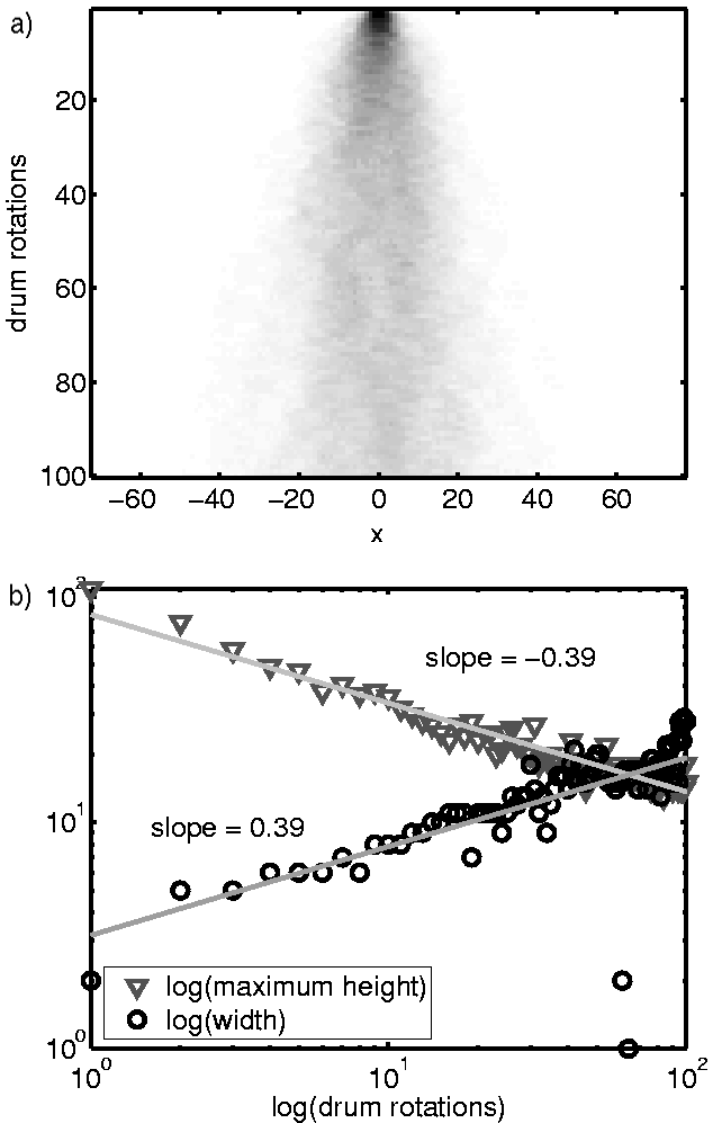

Figure 5.2: a)Space-time diagram of grain type B self-mixing with otherwise identical grain type A, evolving from a small pulse initial condition from Yanagita's cellular automaton model of the rotating drum [71]. b) The FWHM (circles) of the evolving pulse shown in (a) plotted against time on logarithmic scales. The linear fit shows that the pulse width evolves with the power law width $\propto t^{0.39}$. The maximum concentration profile height is also plotted against time (triangles) and the linear fit shows that pulse concentration decays with the power law peak concentration $\propto t^{-0.39}$.

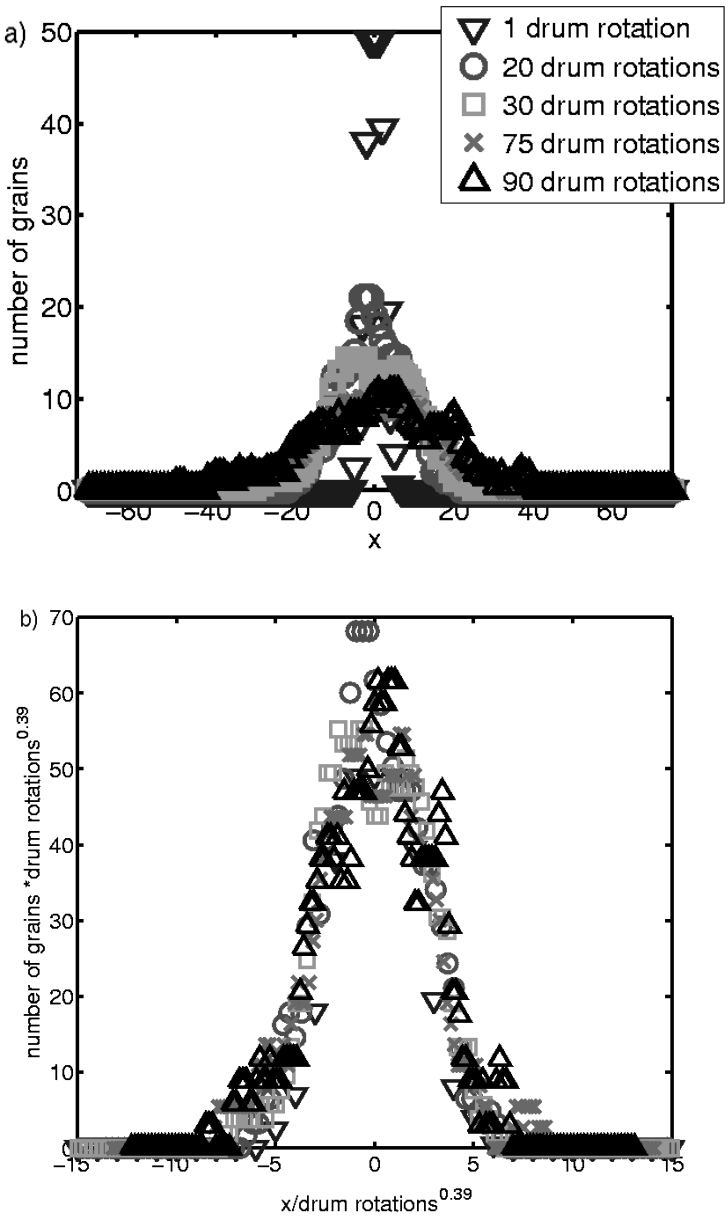

Figure 5.3: a) Concentration profiles of grain type B self-mixing with grain type A, corresponding to the space-time diagram shown in figure 5.2a. b) Collapsed concentration profiles corresponding to (a) with collapse parameter $\alpha = 0.39$.

Chapter 6

Conclusions

In this thesis, we report on a series of experimental results on the segregation and axial transport of grains in a rotating drum. These results have strong implications for any future model of segregation processes in this system. We have provided a consistent experimental picture of the phenomena, and a conceptual framework for future research.

We began our research into the rotating drum system with an experiment designed to test the then current theoretical model for axial segregation in a rotating drum. Our first finding was that the dynamic angle of repose and the surface concentration of grains are coupled throughout segregation process, including the oscillatory transient. This implies that the dynamic angle of repose field does not evolve as predicted, invalidating the theory [38, 39]. As this theory was based on geometrical considerations of surface flows only, our result probably rules out any reasonable elaboration of such a model.

This negative result led us consider the role of the radial core in axial segregation and oscillatory transients. It was already known that the particles in a rotating drum segregated radially prior to axial band formation, forming a radial core made up of the smaller grains. However, this core was ignored by theory and had only recently become an object of active experimental research [20, 21, 23]. We confirmed that axial bands are formed out of bumps on the radial core, and observed that oscillatory band dynamics

are caused by undulations in the core, a periodic mixing and unmixing which shifted these bumps. This brought us to the conclusion that radial core instability is the key to understanding axial segregation.

To resolve this, more insight was needed into how grains move in the bulk. Our next seies of experiments dealt with the axial transport of grains within the radial core in the absence axial banding. Here we found that, contrary to previous assumptions, axial transport is subdiffusive. This applies to both monodisperse and bidisperse mixtures *i.e.* both self-mixing and segregation.

We repeated the experiments for several grain types, grain size ratios, rotation rates, and drum diameters, and in all cases we confirmed that the process remained subdiffusive. With respect to drum diameter and grain size ratio we also found indirect evidence of mixing in the radial core. As drum diameter increased, the inferred core volume increased, which implied that the core was gaining material from outside; as grain size ratio increased the inferred core volume decreased, which implied that the core was losing material.

In another series of experiments that examined axial segregation, we found that the growth rate of axial bands increased as a function of drum diameter, and also as a function of grain size ratio. Combined with the above observations relating drum diameter and grain size ratio to possible mixing in the radial core, these results indicate that faster band growth is associated with enhanced mixing in the radial core. We speculate that many puzzling features of axial segregation, such as the oscillatory transient, may be related to the dynamics of mixing in the radial core.

During the course of this research, we have developed two new visualization and measurement techniques, which may be of use in future investigations of rotating drum phenomena and similar granular systems. The scanning profilometer device was designed to simultaneously measure the streaming surface profile and concentration of flowing grains; this was used to establish our first result. We also devised an optical bulk visualization technique, which was instrumental in our investigation of radial core dynamics.

From our results, and the work of others, we can outline the following phenomenological description of axial segregation: First, we know that a radial core made up of the smaller particles forms very quickly, within five drum rotations. After about 100 drum revolutions, bumps form on the radial core; these may be due to the presence of mixing. These bumps then grow into axial bands, at a rate that depends on certain parameters such as drum diameter and grain size ratio. Since the axial transport is subdiffusive, we surmise that the bands are not strongly damped by the background axial motion of the larger grains. Traveling waves may be the result of a periodic mixing and unmixing of the radial core, but such waves are only observed in certain mixtures.

Partly as a result of the research presented here, there are currently no experimentally validated continuum models specifically intended to describe the phenomenon of axial segregation in the rotating drum system. Promising models have been developed for granular systems that are either highly fluidized or densely packed, but as yet these are not readily applicable to dense flow regimes such as are found in the rotating drum. In the absence of a strong theoretical direction given by an explicit continuum model we must rely on phenomenological descriptions and simulation to guide future work. One simulation technique that seems to have some potential for our particular system are cellular automata models. We implemented one such model, due to Yanagita [71], and found subdiffusive self-mixing of grains consistent with our experimental results.

There is much that can be done to follow up the results presented here. For example, we found that there is a drum diameter cutoff, below which axial bands do not form for a given mixture of grains [25, 27]. We have yet to determine whether radial segration still occurs below this cutoff, and if axial transport of the grains is markedly different within these very small diameters. As well, we have noted that for some sets of parameters the apparent radial core volume is conserved, while for others it increases or deseases in a regular way. It would be worthwhile to conduct a program of experiments to track the apparent radial core volume conservation line through parameter space, and check if

parameter values close to this line are also consistently associated with slower growth of axial bands.

In a more general vein, the parameter space for the rotating drum system is very large, and we have only explored a narrow region of it. In our experiments, we varied the rotation rate, grain type, grain size ratio, and drum diameter independently. There are other parameters that have not been systematically explored. It would be interesting to determine whether such things as polydispersity, filling fraction, or grain density ratio had measurable effects on axial transport and axial band formation.

While 2D visualization was essential in our experiments in establishing the dynamics of the system, it does have definite limitations. In particular, it would be useful to have an investigation of mixing in the radial core using full, 3D bulk imaging. Our visualization method could at most give us indirect evidence of this mixing, by way of the apparent core volume; this could be directly confirmed using non-invasive MRI or X-Ray techniques, or a freeze-and-slice procedure.

Segregation is complicated, perhaps more complicated than anyone previously appreciated. One thing that became increasingly clear through the course of our research was that there needs to be a better understanding of how grains move in the bulk, independent of any segregation effects. Probably the single most profitable avenue of further research would be tracking the movement of a single grain in a monodisperse mixture. If we had a quantitative picture of bulk trapping, the release into the fluidized surface flow, and the transition between the two, it might be possible to construct a model of the simplest dynamical behaviour of grains in a drum. There are various ways this could be done experimentally, for example, using a microwave-tagged particle, determining its position in real time using triangulation methods [82].

In conclusion, while segregation in a rotating drum continues to resist simple formulation, we now have a clearer understanding of the dynamics of this system. Future research along these lines would most certainly be worthwhile.

Bibliography

[1] J. Duran, *Sand, Powders and Grains: An Introduction to the Physics of Granular Materials* (Springer, 2000).

[2] T. Shinbrot and F. J. Muzzio, *Physics Today*, March 2002, p. 25.

[3] P. Umbanhowar, *Nature* **424** , 886 (2003).

[4] P. Umbanhowar, *Nature* **389**, 541 (1997).

[5] F. Melo, P. Umbanhowar, and H. L. Swinney, *Phys. Rev. Lett.* **75**, 3838 (1995).

[6] J. C. Williams, *Powder Technology* **15**, 245 (1976).

[7] A. Rosato, K. J. Strandburg, F. Prinz, and SR. H. Swendsen, *Phys. Rev. Lett.* **58**, 1038 (1987).

[8] T. Shinbrot and F. J. Muzzio, *Phys. Rev. Lett.* **81**, 4365 (1998)

[9] M. A. Naylor, M. R. Swift, and P. J. King, *Phys Rev. E* **68**, 012301 (2003).

[10] M. E. Mobius, B. E. Lauderdale, S. R. Nagel, and H. M. Jaeger, *Nature* **414** , 270 (2001).

[11] H. A. Makse, S. Havlin, P. C. Ivanov, P. R. King, S. Prakash, and H. E. Stanley, *Physica A* **233**, 587 (1996).

[12] J. M. N. T. Gray and K. Hutter, *Continuum Mech. Thermodyn.* **9**, 341 (1997).

[13] H. A. Makse, S. Havlin, P. R. King, and H. E. Stanley, *Nature* **386**, 379 (1997).

[14] H. A. Makse, *Phys. Rev. E* **56**, 7008 (1997).

[15] J. M. Ottino and D. V. Khakar, *Annu. Rev. Fluid. Mech.* **32**, 55 (2000).

[16] K. M. Hill, N. Jain, and J. M. Ottino, *Phys. Rev. E.* **64**, 011302 (2001).

[17] Y. Oyama, *Bull. Inst. Phys. Chem. Res. Rep.* **5**, 600 (1939).

[18] M. B. Donald and B. Roseman, *Brit. Chem. Eng.* **7**, 749 (1962).

[19] D. Levine, *Chaos* **9**, 573 (1999).

[20] K. M. Hill, A. Caprihan and J. Kakalios, *Phys. Rev. Lett.* **78**, 50 (1997).

[21] K. M. Hill, J. Kakalios, K. Yamane, Y. Tsuji and A. Caprihan, *Powders and Grains 97*(A. A. Balkema, 1997), p. 13.

[22] K. M. Hill, A. Caprihan and J. Kakalios, *Phys. Rev. E* **56**, 4386 (1997).

[23] M. Nakagawa, *Chem. Eng. Sci.* **49**, 2540 (1994).

[24] J. Bridgwater, N. W. Sharpe and D. C. Stocker, *Trans. Instn. Chem. Engrs.* **47**, 114 (1969).

[25] A. Alexander. F. J. Muzzio, T. Shinbrot, *Granular Matter* **5**, 171 (2004).

[26] Z. S. Khan and S. W. Morris, *Phys. Rev. Lett.* **94**, 048002 (2005).

[27] C. R. J. Charles, Z. S. Khan and S. W. Morris, *Granular Matter* **8**, 1 (2006).

[28] Z. S. Khan, W. A. Tokaruk and S. W. Morris, *Europhys. Lett.* **66**, 212 (2004).

[29] M. Newey, J Ozik, S. M. van der Meer, E. Ott and W. Losert, *Europhys. Lett.* **66**, 205 (2004).

[30] N. Taberlet, W. Losert, and P. Richard, *Europhys. Lett.* **68**, 522 (2004).

[31] B. Roseman and M. B. Donald, *Brit. Chem. Eng.* **7**, 823 (1962).

[32] K. M. Hill and J. Kakalios, *Phys. Rev. E* **52**, 4393 (1995).

[33] S.B. Savage, in *Disorder and Granular Media*, edited by D. Bideau and A. Hansen (North-Holland, Amsterdam, 1993), p. 255.

[34] O. Zik, D. Levine, S. G. Lipson, S. Shtrikman, and J. Stavans, *Phys. Rev. Lett.* **73**, 644 (1994).

[35] K. Choo, T. C. A. Molteno and S. W. Morris, *Phys. Rev. Lett.* **79**, 2975 (1997).

[36] K. Choo, M. W. Baker, T. C. A. Molteno and S. W. Morris, *Phys. Rev. E* **58**, 6115 (1998).

[37] S. J. Fiedor and J. M. Ottino, *Phys. Rev. Lett.* **91**, 244301 (2003).

[38] I.S. Aranson and L.S. Tsimring, *Phys. Rev. Lett.* **82**, 4643 (1999).

[39] I.S. Aranson, L.S. Tsimring, and V.N. Vinokur, *Phys. Rev. E* **60**, 1975 (1999).

[40] G. H. Ristow and M. Nakagawa, *Phys. Rev. E* **59**, 2044 (1999).

[41] T. Elperin and A. Vikhansky, *Phys. Rev.E* **60**, 1946 (1999).

[42] K. Choo, M. Sc. Thesis, Unpublished (1997).

[43] M. Nakagawa, S. A. Altobelli, A. Caprihan and E. Fukushima, *Chem. Eng. Sci.* **52**, 4423 (1997).

[44] M. Nakagawa, J. L. Moss, K. Nishimura and T. Ozeki, *Powders and Grains 97*, edited by R. P. Behringer and J. T. Jenkins (Balkema, Rotterdam, 1997), p. 495.

[45] G. Metcalfe and M. Shattuck, *Physica A* **233**, 709 (1996).

[46] D. V. Ktitarev and D. E. Wolf, *Gran. Matt.* **1**, 141 (1998).

[47] R. Hogg, D. S. Cahn, T. W. Healy and D. W. Fuerstenau, *Chem. Eng. Sci.*, **21**, 1025 (1966).

[48] D. C. Rapaport, *Phys. Rev. E* **65**, 061306 (2002).

[49] B. Levitan, *Phys. Rev. E* **58**, 2061 (1997).

[50] E. Fried, A. Q. Shen and S. T. Thoroddsen, *Phys. Fluids* **10**, 10 (1998).

[51] A. Q. Shen, *Phys. Fluids* **14**, 462 (2002).

[52] L. C. Evans, *Partial Differential Equations* , (American Mathematical Society, 1998).

[53] G. I. Barenblatt, *Scaling*, (Cambridge University Press, 2003).

[54] W. R. Schneider and W. Wyss, *J. Math. Phys.* **30**, 134 (1989).

[55] R. Metzler and T. F. Nonnenmacher, *J. Phys. A: Math. Gen.* **30**, 1089 (1997).

[56] B. I. Henry and S. L. Wearne, *Physica A* **276**, 448 (2000).

[57] L. S. Tsimring, *personal communication.*

[58] W. H. Press, S. A. Teukolsky, W. T Vetterling and B. P. Flannery, *Numerical Recipes in C, Second Edition*, (Cambridge University Press, 1998).

[59] O. Zik and J. Stavans, *Europhys. Lett.* **16**, 255 (1991).

[60] "Scenic Sand", manufactured by Activa Products Inc., P.O. Box 1296, Marshall, TX.

[61] "8700 Trubore 1.119"IDX36" ", manufacured by Ace Glass Inc., 1430 Northwest Boulevard, Vineland NJ, 08360.

[62] "Larostat FPE S Antistat", manufactured by BASF Corp., 300 Continental Drive North, Mount Olive, NJ, 07828.

[63] C. R. J. Charles, Undergraduate Thesis Project Report, Unpublished (2004).

[64] Z. S. Khan, M. Sc. Project Report, Unpublished (2001).

[65] I.S. Aranson and L.S. Tsimring, *Rev. Mod. Phys.* **78**,641 (2006).

[66] D. C. Rapaport, *Phys. Rev. E* **65**, 061306 (2002).

[67] J. P. Koeppe, M. Enz and J. Kakalios, *Phys. Rev. E* **58**, 4104 (1998).

[68] R. Chicharro, R. Peralta-Fabi and R. M. Velasco, *Powders and Grains 97*, A. A. Balkema, 1997, p. 479.

[69] H. M. Jaeger, S. R. Nagel and R. P. Behringer, *Rev. Mod. Phys.* **68**, 1259 (1996).

[70] N. Taberlet and P. Richard, *Phys. Rev. E* **73**, 041301 (2006).

[71] T. Yanagita, *Phys. Rev. Lett.* **82**, 3488 (1999).

[72] I. Goldhirsch, *Annu. Rev. Fluid Mech.* **35**, 267 (2003) .

[73] E. C. Rericha, C. Bizon, M. D. Shattuck and H. L. Swinney, *Phys. Rev. Lett.* **88**, 014302 (2002).

[74] J. Bougie, J. Kreft, J. B. Swift and H. L. Swinney, *Phys. Rev. E* **71**, 021301 (2005).

[75] V. Garzó, preprint: arXiv:cond-mat/0603232 v2 (2006).

[76] A. Mehta and S. F. Edwards, *Physica A* **157**, 378 (1989).

[77] S. F. Edwards and D. V. Grinev, *Adv. in Phys.* **51**, 1669 (2002).

[78] S. F. Edwards and D. V. Grinev, *Phys. Rev. E* **58**, 4758 (1998).

[79] S. F. Edwards and D. V. Grinev, *Granular Matter* **4**, 147 (2003).

[80] E. R. Nowak, J. B. Knight, M. Povinelli, H. M. Jaeger, and S. R. Nagel, *Powder Technol.* **94**, 79 (1997).

[81] W. A. Strauss, *Partial Differential Equations: An Introduction*, (John Wiley and Sons Inc., 1992).

[82] S. Herminghaus, *personal communication*.